IMPACT OF VARIABILITY OF NAKAGAMI-m PARAMETER ON THE PERFORMANCE OF DIGITAL COMMUNICATION SYSTEMS

BY

Muhammad Imran Azam

A Thesis Presented to the

DEANSHIP OF GRADUATE STUDIES

KING FAHD UNIVERSITY OF PETROLEUM & MINERALS

DHAHRAN, SAUDI ARABIA

In Partial Fulfillment of the
Requirements for the Degree of

MASTER OF SCIENCE

In

ELECTRICAL ENGINEERING

APRIL 2006

KING FAHD UNIVERSITY OF PETROLEUM AND MINERALS

DHAHRAN 31261, SAUDI ARABIA

DEANSHIP OF GRADUATE STUDIES

This thesis, written by **Muhammad Imran Azam** under the direction of his thesis advisor and approved by his thesis committee, has been presented to and accepted by the Dean of Graduate Studies, in partial fulfillment of the requirements for the degree of **MASTER OF SCIENCE In Electrical Engineering.**

THESIS COMMITTEE

Dr. Asrar U.H. Sheikh (Chairman)

Dr. Adil Balghonaim (Member)

Dr. Mohamed Mohandes (Member)

Department Chairman
Dr. Jamil M. Bakhashwain

Dean of Graduate Studies
Dr. Mohammad A. Al-Ohali

Date

٢/٤/١٤٢٧

06 May 2006

Dedicated to

My Beloved Parents and Siblings

ACKNOWLEDGEMENTS

In the name of Allah, the Most Gracious and the Most Merciful

All praise and glory goes to Almighty Allah (Subhanahu Wa Ta'ala) who gave me the courage and patience to carry out this work. Peace and blessings of Allah be upon His last Prophet Muhammad (Sallulaho-Alaihe-Wassalam) and all his Sahaba (Razi-Allaho-Anhum) who devoted their lives towards the prosperity and spread of Islam.

First and foremost gratitude is due to the esteemed university, the **King Fahd University of Petroleum and Minerals** for my admittance, and to its learned faculty members for imparting quality learning and knowledge with their valuable support and able guidance that has led my way through this point of undertaking my research work.

My deep appreciation and heartfelt gratitude goes to my thesis advisor **Professor Asrar Ul Haq Sheikh** for his constant endeavour, guidance and the numerous moments of attention he devoted throughout the course of this research work. His

valuable suggestions made this work interesting and knowledgeable for me. Working with him in a friendly and motivating environment was really a joyful and learning experience. I would also acknowledge him for his cooperation in providing the TRL lab facility.

I extend my deepest gratitude to my thesis committee members Dr. Adil Balghonaim and Dr. Mohamed Mohandes for their constructive and positive criticism, extraordinary attention and thought-provoking contribution in my research. It was surely an honor and an exceptional learning to work with them.

Acknowledgement is due to my senior fellows Muhammad Moinuddin (Bhai) and Saad Azhar and colleagues Mudassir Masood, Imran Naseem and Sheikh Faisal Zaheer for helping me on issues relating to LaTeXand MATLAB. I also appreciate all the deep concerns of all my fellows, all of whom I will not be able to name here.

Family support plays a vital role in the success of an individual.I would like to thank my respected parents, siblings from the core of my heart. Their prayers and encouragement always help me take the right steps in life.

May Allah help us in following Islam according to Quran and Sunnah! *(*Aameen)

Contents

List of Figures

List of Tables

THESIS ABSTRACT

Name: Muhammad Imran Azam

Title: Impact of Variability of Nakagami-m Parameter on the Performance of Digital Communication Systems

Degree: MASTER OF SCIENCE

Major Field: Electrical Engineering

Date of Degree: April 2006

The effect of varying distances between the mobile station and base station on the Nakagami-m parameter is studied. For this purpose a path loss model is developed that finds out the received direct and scattered powers at the mobile station. The effect on the Nakagami-m parameter for different distributions of the reflection co-efficient Γ is presented. It is found that the exponential distribution gives larger values of m as compared to uniform and half Gaussian distribution. Change in the operating frequency also affects the performance of a digital communication link. A new parameter Δm is also introduced in order to study the change in performance behavior of the system with increase in distance. It is, also, observed that the transmitter and receiver antenna heights affect the Nakagami-m parameter and an increase in their effective value enhance the performance of the system. The degraded performance at larger distances for smaller values of Nakagami-m parameter is studied and the error rates are improved by using coherent Equal Gain Combining (EGC) for flat fading and Rake demodulator for frequency selective fading channels. The effect of different parameters such as transmitter and receiver antenna heights, propagation environment, operating frequency, distribution of the reflection coefficient and the distance between the mobile station and the scatterers are studied over the proposed model.

Keywords: *Fading Channels, Multipath Fading, Nakagami Distribution, Path Loss, Propagation, RAKE Receiver, Diversity, Distance.*

King Fahd University of Petroleum and Minerals, Dhahran.
April 2006

خلاصة الرسالة

الأسم : محمد عمران اعظم

عنوان الرسالة: اثر تغير مقدار Nakagami-*m* على اداء انظمة الاتصالات الرقمية

الدرجة الممنوحة: ماجستير في العلوم

حقل التخصص: الهندسة الكهربائية

تاريخ منح الدرجة: ابريل 2006م

لقد تمت دراسة تاثيرتغير المسافة بين النقال و المحطة الثابتة على المقدار Nakagami-*m*. لهذا الغرض تم تطوير نموذج لمسار الفقد و الذي يجد القوة المباشرة و المتشتتة عند المحطة الثابتة. و تم تقديم تاثير هذا الاخير على Nakagami-*m* لمختلف توزيعات معامل الانعكاس Γ . لقد وجد بان التوزيع الاسي يعطي قيم اكبر ل m بالمقارنة مع التوزيع الخطي و النصف Gaussian . التغير في تردد الموجة العاملة يؤثر ايضا على وصلة الاتصالات الرقمية. لقد تم استحداث مقدار جديد Δm لاجل دراسة تغير اداء النظام مع ازدياد المسافة. لقد تم ايضا ملاحظة ان ارتفاع هوائي المرسل و المستقبل يؤثر على Nakagami-*m* و أي ارتفاع في قيمته الفعلية تحسن من اداء النظام. لقد تمت دراسة تدهور الاداء عند مسافات اكبر و قيم اصغر لقيم المقدار Nakagami-*m* و لقد تم تحسين نسب الخطا باستعمال ملتقط EGC لقنوات الفقد المسطح و ملتقط Rake لقنوات الفقد الترددي الانتقائي. لقد تم ايضا دراسة تاثير مقادير مختلفة كارتفاع هوائيات المرسل و المستقبل, محيط الانتشار, تردد الموجة العاملة, توزيعات معامل الانعكاس و المسافة بين الملتقط و المشتتات على النموذج المقترح.

مفردات: القنوات الفقدية, الفقد المتعدد المسارات, توزيع Nakagami, *مسار الفقد, الانتشار, ملتقط* RAKE, *التنوع, المسافة.*

درجة الماجستير في العلوم

جامعة الملك فهد للبترول و المعادن
ابريل 2006م

Chapter 1

Introduction

1.1 Background and Motivation

In a typical mobile communication scenario, the downtown areas of the big cities with tall buildings obstruct the line of sight propagation between transmitter (Tx) and receiver (Rx). In microcells, cell radius is reduced and base station antenna height is lowered below the surrounding high rise buildings. Signal from T_x to R_x is known to propagates via multipaths and the received signal experiences temporal and spatial fading. The multipaths consist of line of sight (LOS), ground reflected, wall refelected and edge diffracted signal components. The small area fading statstics has been reported both as Rayleigh and Rician depending upon the absence and presence of LOS component, respectively. The wider area statistics are reported to be lognormally distributed.

Signal multipath occurs when the transmitted signal arrives at the receiver via multiple propagation paths. Each of these paths may have a separate phase, attenuation, delay and doppler frequency associated with it. Due to the random phase shift associated with each received signal, the multipath components add up constructively or destructively, resulting in a phenomenon called Fading. In personal wireless communications, the radio channel is described as a multipath propagation channel where the mobile station can be standing still or moving. At both the base station and the mobile station, the received signal is a summation of multiple radio waves arriving from different directions and with different magnitudes and phases. Besides Line of Sight (LOS) propagation from transmitter to receiver, the propagation of radio waves is generally described with three basic mechanisms; these are reflection, diffraction and scattering [1] and will be discussed in detail in chapter 2.

Path loss is a large-scale signal condition, which varies with the distance between transmitter and receiver. The path loss between the mobile unit and the base station antenna is usually modeled by a dual-slope curve [2], where the received power is attenuated by $d^{-a}\,(a \approx 2)$ at distances shorter than a turning point, and $d^{-(a+b)}\,(b \approx 2)$ beyond it. The turning point is determined by transmitting and receiving antenna heights, and the operating frequency [3].

Due to the statistical fluctuations of the various phenomena involving mobile radio propagation, the mobile radio signal cannot be treated only by deterministic methods. Accordingly, a great number of distributions exist that well describe the

statistics of the mobile radio signal [4]. Among them the Nakagami-m distribution has been given a special attention for its ease of analytical manipulation and wide range of applicability. Several distributions describe the envelope of the received signal in a mobile environment:

- Lognormal distribution due to shadowing;
- Rayleigh distribution due to multipath propagation;
- Ricean distribution due to multipath propagation with a line-of-sight component;
- Suzuki distribution that combines shadowing and multipath propagation;
- Nakagami distribution, which is a more general distribution that is used to better characterize the rapid fading. Nakagami distribution emulates most of the models given above.

1.2 Thesis Objectives

In this study, we will evaluate the Nakagami-m parameter under changing multipath environment conditions. The effect of varying distances between the transmitter and the receiver on the Nakagami-m parameter at different operating frequencies will be studied. We will develop a channel model that relates the distance between the mobile station and the base station with changing values of m. It is obvious that we

will experience higher values of m closer to the base station and as we move away from the base station, the value of m starts decreasing. Other parameters considered will include the transmitter and receiver antenna heights, the distribution of the reflection co-efficient, the distance between the scatterers and the mobile station, and the distance between the scatterers and the base station.

Once, the channel model is developed that gives us the variability of Nakagami-m parameter with distance, its performance will be studied over different modulation schemes for changing channel conditions. We will consider MPSK (QPSK and 8PSK) and 16QAM modulation schemes for Flat Fading Nakagami-m channels with and without diversity combining and Frequency Selective Nakagami-m channels with Rake reception.

1.3 Thesis Contributions

A path loss model is developed that finds out the received direct and scattered powers at the mobile station. The effect of varying distances between the mobile station and base station on the Nakagami-m parameter is studied. It is found that the Nakagami-m parameter decays at a faster rate for shorter distances than that over larger distances. The effect on the Nakagami-m parameter for different distributions of the reflection co-efficient Γ is studied. It is found that the exponential distribution gives larger values of m as compared to uniform and half Gaussian distribution. Change

in the operating frequency also effects the performance of a digital communication link. It is observed that for shorter distances, operating at higher frequency gives better error rate performance but as we move away from the base station, at larger macrocell distances, the received power and the path loss becomes independent of the frequency thereby providing no considerable improvement. A new parameter Δm is also introduced in order to study the change in performance behavior of the system with incresae in distance. The degraded performance of MPSK system at larger distances for smaller values of Nakagami-m parameter is studied and the error rates are improved by using Rake demodulator at the receiver. It is observed that the transmitter and receiver antenna heights also effects the Nakagami-m parameter and an increase in their effective values enhance the performance of the system.

1.4 Thesis Organisation

The Thesis is organized as follows: Chapter 2 discusses the path loss model and presents the mathematical modeling of the proposed model. Chapter 3 gives explanation on the general features of a multipath fading channel. This chapter also describes the different diversity combining techniques employed to combat fading in flat fading environment and provides an introduction to the Rake receiver to mitigate the Intersymbol Interference (ISI) induced in slow frequency selective multipath fading channels. Chapter 4 provides a detailed discussion on the simulation

results and elaborate the important findings. Finally, chapter 5 concludes the thesis by summarizing important conclusions and contributions and suggesting future avenues of research arising from the work.

Chapter 2

Path Loss Model

2.1 Radio wave propagation

The modes in which electromagnetic wave propagate are diverse; these can generally be attributed to reflection, diffraction, and scattering. Due to multiple reflections from various objects, the electromagnetic waves travel along different paths of varying lengths. The interactions between these waves cause multipath fading at a specific location, and the strength of the waves decrease as the distance between the transmitter and receiver increases.

Propagation models that predict the mean signal strength for an arbitrary transmitter receiver (T-R) seperation distance are useful in estimating the radio coverage area of a transmitter and are called large-scale propagation models, since these characterize signal strength over large T-R seperation distances (several hundredrs or

thousands of meters). On the other hand, propagation models that characterize the rapid fluctuations of the received signal strength over very short travel distances (a few wavelengths) or short time durations (on the order of seconds) are called small-scale fading models.

As a mobile moves over small distances, the instantaneous received signal strength fluctuates rapidly giving rise to small scale fading. The reason for this is that the received signal is a sum of many contributions coming from different directions. Since the phases are random, the sum of the contributions vary widely. As the mobile moves from the transmitter over larger distances, the local average received signal gradually decreases, and it is the local average signal level that is predicted by large-scale propagation models. The local average signal varies with log-normal statistics (shadowing).

2.2 Path loss models

In the analysis of radio wave propagation for mobile communication, one of the major parameters of interest is propagation-path loss. A measure of propagation-path loss is the difference between the effective power transmitted and the average received signal power. The received signal is an indication of the relative signal amplitude at the transmitted carrier frequency. The field strength (in V/m) recorded at the location of a moving mobile receiver fluctuates as a result of the effects of various

multipath phenomena.

General features of the terrain over which signal propagates are roughness and scatterers, tend to defocus the energy reaching the mobile receiver, and these also contribute to the overall path loss. The more substantial differences in terrain and the unique properties of individual scatterers can cause the path losses to be somewhat different in each area [5].

In mobile radio communications, the base station is normally fixed while the mobile subscriber's terminal is free to travel. Therefore, a significant amount of the propagation-path loss is directly related to the general area in which the mobile unit is travelling. This establishes a set of variables for propagation-path loss that are different from those associated with radio communication between two fixed terminal locations, where the elements that cause signal fading are more predictable. Consequently, in mobile radio situations, a more dynamic range of field strength variations is expected at the mobile receiving location. The propagation-path loss characteristics that are attributable to the travelling mobile unit can be classified according to the different general areas in which they occur.

2.2.1 Free space propagation model

The free space propagation model is used to predict received signal strength when the transmitter and receiver have a clear, unobstructed line-of-sight path between them. Satellite communication systems and microwave line-of-sight radio links typically

rely free space propagation. The free space model predicts that the received power decays as a function of the T-R seperation distance raised to power (i.e. a square law function) two. The free space power received by a receiver antenna which is seperated from a radiating transmitter antenna by a distance d, is given by the Friis free space equation,

$$P_r(d) = \frac{P_t G_t G_r \lambda^2}{(4\pi)^2 d^2 L} \tag{2.1}$$

where $P_r(d)$ is the received power which is a function of the T-R seperation, P_t is the transmitted power, G_t is the transmitter antenna gain, G_r is the receiver antenna gain, d is the T-R seperation distance in meters, L is the system loss factor not related to propagation and λ is the wavelength in meters. The gain of the antenna is related to its effective aperture, A_e, by

$$G = \frac{4\pi A_e}{\lambda^2} \tag{2.2}$$

The effective aperture A_e is related to the physical size of the antenna, and λ is related to the carrier frequency by

$$\lambda = \frac{c}{f} = \frac{2\pi c}{\omega_c} \tag{2.3}$$

where f is the carrier frequency in Hertz, ω_c is the carrier frequency in radians per second, and c is the speed of light given in meters/second. The values of P_t and P_r must be expressed in the same units, while G_t and G_r are dimensionless quantities.

The Friis free space equation (eq. 2.1) shows that the received power falls off as the square of the T-R seperation distance. This implies that the received power decays with distance at a rate of 20 dB/decade.

The path loss, which represents signal attenuation as a positive quantity measured in dB, is defined as the difference (in dB) between the effective transmitted power and the received power, and may or may not include the effect of the antenna gains. The path loss for the free space model when antenna gains are included is given by

$$P_L(dB) = 10log\frac{P_t}{P_r} = -10log\left(\frac{G_tG_r\lambda^2}{(4\pi)^2d^2}\right) \tag{2.4}$$

When antenna gains are excluded, that is when the antennas are assumed to have unity gain, the path loss is given by

$$P_L(dB) = 10log\frac{P_t}{P_r} = -10log\left(\frac{\lambda^2}{(4\pi)^2d^2}\right) \tag{2.5}$$

Large-scale propagation models use a close-in distance d_o, as a known received power reference point. The received power, $P_r(d)$ at any distance $d > d_o$, may be related to P_r at d_o. The value $P_r(d_o)$ may be predicted from equation (2.1) or may be measured in the radio environment by taking the average received power at many points located at a close-in radial distance d_o from the transmitter. Thus, using equation (2.1), the received power in free space at a distance greater than d_o is

given by

$$P_r(d) = P_r(d_o)\left(\frac{d_o}{d}\right)^2 \tag{2.6}$$

In mobile radio systems, it is not uncommon to find that P_r changes by many orders of magnitude over a typical coverage area of several square kilometers. Because of the large dynamic range of received power levels, often dBm or dBW units are used to express received power levels. Equation (2.6) may be expressed in units of dBm as,

$$P_r(d)(dBm) = 10log\left(\frac{P_r(d_o)}{0.001W}\right) + 20log\left(\frac{d_o}{d}\right) \tag{2.7}$$

where $P_r(d_o)$ is in watts.

The reference distance d_o for practical systems using low gain antennas in the 1-2 GHz region is typically chosen to be $1m$ in indoor environments and $100m$ or $1km$ in outdoor environments [1], so that the numerator in equations (2.6) and (2.7) is a multiple of 10. This makes path loss computations easy in dB units.

2.2.2 Ground reflection (two-ray) model

In a mobile radio channel, a single direct path between the base station and a mobile is seldom the only propagation mode, and hence the free space propagation model of equation (2.4) is in most cases inaccurate when used alone. The two-ray ground reflection model is a useful propagation model that is based on geometric optics, and considers both a direct path and a ground reflected propagation path

between transmitter and receiver. This model is found to be reasonably accurate for predicting the large-scale signal strength over distances of several kilometers for mobile radio systems that use tall towers as well as for line-of-sight microcell channels in urban environments [6]. In most mobile communication systems, the

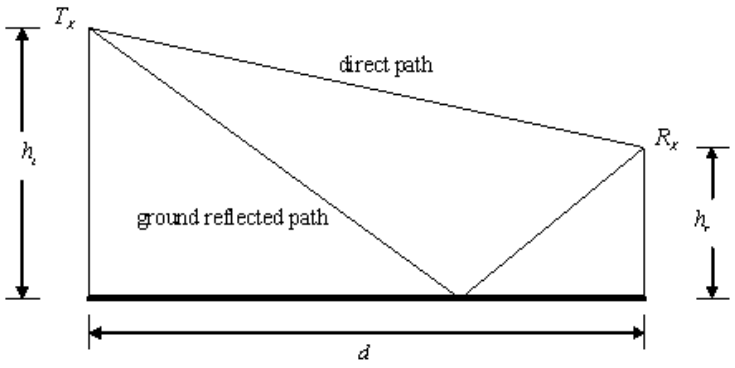

Figure 2.1: Two-ray ground reflection model

maximum T-R seperation distance is at most only a few tens of kilometers, and the earth may be assumed to be flat. Therefore, the received power at the receiver is due to the direct line-of-sight component and the ground reflected component. From [1], the received power at a distance d from the transmitter for the two-ray ground bounce model can be expressed as

$$P_r = P_t G_t G_r \frac{h_t^2 h_r^2}{d^4} \tag{2.8}$$

where, h_t is the transmitter antenna height and h_r is the receiver antenna height. As seen from equation (2.8), at large distances ($d >> \sqrt{h_t h_r}$), the received power falls off with distance raised to the fourth power, or at a rate of 40 dB/decade. This

is a much more rapid path loss than is experienced in free space. The path loss for the two ray model can be expressed in dB as [1],

$$P_L(dB) = 40logd - (10logG_t + 10logG_r + 20logh_t + 20logh_r) \tag{2.9}$$

2.3 Multipath propagation

Signal multipath occurs when the transmitted signal arrives at the receiver via multiple propagation paths. Each of these paths may have a separate phase, attenuation, delay and doppler frequency associated with it. Due to the random phase shift associated with each received signal, these paths add up constructively or destructively, resulting in a phenomenon called Fading.

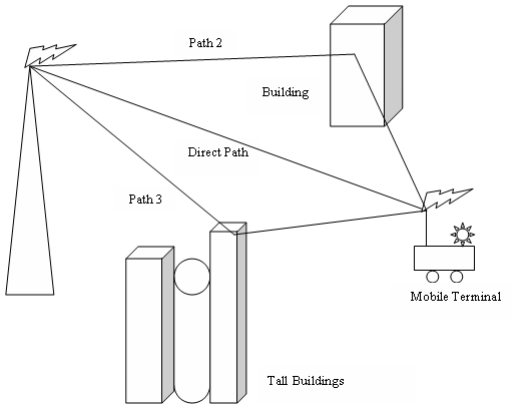

Figure 2.2: Illustration of a Multipath channel in an urban environment.

The propagation of radio waves is generally described with three basic mechanisms; these are reflection, diffraction and scattering [1]. These mechanisms are

illustrated in Fig. (2.3) as (1)reflection, (2)scattering, (3)diffraction, (4)transmission and (5)penetration into a building.

2.3.1 Reflection

Reflection occurs when a propagating electromagnetic wave impinges upon an object of large dimensions when compared to that of incident signal wavelength. Reflections from the surface of the earth and from buildings or walls produce reflected waves, which may interfere either constructively or destructively at the receiver.

When a radio wave propagating in one medium enters into another medium with different electrical, dielectric and conductive properties, the wave is partially reflected, transmitted, and absorbed. If the plane wave is incident on a perfect dielectric, part of the energy is transmitted into the second medium and part of the energy is reflected back into the first medium, and there is no loss of energy due to absorption. The reflection depends on the ratio of the dielectric constant. If the second medium is a perfect conductor, then all the incident energy is reflected back into the first medium without loss. The electric field intensity of the reflected and transmitted waves is related to the incident wave in the medium of origin through the Fresnel reflection coefficient (Γ). The term reflection coefficient is used when wave propagation in a medium containing discontinuities is considered. In general, the reflection coefficient describes the amplitude of a reflected wave relative to an incident wave. The reflection coefficient is a function of the material properties, and

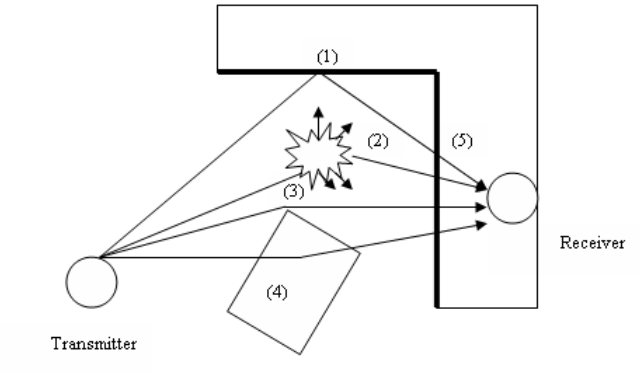

Figure 2.3: Representation of the propagation mechanisms

generally depends on the wave polarization, angle of incidence, and the frequency of the propagating wave.

2.3.2 Diffraction

Diffraction occurs when the radio path between the transmitter and receiver is obstructed by a surface that has sharp irregularities or edges. Diffraction allows radio signals to propagate around the curved surface of the earth, beyond the horizon, and may propagate around obstructions. Although the received field strength decreases rapidly as a receiver moves deeper into the obstructed (shadowed) region, the diffraction field still exists and often has sufficient strength to produce a useful signal.

If an ideal, straight, perfectly absorbing screen is interposed between T_x and R_x then when the top of the screen is well below the LOS path, it will have little effect and the field at R_x will be the 'free space' value. The field at R_x begin to oscillate

as the height is increased, hence blocking more of the Fresnel zones below the line-of-sight path. The amplitude of the oscillation increases until the obstructing edge is just in line with T_x and R_x. As the height is increased above this value, the oscillation ceases and the field strength decreases steadily.

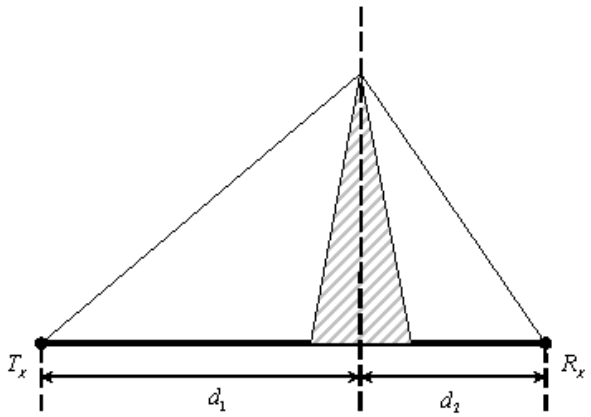

Figure 2.4: Illustration of knife-edge diffraction

2.3.3 Scattering

Scattering occurs when the radio path contain objects with dimensions that are small compared to the incident wavelength, and where the number of obstacles per unit volume is large. In a typical urban environment, lamp posts, street signs, foliage and rough surfaces scatter the transmitted radio signal in many directions, thereby providing RF coverage to locations which might not receive any signal via reflection or diffraction. Scattering, which follows the basic principles of diffraction

is the most difficult to predict due to its random nature. The actual received signal in a mobile radio environment is often stronger than what is predicted by reflection and diffraction models alone. This is because when a radio wave impinges on a rough surface, the reflected energy is spread out (diffused) in all directions due to scattering. Flat surfaces that have much larger dimension than a wavelength are modeled as reflective surfaces. However, the roughness of such surfaces often induces propagation effects different from the specular reflection described in section (2.3.1). For rough surfaces, the flat surface reflection coefficient needs to be multiplied by a scattering loss factor ρ_s, to account for the diminished reflected field.

$$\Gamma_{rough} = \rho_s \Gamma \tag{2.10}$$

The number of multipaths at the receiver are generally large, but the power content of each path would be different due to different physical lengths, caused by propagation mechanism of reflection, scattering and diffraction. The paths of larger lengths due to multiple reflections are quite weaker as compared to LOS path because of reflection and transmission losses and if these fall below the receiver noise threshold could be ignored [7].

It is shown in [8], [9] that a few paths are generally sufficient to describe path loss and statstics of microcellular mobile radio channel, namely, i) LOS, ii) ground reflected, iii) primary and secondary buildings reflected. However it is observed in [7] that inclusion of more paths, e.g. edge diffracted, will be useful to enhance the

details of the received signal envelope and consequently the envelope statistics.

2.4 Proposed Model

For simulation purposes, we used equation (2.8) for the calculation of direct power at different distances, d. G_t and G_r are assumed to be 1. The transmitted power is 10 W (10 dBW). The cellular region is divided into two parts based on the distance measure.

- *Microcell* - Distance between 100 m and 1 km (with intervals of 100 m).
- *Macrocell* - Distance between 1 km and 10 km (with intervals of 1 km).

2.4.1 Analytical formulation

Usually a propagation path extends over more than one type of terrain features. Refering to figure (2.5), assuming a transmitter T_x and a receiver R_x seperated by a distance d and the propagation path extends over two different types of terrain with α_1 be the propagation path loss slope in terrain type 1 and α_2 be the propagation path slope in terrain type 2. We define d_1 as the distance between the base station T_x and the scatterer and distance d_2 between the mobile station R_x and the scatterer. P_t is termed as the transmitted power at the base station T_x, P_{r_1} as the received power at the scatterer, P_{t_1} as the trasmitted power at the scatterer and P_r as the

received power at the mobile station R_x. P_{L_1} is the path loss for terrain type 1 and P_{L_2} is the path loss for terrain type 2.

Therefore the received power at the mobile station R_x can be expressed as,

$$P_{r_s} = \frac{P_{t_1}}{P_{L_2}}$$

where,

$$P_{t_1} = \Gamma P_{r_1}$$

and,

$$P_{r_1} = \frac{P_t}{P_{L_1}} \tag{2.11}$$

Therefore, the received scattered power will be,

$$P_{r_s} = \frac{\Gamma \frac{P_t}{P_{L_1}}}{P_{L_2}} \tag{2.12}$$

where, Γ is the reflection coefficient.

P_{L_1} over terrain type 1 and P_{L_2} over terrain type 2 can be expressed as

$$P_{L_1} = \left(\frac{4\pi}{\lambda}\right)^2 d_1^{\alpha_1} \tag{2.13}$$

and,

$$P_{L_2} = \left(\frac{4\pi}{\lambda}\right)^2 d_2^{\alpha_2} \left(\frac{1}{d_1}\right)^{\alpha_2 - \alpha_1} \tag{2.14}$$

where, $\left(\frac{4\pi}{\lambda}\right)^2$ is the aperture area of the antenna and is independent of distance.

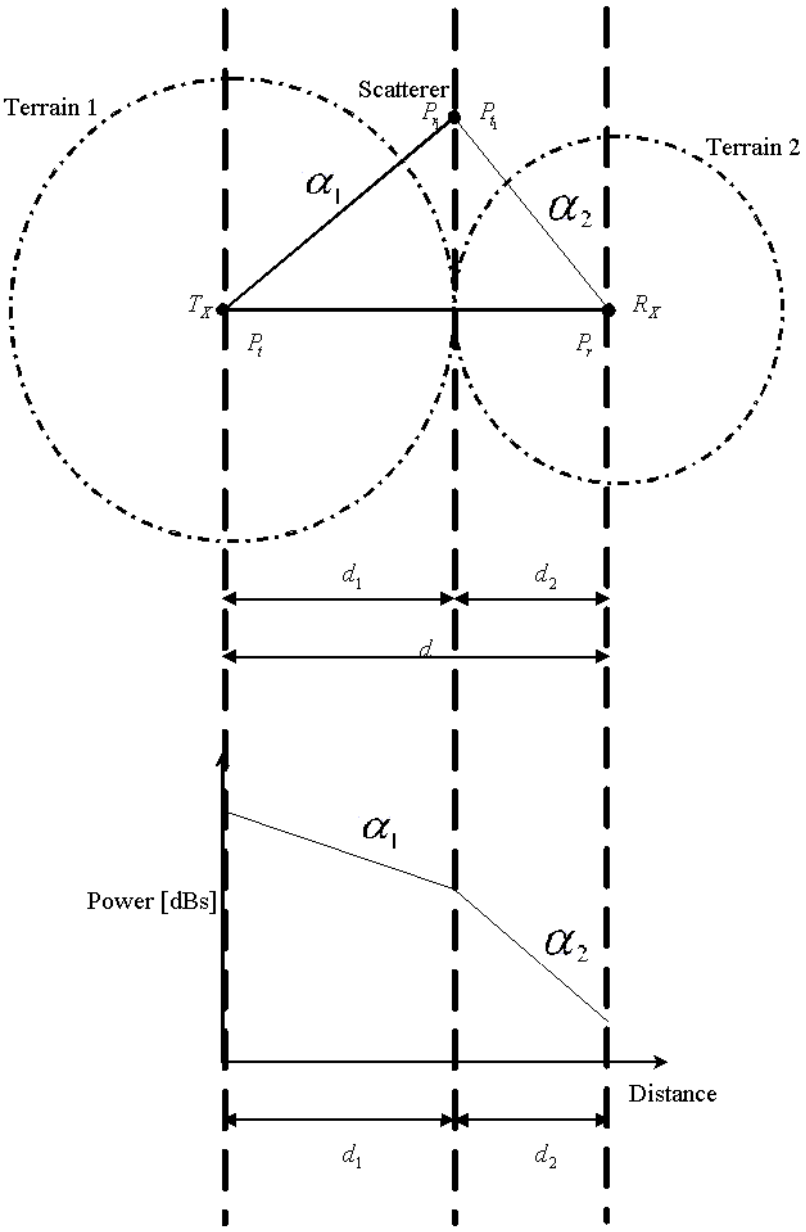

Figure 2.5: Illustration of proposed model

Therefore, equation (2.12) becomes

$$P_{r_s} = \frac{\Gamma \frac{P_t}{\left(\frac{4\pi}{\lambda}\right)^2 d_1^{\alpha_1}}}{\left(\frac{4\pi}{\lambda}\right)^2 d_2^{\alpha_2} \left(\frac{1}{d_1}\right)^{\alpha_2 - \alpha_1}} \tag{2.15}$$

$$P_{r_s} = \frac{\Gamma P_t}{\left(\frac{4\pi}{\lambda}\right)^2 \left(\frac{4\pi}{\lambda}\right)^2 d_1^{\alpha_1} d_2^{\alpha_2} \left(\frac{1}{d_1}\right)^{\alpha_2 - \alpha_1}} \tag{2.16}$$

$$P_{r_s} = \frac{\Gamma P_t}{\left(\frac{4\pi}{\lambda}\right)^4 d_2^{\alpha_2} d_1^{2\alpha_1 - \alpha_2}} \tag{2.17}$$

$$P_{r_s} = \Gamma P_t \left(\frac{\lambda}{4\pi}\right)^4 d_2^{-\alpha_2} d_1^{\alpha_2 - 2\alpha_1} \tag{2.18}$$

Since, the Rician factor K is defined as the ratio of the direct (line-of-sight) power to the received scattered power, thus using equation (2.8) and (2.18), we can say that

$$K = \frac{P_t \frac{h_t^2 h_r^2}{d^4}}{\Gamma P_t \left(\frac{\lambda}{4\pi}\right)^4 d_2^{-\alpha_2} d_1^{\alpha_2 - 2\alpha_1}} \tag{2.19}$$

$$K = \frac{\left(h_t h_r\right)^2}{\Gamma \left(\frac{\lambda}{4\pi}\right)^4 d^4 d_2^{-\alpha_2} d_1^{\alpha_2 - 2\alpha_1}} \tag{2.20}$$

In a situation, when there is a dominant stationary (nonfading) signal component present, such as a line-of-sight propagation path, the small-scale fading envelope distribution is Ricean. Random multipath components arriving at different angles are superimposed on a stationary dominant signal. At the output of an envelope detector, this has the effect of adding a dc component to the random multipath. As

the dominant signal becomes weaker, the composite signal resembles a noise signal which has an envelope that is Rayleigh. Thus the Ricean distribution degenerates to a Rayleigh distribution when the dominant component fades away.

It is observed from equation (2.20), that the Ricean factor depends on the following parameters.

- h_t - height of the transmitting antenna.
- h_r - height of the receiving antenna.
- Γ - reflection coefficient.
- d - distance between T_x and R_x.
- d_1 - distance between T_x and scatterer.
- d_2 - distance between R_x and scatterer.
- α_1 - propagation path loss slope for terrain type 1.
- α_2 - propagation path loss slope for terrain type 2.

The effect of these parameters is studied through simulations.

2.4.2 Relationship between K and m

The Ricean factor K and the Nakagami parameter m are related to each other as [10];

$$K = \frac{\sqrt{m^2 - m}}{m - \sqrt{m^2 - m}} \tag{2.21}$$

Factorizing,

$$\begin{aligned} K &= \frac{\sqrt{m^2 - m}}{m - \sqrt{m^2 - m}} \frac{m + \sqrt{m^2 - m}}{m + \sqrt{m^2 - m}} \\ &= \frac{\left(m\sqrt{m^2 - m}\right) + (m^2 - m)}{m^2 - m^2 + m} \\ &= \frac{m\left(\sqrt{m^2 - m} + m - 1\right)}{m} \\ K &= \sqrt{m^2 - m} + m - 1 \\ K + 1 - m &= \sqrt{m^2 - m} \\ K - (m - 1) &= \sqrt{m^2 - m} \end{aligned}$$

Squaring both sides

$$(K-(m-1))^2 = \left(\sqrt{m^2-m}\right)^2$$

$$K^2 + (m-1)^2 - 2K(m-1) = m^2 - m$$

$$K^2 + m^2 + 1 - 2m - 2Km + 2K = m^2 - m$$

$$K^2 + 2K + 1 = 2m + 2Km - m$$

$$(K+1)^2 = m(2+2K-1)$$

$$(K+1)^2 = m(2K+1)$$

$$m = \frac{(K+1)^2}{2K+1} \tag{2.22}$$

Chapter 3

Disruptive Properties of Mobile Radio Channel

Radio channel is the link between the transmitter and the receiver that carries information bearing signal in the form of electromagnetic waves. The radio channel is commonly characterized by scatterers discussed in section (2.3.3) and reflectors discussed in section (2.3.1).

Mobile radio links often require communication between fixed base stations and mobile transceivers. The channel will be non-stationay in this case. However, characterization of mobile radio channel proves extremely difficult unless stationarity is assumed over short intervals of time. In order to obtain a fairly complete statistical description of the channel, a two-stage characterization is proposed [11]. Firstly, the channel is charaterized over a period of time, or a geographical area, which is

small as compared to the period of the slow channel variations, so that the mean received signal strength appears virtually constant. It is further assumed that in this small interval, the prominent features of the environment remain unchanged. The large-scale behavior of the channel is then obtained by examining the behavior of the small-scale statistics over large areas. A further simplification in the characterization of mobile radio channels is done by assuming that contributions from scatterers with different path delays are uncorrelated. Then the channel is described in terms of *wide-sense stationary uncorrelated scattering (WSSUS)* statistics. This two-stage model was first proposed by Bello [12], and was subsequently used by Cox [13].

3.1 Modeling of Mobile Radio Channels

In last few decades, modeling and characterization of fading channels gained considerable interest. Over many years, a large number of experiments are carried out to investigate fading channels. Earlier work in this area includes the contributions of Bello [12], Clarke [14] and Jakes [15].

3.1.1 Narrowband Modeling

In narrowband modeling the fluctuations of the received signal envelope and phase over time and space are characterized. A radio wave traveling through a certain

environment attenuates due to the above-mentioned mechanisms and free space loss. These effects are characterized as a superposition of path loss, large-scale fading and small-scale fading. The concepts of large and small-scale refer to the dimensions of the area studied. Large-scale effects are noticed over longer distances while small-scale effects are noticed over smaller distances (a few wavelengths).

In the case of the MS movements in a small local area, it is reasonable to assume that the compositions of the impinging radio waves will not change, but only the phases of these radio waves. These changes of phase cause rapid fluctuations in the received signal called small-scale or fast fading. Also, proportional to the speed of movement of the MS, the multipath components experience an apparent shift in frequency called doppler shifts. Even when the MS is stationary, the received signal experiences fast fading due to the movement of objects in the surroundings.

When the MS moves over larger areas, the composition of waves change. Existing components are obstructed while new ones arise and relative directions and distances to scatterers also change. The fluctuations resulting from movements over wider areas are called large-scale fading, slow fading or shadowing. The path loss is determined from the average received signal and depends on the distance between transmitter and receiver and the environment characteristics.

3.1.2 Wideband Modeling

Due to multipath propagation the radio channel is time-dispersive. This means that the channel impulse response is not a single echo, but a sequence of pulses spread in time and space. If the time of arrival between the first and last significant echoes is much smaller than the duration of a digital symbol, then the system is defined to be a narrowband system. However, if this is not the case, the time dispersion of the channel have an effect on the shape of the received signal. In such a case the system is defined as a wideband system.

Thus, the statement whether a system is narrowband or wideband, depends on both the duration of a symbol and the channel characteristics.

In wideband characterization, the impulse response is often used to describe the channel. From the impulse response (power delay profile), a number of parameters are extracted to characterize the time dispersion of the channel. These are the mean excess delay, rms delay spread, maximum excess delay and coherence bandwidth [1].

Assuming a low-pass equivalent model for the channel, the received signal $r(t)$ over a fading multipath channel can be represented by [16],

$$r(t) = \int_{-\infty}^{+\infty} h(\tau, t)s(t-\tau)d\tau \tag{3.1}$$

where $s(t)$ is the transmitted signal and $h(\tau, t)$ is the channel impulse response at delay τ and time instant t. In discrete form,

$$r(n) = \sum_{i=-\infty}^{\infty} h(iT_s, n)s(n-iT_s) \tag{3.2}$$

where T_s is the symbol duration and n represents the sampling index. Defining a compact notation for the time varying channel coefficients in the form,

$$h_i(n) = h(iT_s, n)$$

Equation (3.2) can be written as

$$r(n) = \sum_{i=-\infty}^{\infty} h_i(n)s(n - iT_s) \tag{3.3}$$

The form of received signal in Equation (3.3) suggests that the impulse response of fading multipath channel is modeled as a tapped delay line filter, a finite impulse response filter, with tap spacing T_s and time varying coefficients $h_i(n)$. The time varying coefficients are characterized as random processes because of the constantly changing physical characteristics of the channel. The tap weights, $h_i(n)$, can be expressed as,

$$h_i(n) = \sqrt{\rho_i}G_i(n) \tag{3.4}$$

where ρ_i is the strength of the ith path and $G_i(n)$ is the complex stochastic process specified by its mean square value and power spectrum density.

3.2 Parameters of Mobile Multipath Channels

In an ideal radio channel, the received signal consists of only a single direct path signal, which is a perfect reconstruction of the transmitted signal. However, in a

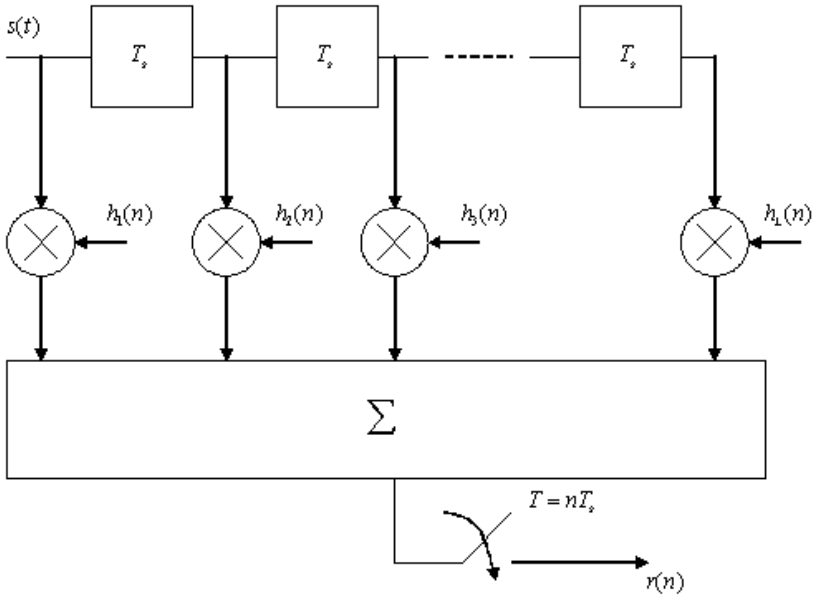

Figure 3.1: Tapped delay line model

real channel, the signal is modified during transmission. The received signal consists of a combination of attenuated, reflected, refracted, and diffracted replicas of the transmitted signal. On top of all this, the channel adds noise to the signal. Understanding of these effects on the signal is important because the performance of a radio system is dependent on the radio channel characteristics.

A radio channel can be either *static* or *dynamic*. In a *static channel*, the transmitter, the receiver and all objects in the environment are standing still. In a *dynamic channel*, at least one of them is moving. First, we will discuss briefly that what will happen to the amplitude, phase and the time of arrival when a continuous wave is transmitted in a static channel.

3.2.1 Amplitude fading

The received amplitude is of interest since it is directly related to the received power and the received power has influence on the average bit error rate. Amplitude fading is the decrease of the amplitude of a continuous wave. This decrease is caused by numerous effects, such as the distance between the transmitter and receiver, the objects between them and interference with other waves. There are quite a few models that try to describe that fading. Some of those models are deterministic models which will predict the average received power at a certain distance from the receiver. However, the actual received power at a certain point can be very different compared to that prediction. This difference is caused by countless factors

and cannot easily be taken into account in a deterministic model. Therefore, it is better to treat the signal as a random process that gives signal strengths with certain probabilities and to analyze that process on a statistical basis.

3.2.2 Time dispersion parameters

The time of arrival of a pulse depends on the distance that the pulse has to travel between transmitter and receiver, and on the objects that it has to penetrate on its path. A reflection against an object causes a longer path length and therefore a longer delay. A penetration also causes a longer delay, since the velocity of the pulse inside the object is less than the velocity of the pulse in vacuum (which is c, the speed of light). The amount of reflections and penetrations are unknown and therefore, a deterministic approach for the time of arrival is not possible, and the time of arrival has to be analyzed statistically. The time of arrival of the i^{th} received pulse is modeled as,

$$t_i = t_0 + \tau_i \tag{3.5}$$

where t_0 is the delay of the first pulse and τ_i is the excess delay for that pulse (which is the extra time it takes for a pulse to arrive compared to the pulse that arrived first; hence, $(\tau_0 = 0)$.

The mean excess delay, rms delay spread, and excess delay spread are multipath channel parameters that can be determined from a power delay profile. The time

dispersive properties of wideband multipath channels are most commonly quantified by their mean excess delay $\overline{\tau}$ and rms delay spread σ_τ. The mean excess delay is the first moment of the power delay profile. The rms delay spread is the square root of the second central moment of the power delay profile and is defined to be,

$$\sigma_\tau = \sqrt{\overline{\tau^2} - (\overline{\tau})^2} \tag{3.6}$$

The received radio signal from a transmitter consists of a direct signal plus signals reflected off objects such as buildings, mountains, and other structures. The reflected signals arrive at a later time than the direct signal because of the extra path length, giving rise to a slightly different arrival time of the transmitted pulse. The signal energy confined to a narrow pulse is spreading over a longer time. Delay spread is a measure of how the signal power is spread over the time between the arrival of the first and last multipath signal seen by the receiver.

In a digital system, the delay spread leads to inter-symbol interference. This is due to the delayed multipath signal overlapping symbols that follows. This causes significant errors in high bit rate systems. As the transmitted bit rate is increased the amount of inter-symbol interference also increases. The effect starts to become very significant when the delay spread is greater then 50% of the bit time.

3.2.3 Coherence Bandwidth

The coherence bandwidth B_c of a channel is derived from the rms delay spread. Coherence bandwidth is a stastical measure of the range of frequencies over which the channel can be considered "flat" (i.e. a channel which passes all spectral components with approximately equal gain and linear phase). In other words, it is the maximum bandwidth between two frequencies where the frequencies within that band have a sufficiently large amplitude correlation. Thus, the channel effects all of those frequencies in the same way with respect to the amplitude and one can think of the channel as a filter with bandwidth B_c. Although the meaning of B_c given above is generally accepted, there are a few different formulas to compute B_c [1]:

$$B_c = \frac{1}{50\sigma_\tau} \qquad \text{(for correlation higher than 0.9)} \tag{3.7}$$

$$B_c = \frac{1}{5\sigma_\tau} \qquad \text{(for correlation higher than 0.5)} \tag{3.8}$$

3.2.4 Doppler Shifts

Doppler spread is a parameter that describes the time varying nature of the channel. When a signal source and/or a receiver are moving relative to one another, the frequency of the received signal is not the same as the source. When they are moving away, the frequency of the received signal is lower than the source, and when they are approaching each other the frequency increases. This is called the Doppler effect.

When a pure sinusoidal tone of frequency f_c is transmitted, the received signal spectrum, called the Doppler spectrum, will have components in the range $f_c - f_d$ to $f_c + f_d$, where f_d is the Doppler shift. The amount of spectral broadening depends on f_d which is the function of the relative velocity of the mobile, and the angle θ between the direction of motion of the mobile and direction of arrival of the scattered waves.

3.2.5 Coherence time and distance

Coherence distance d_c is the maximum distance over which two received signals have a strong potential for amplitude correlation. After moving the receiver more than d_c meters, one cannot expect that the channel is still the same, and perhaps a new pilot symbol should be transmitted to update the information about how the channel effects the transmitted symbols. The coherence distance is also important when one wants to design a radio system that uses multiple antennas to combat fading.

Coherence time T_c is closely related to coherence distance. Coherence time is the maximum time during which one can assume the channel to be static (and thus during which the coherence bandwidth doesn't change). If only the receiver (or only the transmitter) is moving with speed v and the channel is otherwise static, then

the relation between coherence distance d_c and coherence time T_c is simple.

$$T_c = \frac{d_c}{v} \tag{3.9}$$

For a pure Rayleigh fading channel, the coherence time is [1],

$$T_c \approx \frac{9}{16\pi f_m} \tag{3.10}$$

where $f_m = v/\lambda$ is the maximum doppler shift.

Fast fading channel

If the symbol time T_s is much larger than T_c, then the channel changes much faster than one symbol time and a transmitted symbol is deformed by the channel in an unknown way since the channel changes too fast. This is called a *fast fading channel*.

Slow fading channel

If the symbol time T_s is much smaller than T_c, most of the transmitted symbols are deformed in a known way and the receiver is able to reconstruct the transmitted symbols. This is known as a *slow fading channel*.

3.3 Fading Channels

Fading channels are typically produced by scattering or multipath processes, and are characterized by a randomly varying received signal amplitude and phase. For

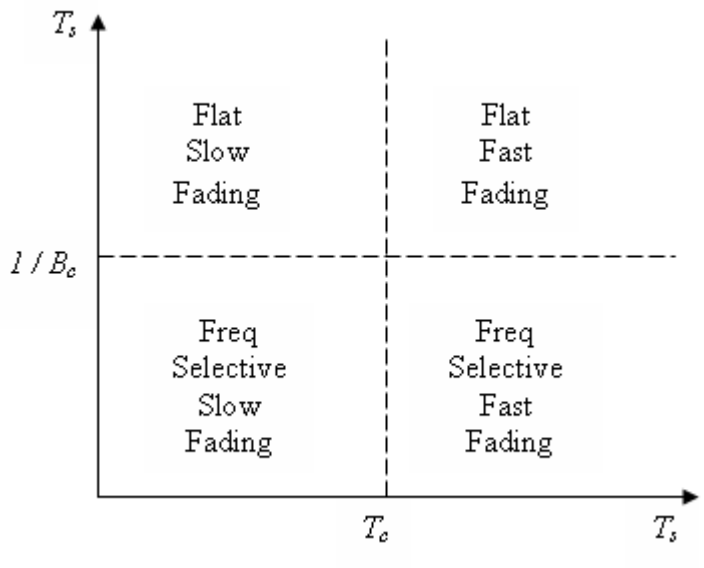

Figure 3.2: Effect of different parameters on the type of channel

coherent modulations, the fading effects on the phase can severely degrade performance unless measures are taken to compensate for them at the receiver. Most often, analyses of systems employing such modulations assume that the phase effects due to fading are perfectly corrected at the receiver resulting in what is referred to as "ideal" coherent demodulation. For non-coherent modulations, phase information is not needed at the receiver and therefore the phase variation due to fading does not affect the performance. Hence, performance analyses for both ideal coherent and non-coherent modulations over fading channels requires knowledge of only the fading envelope statstics [10].

3.3.1 Frequency-Flat and Frequency-Selective Fading

The fading process is considered frequency-nonselective or equivalently frequency-flat when the signal bandwidth is much smaller than the coherence bandwidth of the channel (that is, when all spectral components within the signal bandwidth are affected equally by the channel). When the received signal is comprised solely of uncorrelated scattered components, the fading process is described as Rayleigh. When a strong signal component is present in the received waveform, such as from a direct signal path or a fixed reflector in the medium, the fading process is described as Ricean.

3.3.2 Modeling of Flat Fading Channels

When fading effects narrowband systems, the received carrier amplitude is modulated by the fading amplitude α, where α is a RV (Mathematically, a random variable is defined as a measurable function from a probability space to some measurable space. This measurable space is the space of possible values of the variable, and it is usually taken to be the real numbers) with mean-square value $\Omega = \overline{\alpha^2}$ and probability density function (PDF) $p_\alpha(\alpha)$, which is dependent on the nature of the radio propagation environment. After passing through the fading channel, the signal is perturbed at the receiver by additive white Gaussian noise (AWGN), which is typically assumed to be statstically independent of the fading amplitude α, and which is

characterized by a one-sided power spectral density N_o Watts/Hertz. Equivalently, the received instantaneous signal power is modulated by α^2. Thus, we define the instantaneous signal-to-noise power ratio (SNR) per symbol by $\gamma = \alpha^2 E_s/N_o$ and the average SNR per symbol by $\overline{\gamma} = \Omega E_s/N_o$, where E_s is the energy per symbol. In addition the PDF of γ is obtained by introducing a change of variables in the expression for the fading PDF $p_\alpha(\alpha)$ of α, yielding [10],

$$p_\gamma(\gamma) = \frac{p_\alpha\left(\sqrt{\frac{\Omega\gamma}{\overline{\gamma}}}\right)}{2\sqrt{\frac{\gamma\overline{\gamma}}{\Omega}}} \tag{3.11}$$

The amount of fading (AF) or "fading figure", associated with the fading PDF is defined as,

$$AF = \frac{var\left[\alpha^2\right]}{\left(E\left[\alpha^2\right]\right)^2} = \frac{E\left[(\alpha^2-\Omega)^2\right]}{\Omega^2} = \frac{E\left[\gamma^2\right]-\left(E\left[\gamma\right]\right)^2}{\left(E\left[\gamma\right]\right)^2} \tag{3.12}$$

where $E\left[\cdot\right]$ statstical average and $var\left[\cdot\right]$ denotes variance.

3.3.3 Modeling of Frequency-Selective Fading Channels

When wideband signals propagate through a frequency-selective channel, their spectrum is affected by the channel transfer function, resulting in a time-dispersion of the waveform. This type of fading is modeled as a linear filter characterized by the following complex-valued lowpass equivalent impulse response [10],

$$h(t) = \sum_{l=1}^{L_p} \alpha_l e^{-j\theta_l} \delta\left(t-\tau_l\right) \tag{3.13}$$

where $\delta(\cdot)$ is the Dirac delta function, l is the channel index, and $\{\alpha_l\}_{l=1}^{L_p}$,$\{\theta_l\}_{l=1}^{L_p}$ and $\{\tau_l\}_{l=1}^{L_p}$ are the random channel amplitudes, phases and delays, respectively. In equation (3.13), L_p is the number of resolvable paths (the first path is the reference path whose delay $\tau_1 = 0$ and is related to the ratio of the maximum delay spread to the symbol time. Under the slow-fading assumption, L_p is assumed to be constant over a certain period of time, and $\{\alpha_l\}_{l=1}^{L_p}$, $\{\theta_l\}_{l=1}^{L_p}$ and $\{\tau_l\}_{l=1}^{L_p}$ are all constant over a symbol interval. Extending the flat fading notations, the fading amplitude α_l of the lth resolved path is assumed to be a RV whose mean-square value $\overline{\alpha_l^2}$ is denoted by Ωl and whose PDF p_{α_l} can be any one of the PDFs (Rayleigh, Rician, or Nakagami) discussed in the following section.

The first arriving path in the impulse response exhibits a lower amount of fading than do subsequent paths, since it contains the line of sight path [17, 18, 19]. Furthermore, since the specular power component decreases with respect to delay, the last arriving paths exhibit higher amounts of fading. The $\{\Omega_l\}_{l=1}^{L_p}$ are related to the channel's *power delay profile (PDP)*, which is also refered to as the *multipath intensity profile (MIP)* and that is typically the decreasing function of the delay. The PDP model can assume various forms depending on whether the model is designed for indoor or outdoor environments and, for each environment, the general propagation conditions. Experimental measurements indicate that the mobile radio channel is well characterized by an exponentially decaying PDP for indoor office

buildings [20] and conjested urban areas [21]:

$$\Omega_l = \Omega_l e^{-\tau_l/\tau_{max}}, \qquad l = 1, 2, , ..., L_p \tag{3.14}$$

where Ω_l is the average fading power corresponding to the first (reference) propagation path and τ_{max} is the channel maximum delay spread. Other idealized PDP profiles reported or used in the literature include the constant (flat) [22], the flat exponential [23], the double-spike [22], the Gaussian [22], the power function (polynomial) [24] and other more complicated composite profiles [25].

3.3.4 Multipath Fading

Multipath fading is due to the constructive and destructive combination of randomly delayed, reflected, scattered and diffracted signal components. This type of fading is relatively fast and is therefore responsible for the short-term signal variations. Depending on the nature of the radio propagation environment, there are different models describing the statstical behavior of the multipath fading envelope.

Rayleigh

The Rayleigh distribution is commonly used to model multipath fading when there is no direct line-of-sight signal component. In this case the channel fading amplitude α is distributed as,

$$f_\alpha(\alpha) = \frac{\alpha}{\sigma^2} \exp(-\frac{\alpha^2}{2\sigma^2}), \quad \alpha \geq 0 \tag{3.15}$$

where σ^2 is the variance of the fading amplitude. In general, the Rayleigh distribution is obtained for any quantity R given by,

$$R^2 = X^2 + Y^2$$

if X and Y are independent and both Gaussian (normal) with the same variance and zero mean. The instantaneous signal power, $\gamma = \alpha^2$ is distributed according to an exponential distribution given by,

$$f_\gamma(\gamma) = \frac{1}{\Omega} \exp(-\frac{\gamma}{\Omega}) \tag{3.16}$$

where we define,

$$\Omega = E[\alpha^2]$$

Rayleigh fading model agrees very well with experimental data for mobile radio channels where no line-of-sight (LOS) path exists between the transmitter and receiver antennas [26, 1], which is the case in urban areas.

Realization of Rayleigh fading in simulations

In this section, we describe the simulator that is used to simulate the channel. Basically, we need colored Gaussian noise to realize fading channel statistics which may be Rayleigh, Ricean or any other. These colored Gaussian processes can be generated either by filtering white Gaussian noise [14] or by deterministic methods [15] or by Monte Carlo approach [27].

Filtering method requires large number of filter taps to reshape the spectrum and it is based on Clarkes model. A deterministic method to simulate mobile fading channels is based on Rice's sum of sinusoids [15]. In this case, a colored Gaussian noise is approximated by a finite sum of sinusoids with proper weights and frequencies. Jakes also presented a realization for the simulation of fading channel model which generates real and imaginary parts of the channel taps coefficients as weighted sum of sinusoids. Jakes simulator has been widely used and extensively studied over the past three decades [26]. Recently, Pop and Beaulieu [28] have highlighted few shortcomings in the Jakes model. They propose to include a random phase in the low frequency oscillators of the Jakes model. We have implemented this modified Jakes model as fading channel simulator.

The real and imaginary parts of the channel taps are generated as [15]

$$g_I(t) = 2\sum_{n=1}^{N_0} \cos\beta_n \cos(\omega_n t + \phi_n) + \sqrt{2}\cos\alpha\cos(\omega_m t) \tag{3.17}$$

$$g_Q(t) = 2\sum_{n=1}^{N_0} \sin\beta_n \cos(\omega_n t + \phi_n) + \sqrt{2}\sin\alpha\cos(\omega_m t) \tag{3.18}$$

where

$$\beta_n = \frac{n\pi}{N_0 + 1} \qquad \omega_n = \omega_m \cos(\frac{2\pi n}{N}) \qquad N_0 = \frac{1}{2}(\frac{N}{2} - 1)$$

where $t = kT_s$ and $\phi_1, ..., \phi_{N_0}$ are uniformly distributed random variables over $[0, 2\pi]$. We have implemented the technique proposed by Jakes [15] and modified it according to model proposed by Beaulieu [28]. In this technique, the nth oscillator is given an additional phase shift $\gamma_{nl} + \beta_n$ while retaining gains. For lth path the in-phase

component of the fading can be written as:

$$g_\ell(t) = 2\sum_{n=1}^{N_0} \cos\beta_n \cos(\omega_n t + \phi_n + \theta_{nl}) + \sqrt{2}\cos\alpha\cos(\omega_m t) \tag{3.19}$$

where,

$$\theta_{nl} = \gamma_{nl} + \beta_n \qquad \beta_n = \frac{n\pi}{N_0 + 1} \qquad \gamma_{nl} = \frac{2\pi(\ell - 1)n}{N_0 + 1}$$

The quadrature component can be modified in the same manner. The normalized complex channel tap for lth path is,

$$G_\ell(t) = g_\ell^I(t) + jg_\ell^Q(t) \tag{3.20}$$

which will be normalized such that $E[G_\ell G_\ell^*] = 1$.

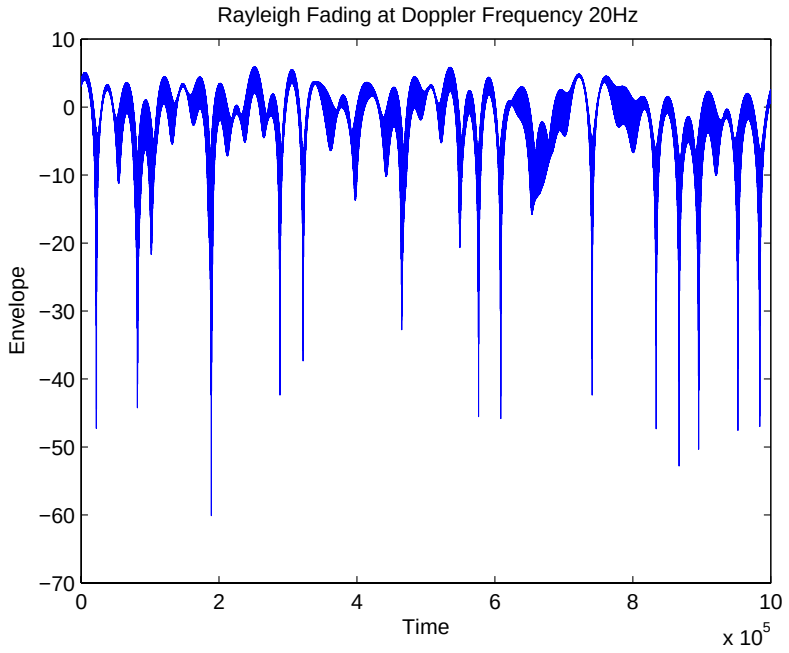

Figure 3.3: Envelope of simulated Rayleigh faiding process

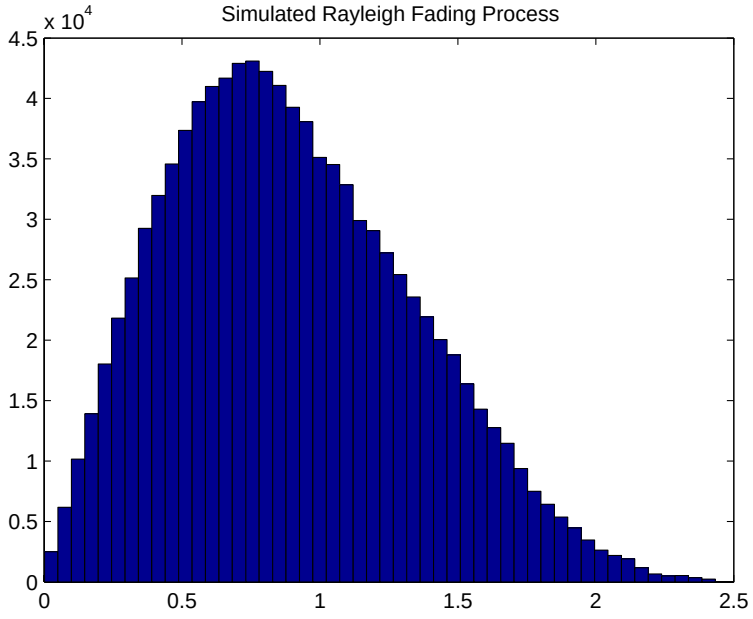

Figure 3.4: Histogram of simulated Rayleigh fading process

Nakagami-m

The Nakagami m distribution is well-known to capture the envelope distribution of various fading channel conditions in wireless communications [26]. The value of m is an indicator of the severity of fading, channel quality and influences the bit error rate. Accurate estimation of m is of paramount importance in wireless communications. There are several methods [29, 30, 31, 32, 33] that are employed in the literature to estimate m. The Nakagami-m distribution is given by

$$f_\alpha(\alpha) = \frac{2}{\Gamma(m)} \left(\frac{m}{\Omega}\right)^m \alpha^{2m-1}\, e^{-m\gamma/\Omega}, \tag{3.21}$$

where $\Gamma(.)$ denotes the Gamma function.

$$\Gamma(z) = \int_0^\infty t^{z-1} e^{-t} dt.$$

The parameter m is defined as the ratio of moments, called the *fading figure*,

$$m = \frac{\Omega^2}{E[(\alpha^2 - \Omega)^2]}, \quad m \geq \tfrac{1}{2} \tag{3.22}$$

In fact, both the Rayleigh distribution ($m = 1$) and the Rice distribution are special cases of Nakagami-m distribution.

The amount of fading for Nakagami-m distribution is given as,

$$AF_m = \frac{1}{m}, \qquad m \geq \frac{1}{2} \tag{3.23}$$

Hence, the Nakagami-m distribution spans, via the m parameter, the widest range of AF (from 0 to 2) among all the multipath distributions. For instance, it includes the

one-sided Gaussian distribution $\left(m = \frac{1}{2}\right)$ and the Rayleigh distribution $(m = 1)$ as special cases. In the limit as $m \to +\infty$, the Nakagami-m fading channel converges to a non-fading AWGN channel. Furthermore, when $m > 1$, we obtain one-to-one mapping between the m parameter and the n parameter (or equivalently the Rician K factor since, $n = \sqrt{K}$) allowing the Nakagami-m distribution to closely approximate the Rician distribution, and this mapping is given by [10],

$$m = \frac{(1+n^2)^2}{1+2n^2}, \qquad n \geq 0 \tag{3.24}$$

$$n = \sqrt{\frac{\sqrt{m^2-m}}{m-\sqrt{m^2-m}}}, \qquad m \geq 1 \tag{3.25}$$

$$n = \sqrt{K} \tag{3.26}$$

The fading parameter of the Nakagami-m distribution can describe the presence or absence of the line of sight (LOS) between MS and BS.

The rationale for using the Nakagami distribution to model multipath fading is based on the following characteristics of the Nakgami distribution:

- The Nakagami distribution takes the Rayleigh distribution as a special case as does the Ricean distribution, and it has a simpler probability density function expression.

- The Nakagami distribution approximates the Ricean distribution and log-normal distribution very well [34].

- The Nakagami distribution models fading conditions which are more or less severe than that of Rayleigh.

- Most importantly, the Nakagami distribution fits experimental data better than Rayleigh, Ricean or log-normal distributions in many cases [35].

It is believed that the approach via Nakagami distribution is an alternative to that via Rayleigh or Ricean distributions. Moreover, for calculating important system performance measures, such as bit-error rates with single and multi-channel reception in fading channels, the Nakagami distribution usually results in closed form expressions.

There are several methods that are employed in the literature to estimate the Nakagami-m parameter since its estimation effects many performance characterstics in mobile radio environment. Among them, some important methods are discussed here in brief. The performace of the inverse-noramilzed variance, Tolparev-Polyakov and the Lorenz estimators are compared in [36] through monte-carlo simulations. It is observed that the inverse-normalized variance estimator is superior to the others over a broad range of m-values. In [29], the Maximum-Likelihood Estimation of the Nakagami-m parameter is considered. It is found that the two estimators proposed have smaller variance than the best reported estimator which is based on the moment method. Moreover, a family of moment-based estimators which uses lower order fractional sample momets is proposed [30] for estimating the Nakagami-m

parameter in a noiseless environment. A new integer-moment estimator that outperforms known integer-moment estimators is also presented in [31], which is based on real (integer and possibly non-integer) sample moments. A class of moment based estimators is proposed in [37] that analyzes the performance of all known moment-based estimators by deriving their asymptotic variance and comparing it with the Cramer-Rao Bound (CRB). It is demonstrated by Zhang [38] that none of the recently proposed estimators exceeds the performance of the classical one proposed more than four decades ago by Greenwood and Durand. Cihan presented discussions on some of the practical issues including presence of AWGN, adaptation and computational complexity in [32]. It is shown that the new estimator developed is robust to any symmetrical distributed noise. Noisy sample based Maximum-Likelihood(ML) and moment-based estimators for the Ricean and Nakagami-m fading distribution parameters are derived in [33]. The problem of estimating these parameters in noisy slowly fading channels is also studied. To apply the Nakagami-m distribution to the received signal-level distribution from narrowband to wideband transmissions, the m-parameter is mathematically derived in [39] as a function of equivalent received bandwidth in the case of non-line of sight. An efficient method for generating correlated Nakagami-m fading envelope samples is presented in [40], and is compared to other methods used to generate Nakagami-m variates. In the literature, there are algorithmns only for generating correlated Nakagami branches with the same fading parameter. In [41, 42], a novel approach is adopted to generate Nakagami

fading signals with arbitrary fading parameters and any correlation structure. The Equivalent Transmission Path model(ETP) has a function to assess BER due to ISI in a Nakagami-Rice fading environment [43]. Finally, the Nakagami-m distribution often gives the best fit to land-mobile [35, 44, 18] and indoor [45] mobile multipath propagation, as well as scintillating ionospheric radio links [46].

3.3.5 Diversity Combining

Diversity combining consists of receiving redundantly the same information-bearing signal over two or more fading channels; combining these multiple replicas at the receiver in order to inrease the overall received SNR. The intuition behind this concept is to exploit the low probability of concurrence of deep fades in all the diversity channels in order to lower the probability of error and outage. These multiple replicas are obtained by extracting the signals via different radio paths:

- In space by using multiple-receiver antennas (antenna or site diversity).
- In frequency by using multiple-frequency channels seperated by at least the coherence bandwidth of the channel (frequency hopping or multicarrier systems).
- In time by using multiple time slots seperated by at least the coherence time of the channel (coded systems).

- Via multipath by resolving multipath components at different delays (direct-sequence spread spectrum systems with RAKE reception).

The model consists of a multilink channel where the transmitted signal is received over L independent slowly varying flat-fading channels, where l is the channel index and $\{\alpha_l\}_{l=1}^{L}$, $\{\theta_l\}_{l=1}^{L}$, and $\{\tau_l\}_{l=1}^{L}$ are the random channel amplitudes, phases and delays, respectively. We assume that $\{\alpha_l\}_{l=1}^{L}$, $\{\theta_l\}_{l=1}^{L}$, and $\{\tau_l\}_{l=1}^{L}$ are all constant over atleast a symbol interval. When we talk about independent combined paths, we mean that the fading amplitudes $\{\alpha_l\}_{l=1}^{L}$ are assumed to be statistically independent random variables (RVs) where α_l has mean square value $\overline{\alpha_l^2}$ denoted by Ω_l and a probability density function (PDF) described by any of the family of the distributions Rayleigh, Nakagami-n (Rice), or Nakagami-m described in section (3.3.4).

Diversity techniques are classified according to the nature of the fading that they are intended to mitigate. For instance, microdiversity schemes are designed to combat short-term multipath fading whereas macrodiversity techniques mitigate the effect of long-term shadowing caused by obstructions such as buildings, trees and hills. Diversity schemes can also be classified according to the type of combining employed at the receiver. e.g. *pure combining techniques* such as *Maximal-Ratio Combining*, *Equal Gain Combining*, *Selection Combining* and *Switched Combining* and the most recently proposed *hybrid techniques* such as *mutidimensional diversity techniques*.

Coherent Equal Gain Combining

Maximal-Ratio Combining provides the maximum performance improvement relative to all other diversity combining techniques by maximizing the signal-to-noise ratio at the combiner output. Alternative combining techniques such as EGC are often used in practice because of their reduced complexity relative to the optimum MRC scheme. Indeed, EGC equally weights each branch before combining, and therefore doesn't require estimation of the channel (path) fading amplitudes.

The EGC receiver processes the L received replicas, equally weights them, and then sums them to produce the decision statistic. For equiprobable transmitted symbols, it can be shown that the total conditional SNR per symbol γ_{EGC} at the output of the EGC combiner is given by,

$$\gamma_{EGC} = \frac{\left(\sum_{l=1}^{L} \alpha_l\right)^2}{\sum_{l=1}^{L} N_l} \tag{3.27}$$

where E_s is the energy (in joules) per symbol and N_l is the AWGN power spectral density on the lth path.

Abu-Dayya and Beaulieu [47, 48] employed an infinite series representation for the PDF of the sum of Nakagami-m and Rice RVs [49] to analyze the performance of binary modulations when used in conjunction with EGC. The same approach was adopted by Dong [50] to extend the results to several two-dimensional constellation of interest. Another approach based on the Gil-Pilaez lemma [51] was proposed by Zhang [52] and lead to closed-form solutions for binary modulations with two or

three branch EGC receivers over Rayleigh fading channels. Zhang extended this approach to Nakagami-m fading channels [53]. Annamalai [54] used a frequenecy-domain-based approach and Parseval's theorem to compute the average symbol error rate with EGC over Nakagami-m fading channels.

3.4 Rake Receiver

Multipath impairments are encountered by Rake receiver, so called by its inventors, Price and Green [55]. The receiver takes the advantage of the resolved multipaths to provide diversity gain. Such a diversity is termed as *implicit diversity*, *multipath diversity*, *internal diversity* or simply, *Rake diversity*.

A rake receiver combines the signal components from multipath using any diversity combining method like Equal Gain Combining (EGC) or Maximal-Ratio Combining (MRC). A generic block diagram of Rake receiver with L branches is shown in figure (3.5).

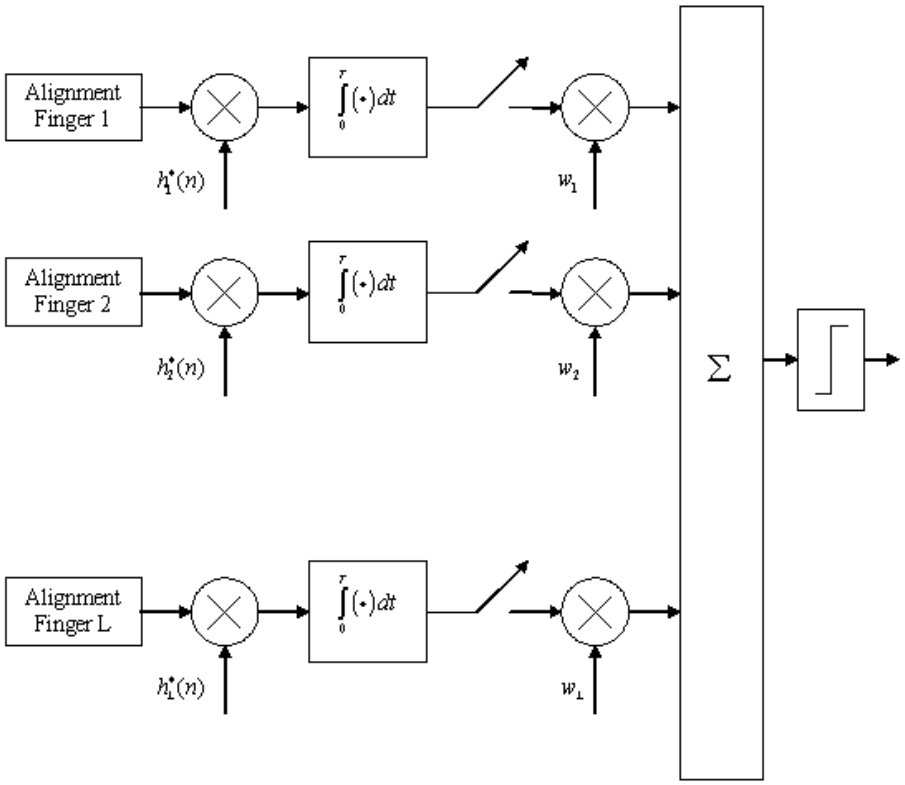

Figure 3.5: Implementation of Rake receiver

Chapter 4

Results and Discussion

The distribution of the reflection co-efficient is described according to three common distributions that covers the wide range of the reflecting surfaces in practical scenarios. i.e. Uniform distribution, Exponential distribution and Half Gaussian distribution. The magnitude of the reflection co-efficient typically ranges from $0.5 - 1$ for ideal smooth surfaces, and from $0 - 1$ for Gaussian rough surfaces depending upon the angle of incidence. It is found that exponential distribution of the reflection co-efficient gives larger values of m and if operating in an environment where the reflections from the material surfaces is best described by the exponential distribution, error performance is enhanced for any modulation scheme used. Further, while operating at higher frequencies, better performance is acheived than operating at lower frequencies at shorter distances.

The exponential distribution of the reflection co-eficient is studied over frequency

non-selective and frequency selective Nakagami-m fading channels. It is obvious that as we move from microcell to macrocell and as the distance between the T_x and R_x increases, the error rates starts increasing and there is a degradation in performance of the digital communication system. Therefore, in order to ovecome this degradation, diversity techniques are employed to improve the error rates. Equal Gain Combining approach is used for MPSK systems. At higher distances, the error rates showed imrovements for smaller values of m. All the three modulation schemes (QPSK, 8PSK and 16QAM) are compared and their variations in performance with increase in distances and varying Nakagami-m parameter is shown. The 3D representation also gives us an indication on how the bit error rate curves (for SNR range of $0dB$ to $30dB$ with intervals of $5dB$) for different modulation schemes vary with increase in distance in micro and macrocellular structure. The information represented by these 3D plots has not been reported in the literature yet.

Since, the channel is assumed to be flat, therefore the diversity combining techniques provide improvements in error rates while operating for smaller values of m at which system undergoes degradation. When the channel is frequency-selective, then the delayed (multipath) components give rise to InterSymbol Interference (ISI) and we have degraded performance of the system. Therefore, in order to study the effect of changing Nakagami-m parameter over frequency-selective channels (more realistic scenario), we apply Rake diversity at the receiver. It is seen from figure (3.5) that the basic function of the Rake receiver is to combine different multipath com-

ponents that are delayed in time and attenuated by a weight defined by the power delay profile (PDP), according to a certain criteria in order to enhance the system performance at the receiver. Since, we assume perfect channel estimation i.e. the strengths of the paths and the interpath delays are known to us, therefore, no estimation of the channel is required. We applied the EGC diversity technique for the implementation of the Rake receiver and obtain the BER curves for MPSK (QPSK and 8PSK) systems. It is observed that there is a degradation of performance for uniform and half Gaussian distributions of the reflection co-efficient as compared to the exponential distribution.

4.1 Simulation Modeling

The simluation methodology consists of the following steps:

- Defining frequency (f), heights of the transmitter and receiver antennas (h_t and h_r), transmitted power (P_t taken as constant $10W$), path loss slopes for terrain types 1 and 2 (α_1 and α_2) and the number of iterations.

- Calculating the direct received power at the mobile station using two ray ground reflection model using equation (2.8).

- Positioning (random) the scatterers local to the receiver with Gaussian (Normal distribution).

- Defining the position of the base station.
- Calculating the distances d_1 (distances between the scatterers and the base station) and d_2 (distances between the scatterers and the mobile station).
- Defining the distribution of the modified Fresnel Reflection Coefficient Γ (Uniform, Exponential or Half Gaussian).
- Defining the Diffraction Losses between $8-12dB$ with $10dB$ mean considering different propagation environments.
- Calculating the total average received scattered power at the mobile station from the proposed model using equation (2.18).
- Calculating the Rician K factor and introducing the Nakagami-m parameter with varying distances for micro and macro cellular structures.
- Simulating the Nakagami channel for a particular value of m corresponding to a certain distance d between the mobile station and the base station.
- Finding the BER curves for $QPSK$, $8PSK$ and $16QAM$ for specific determined values of m for different distributions of Γ at $900MHz$ and $1800MHz$ frequencies over Flat Fading and Frequency Selective Fading Nakagami-m channels.
- Improving the degraded error performance at larger distances by employing

Equal Gain Combining (EGC) Diversity technique (Flat Fading case) and Rake Receiver (Frequency Selective Fading case).

- Representing $3D$ curves showing the relationship between Nakagami-m parameter, distance d and the error performance of a particular modulation scheme.

4.2 Parameter Δm

A new parameter Δm is also introduced in order to study the change in performance of the communication system with incresae in distance. It is seen with the help of figures (4.1 to 4.24) that the Nakagami-m parameter decreases at a faster rate initially for smaller distances and then at a slower rate afterwards for longer distances. Therefore, the parameter Δm will be of higher value initially (close to the base station) and starts decreasing as we move towards the edge of the cellular structure. It is observed that the transmitter and receiver antenna heights and the distance between the mobile station and the scatterers effect the parameter Δm. From the same set of figures, it is inferred that m changes (reduces) at a faster rate for model B (discussed in section 4.3) where the average distances between the receiver and the scatterers is increased, thereby reducing the received scattered power (see figure 2.5 for both cellular (micro and macro) structures).

This behavior of Δm indicates that the performance of the digital communication system defined by the channel link parameter m obeys an exponential decay.

Initially, the performance degrades faster and after reaching a certain distance, the change in performance becomes less severe at higher distances.

In microcellular structure, the performance of MPSK systems is represented with the help of 3D plots to obtain a relationship between the error performance criteria (BER) and the increasing distance with varying values of m.

4.3 Variations of Nakagami-m parameter with Distance: Comparison of distributions of reflection co-efficient Γ

We considered three models (model A, model B, and model C) depending on different parameters such as the transmitter antenna height h_t, receiver antenna height h_r and the ditance between the mobile station and the scatterers d_2 local to the receiver. All of these parameters have an impact on the Nakagami-m parameter. The three models are defined as follows:

Parameters of Model A:

- Transmitting Antenna Height $h_t = 50m$
- Receiving Antenna Height $h_r = 3m$
- Ditance between the Mobile Station and the Scatterers $d_2 = 12m$

Parameters of Model B:

- Transmitting Antenna Height $h_t = 50m$
- Receiving Antenna Height $h_r = 3m$
- Ditance between the Mobile Station and the Scatterers $d_2 = 16m$

Parameters of Model C:

- Transmitting Antenna Height $h_t = 40m$
- Receiving Antenna Height $h_r = 5m$
- Ditance between the Mobile Station and the Scatterers $d_2 = 12m$

Refering to figure (4.1) and (4.2), it is observed that the value of m decreases as the distance between the mobile station and the base station increases. Similarly depending on the distribution of reflection co-efficient which is represented by Γ in equation (2.20), three types of distribution are considered. Since its value depends on the type of reflecting/scattering material and the angle of the incidence on the surface of the material, we consider *Uniform distribution* (see figure (4.25)), *Exponential distribution* (see figure (4.27)), and *Half Gausian distribution* (see figure (4.26)) of the reflection coefficient that covers the wide range of reflecting surfaces. The diffraction losses are taken to be normally distributed between $8-10dB$ with a mean of $10dB$ (see figure (4.28)). The cellular structure is divided into *Microcell* $100m-1km$ and *Macrocell* $1km - 10km$.

The comparison of different distributions of the reflection coefficient Γ for different models at $900MHz$ and $1800MHz$ for micro and macrocellular structure is shown in figures (4.1 to 4.12). It is observed that the exponential distribution gives higher values of m at a particular distance than any other distribution. All of these distributions have practical implications because these distributions represent the nature of the terrain in which the mobile is operating. Refering to figure (4.1) and (4.3), it is observed that if the mobile is $400m$ away from the base station in an environment whose properties are best described by exponential distribution, then the value of Nakagami-m parameter is $3.09dB$ at $900MHz$ and $13.17dB$ at $1800MHz$. Similarly, at the same distance, if the environment characteristics are described by uniform distribution, then m changes to $0.84dB$ at $900MHz$ and $8.2dB$ at $1800MHz$. And for half gaussian distribution of the reflection co-efficient, m is shown to be $1.84dB$ at $900MHz$ and $10.82dB$ at $1800MHz$. This analysis shows that the exponential distribution of the reflection co-efficient gives higher values of m at a specified distance. Further, at shorter distances $(100m - 1km)$, the change in frequency also effects the value of m. Higher the frequency, higher will be the m. Similar behavior is observed for other models (model B and model C), refer to figures (4.5 to 4.12).

4.3.1 Effect of distribution of the refelection co-eficient

It is observed that in each case, the exponential distribution of the reflection co-efficinet gives higher values of Nakagami-m parameter as compared to the other distributions. This is because exponential distribution has more values closer to zero indicating the roughness of the surface to be more severe and low scattered power henceby increasing the value of m.

4.3.2 Effect of frequency

The operating frequency is another parameter that affects the value of m at a particular distance. The higher the frequency, the larger the value of m. Refering to equations (2.13) and (2.14), it is observed that $(4\pi/\lambda)^2$ is the aperture area of the antenna. By looking at the received scattered power (equation (2.18)), higher values of f decreases the received scattered power and results in larger value of m.

Tables (4.1 to 4.18) gives the tabular representation of variations of Nakagami-m parameter with distance for varying parameters such as f, h_t, h_r, d_2, and Γ. The tabular representation indicates that the values of m are not integer values as considered in the previous studies on more than one occassion. However, it is shown that the Nakagami-m parameter describing the link quality is continuously changing with an increase in distance.

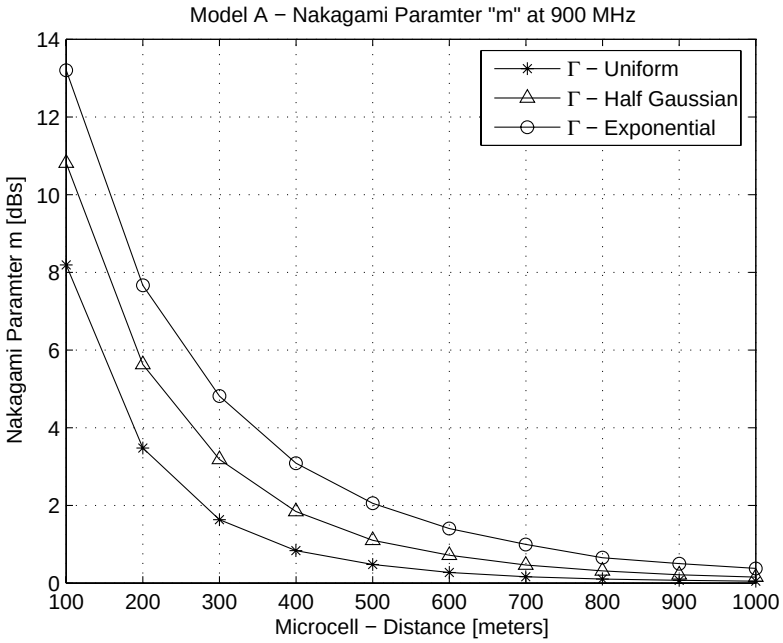

Figure 4.1: Nakagami m variations:Model A, Microcell, 900 MHz

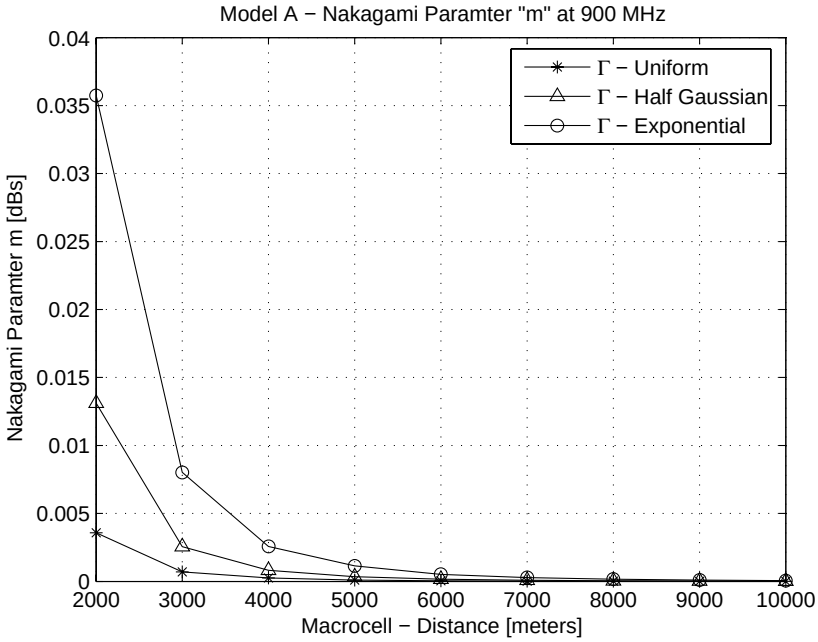

Figure 4.2: Nakagami m variations:Model A, Macrocell, 900 MHz

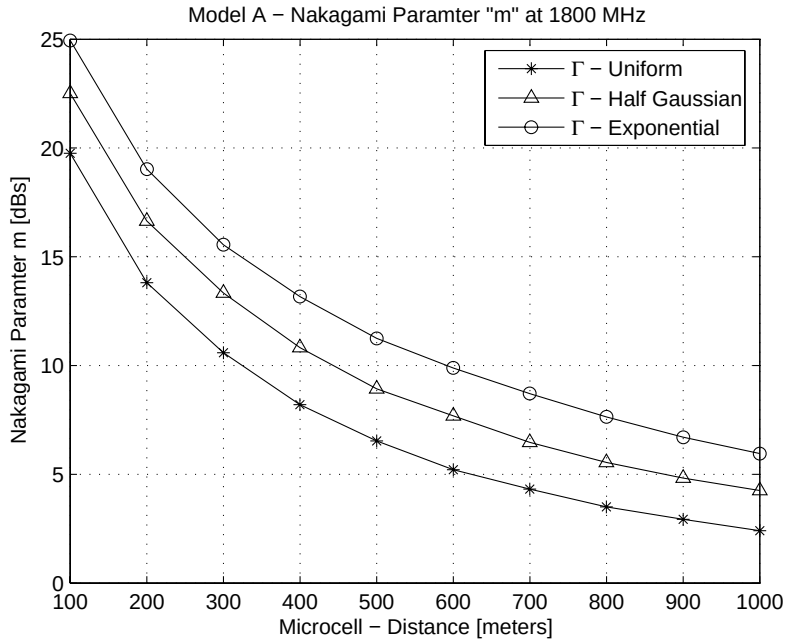

Figure 4.3: Nakagami m variations:Model A, Microcell, 1800 MHz

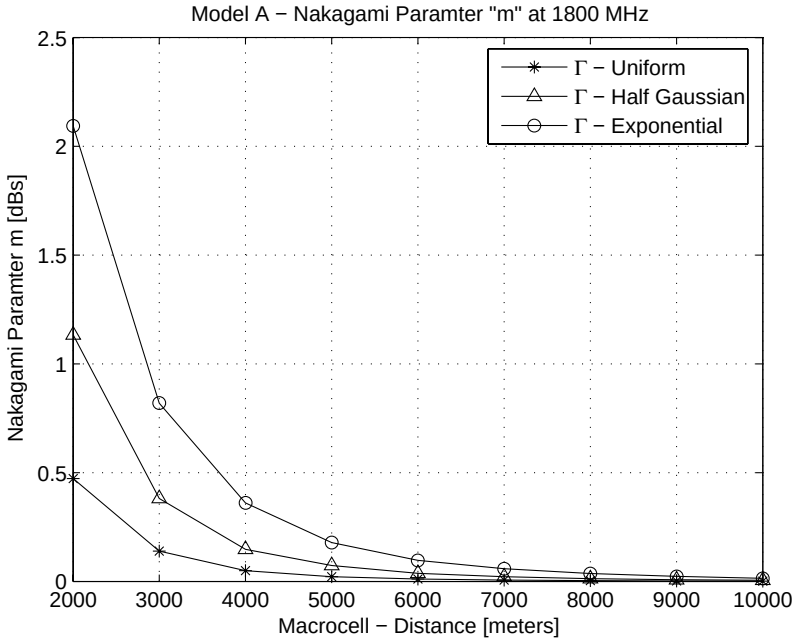

Figure 4.4: Nakagami m variations:Model A, Macrocell, 1800 MHz

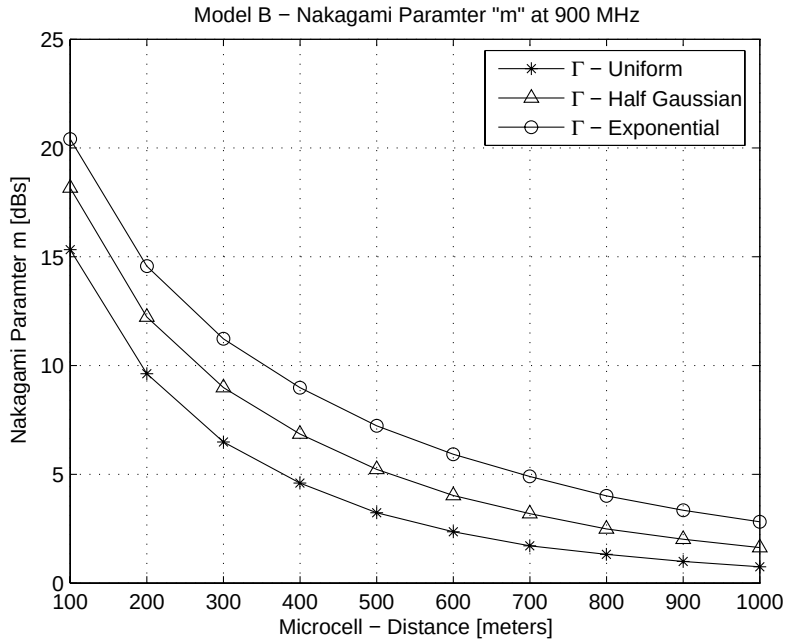

Figure 4.5: Nakagami m variations:Model B, Microcell, 900 MHz

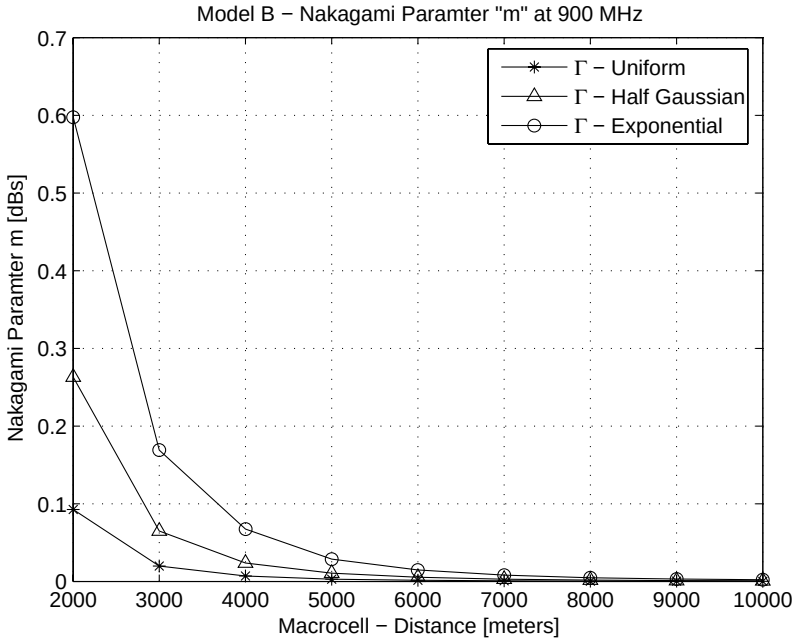

Figure 4.6: Nakagami m variations:Model B, Macrocell, 900 MHz

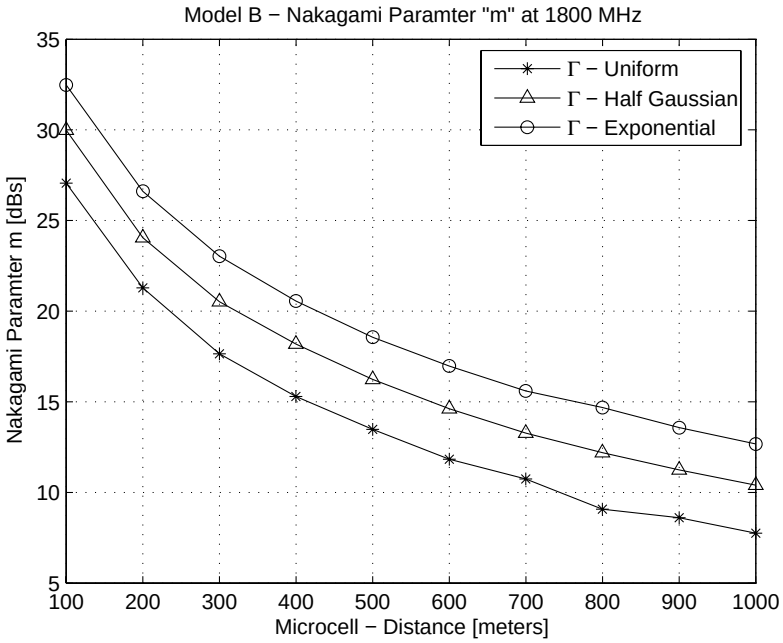

Figure 4.7: Nakagami m variations:Model B, Microcell, 1800 MHz

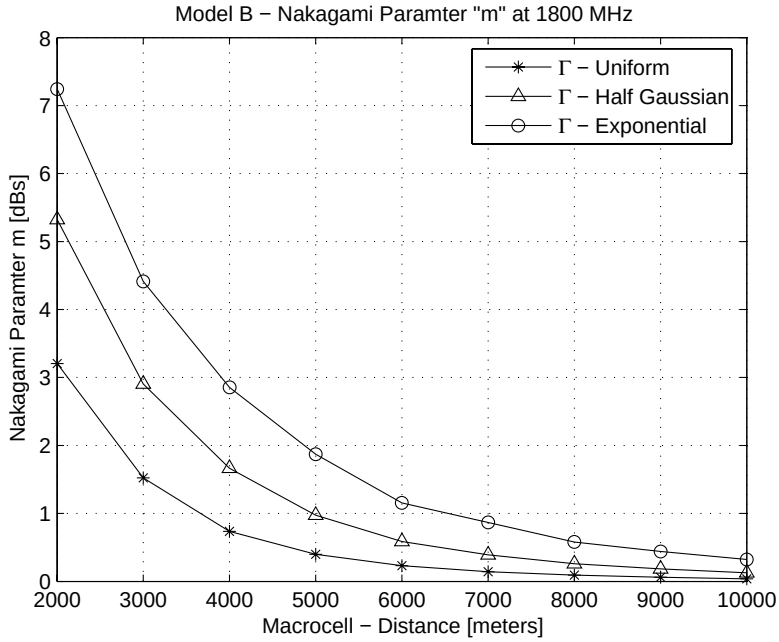

Figure 4.8: Nakagami m variations:Model B, Macrocell, 1800 MHz

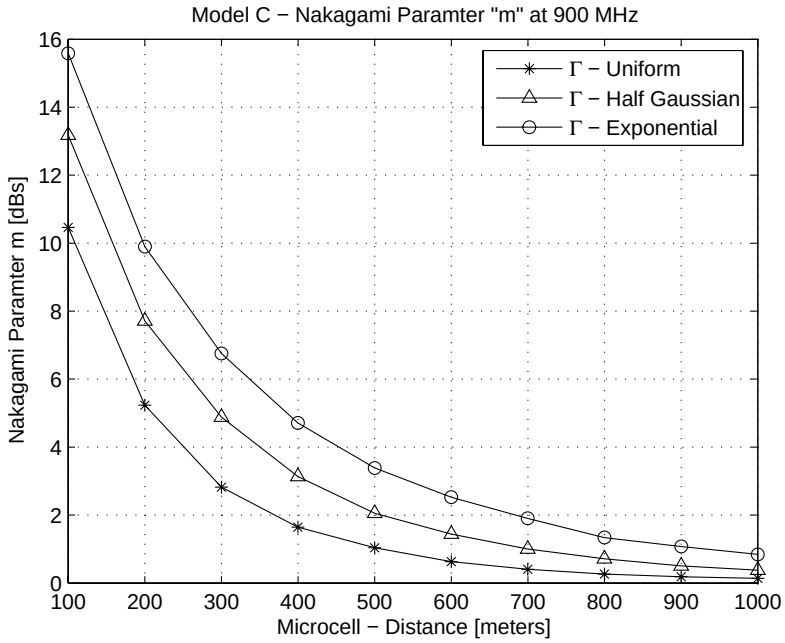

Figure 4.9: Nakagami m variations:Model C, Microcell, 900 MHz

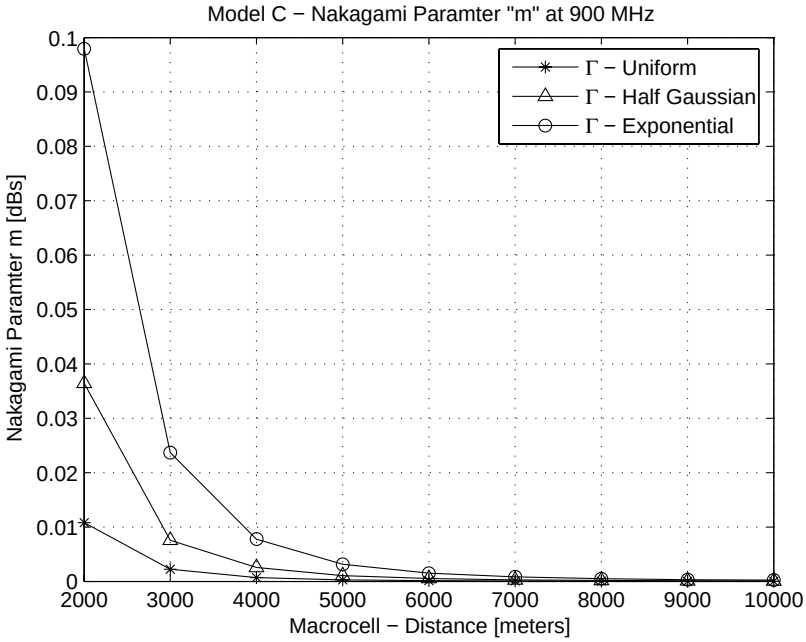

Figure 4.10: Nakagami m variations:Model C, Macrocell, 900 MHz

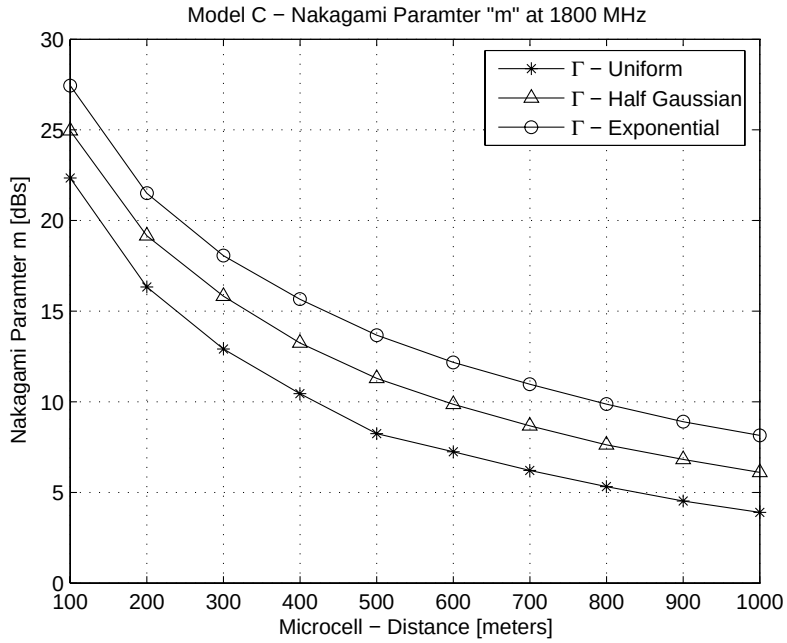

Figure 4.11: Nakagami m variations:Model C, Microcell, 1800 MHz

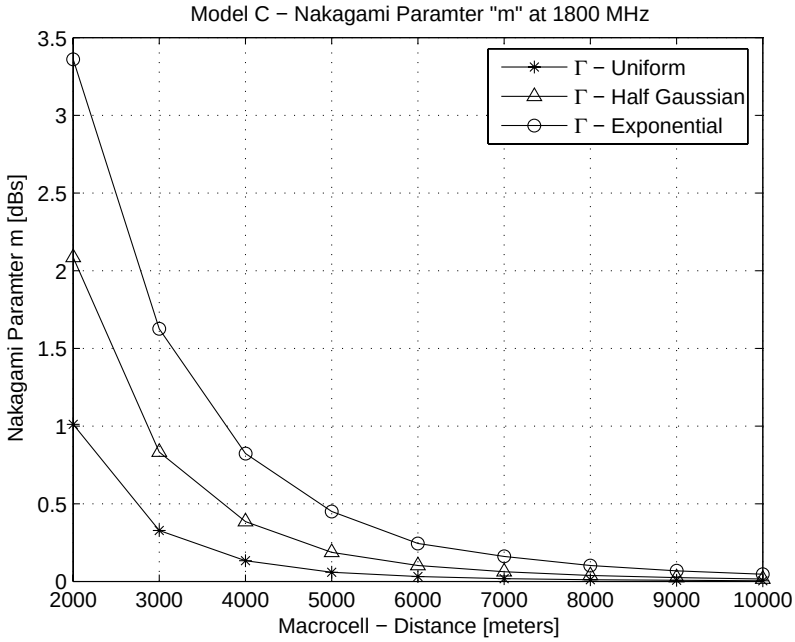

Figure 4.12: Nakagami m variations:Model C, Macrocell, 1800 MHz

4.4 Variations of Nakagami-m parameter with Distance: Comparison of Models A, B, and C

As described in section (4.3), we considered three models (A, B, and C) depending on the type of environment and cellular conditions. The three variable parameters in these models are:

- Transmitter Antenna Height h_t
- Receiver Antenna Height h_r
- Distance between the Mobile Station and the Scatterers d_2

4.4.1 Effect of h_t, h_r and d_2

Figures (4.13 to 4.24) provide a comparison between different models for a paricular distribution of the reflection coefficient Γ. It is found that model B gives larger values of m since it has larger distances d_2 between the mobile station and the scatterers. In another way, we can say that the breakpoint distance is decreased from the base station thereby providing diminshed scattered power at the receiver and higher values of m.

Model C gives higher values of m than model A since the effective heights of the transmitting and receiving antennas are increased. As discussed earlier, there are larger values of m at higher frequency.

By looking at figure (4.15), it is observed that at a particular distance, if we compare the three models described above, the difference between them is not same. Let's say, at $d = 500m$, and $f = 1800MHz$ and Γ uniformly distributed, the values of m are $6.53dB$, $13.48dB$, and $8.67dB$ corresponding to model A, model B, and model C. It is observed that if we move from model B to model A, i.e. the distance between the mobile and the scatterers is increased, we have a severe degradation in performance while moving from model C to model A, i.e. changing the effective value of transmitter and receiver antenna heights. This behavior is observed for all the types of reflection co-efficient distribution for both micro and macrocellular structures by refering to figures (4.13 to 4.24).

4.4.2 Effect of frequency

The operating frequency also affects the value of m at a particular distance. The higher the frequency, the larger the value of m. By looking at the received scattered power (equation (2.18)), higher values of f decreases the received scattered power and results in larger values of m. It will be shown in the coming discussion that the performance of the digital communication system (BER, SER, outage etc.) highly depends on the parameter Δm (i.e. change in value of Nakagami-m parameter with distance). At larger distances, this change becomes smaller and becomes independent of frequnecy. The representation of the distribution of reflection co-efficient and diffraction losses are shown in figures (4.25 to 4.28).

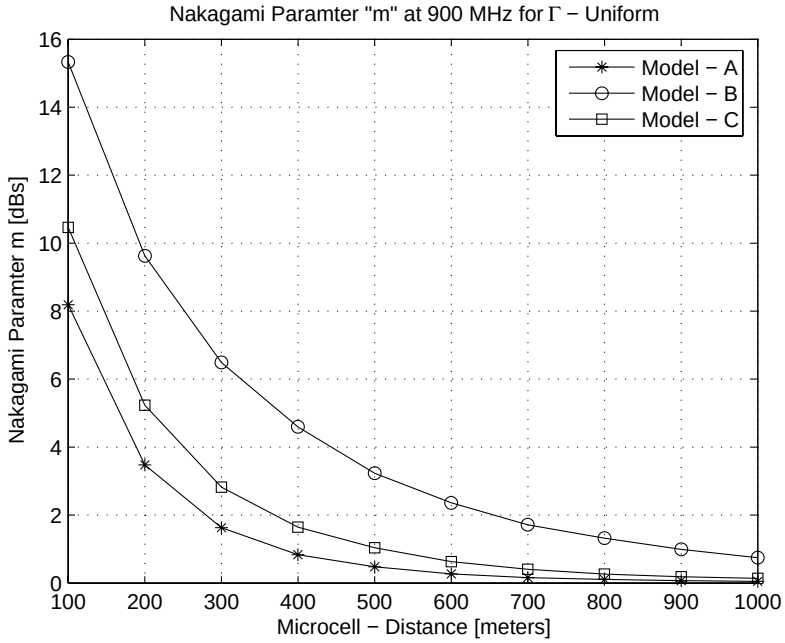

Figure 4.13: Nakagami m variations: Γ uniform, Microcell, 900 MHz

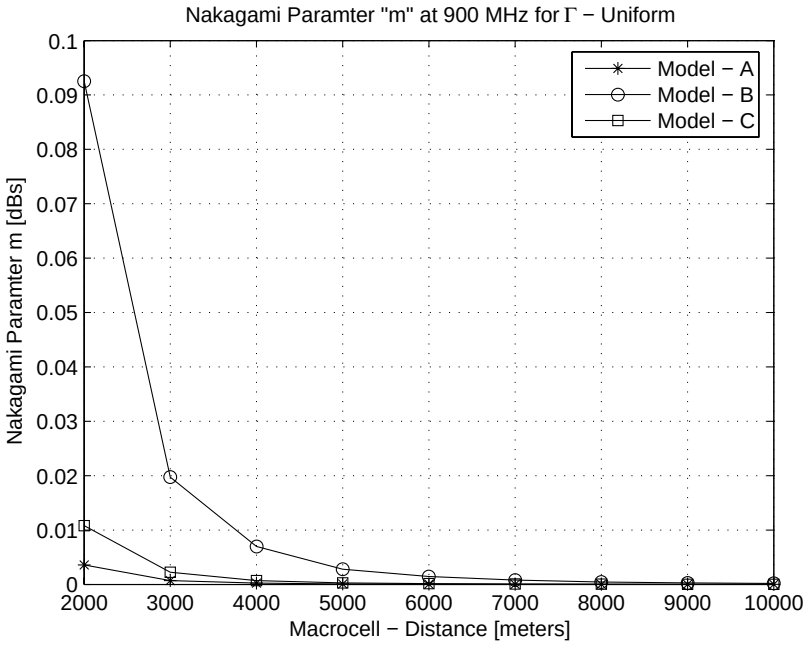

Figure 4.14: Nakagami m variations: Γ uniform, Macrocell, 900 MHz

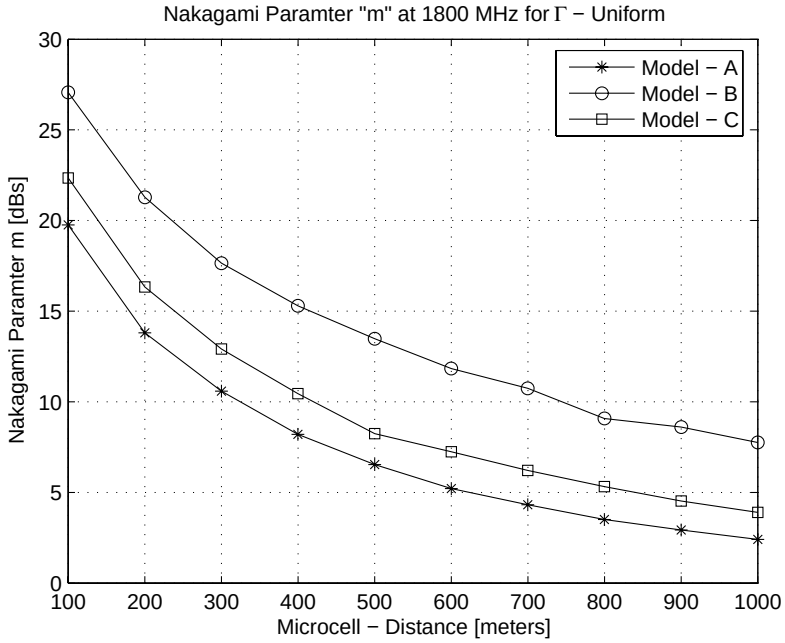

Figure 4.15: Nakagami m variations: Γ uniform, Microcell, 1800 MHz

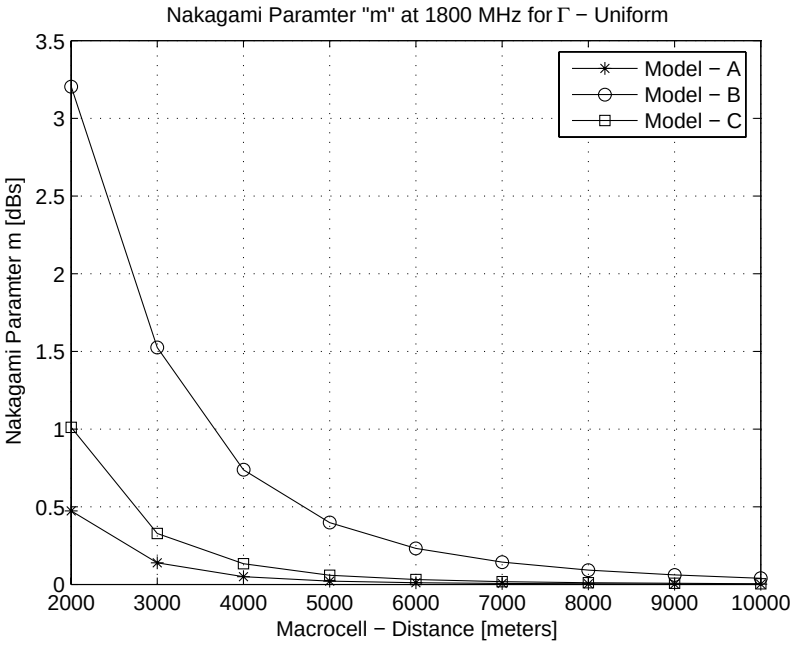

Figure 4.16: Nakagami m variations: Γ uniform, Macrocell, 1800 MHz

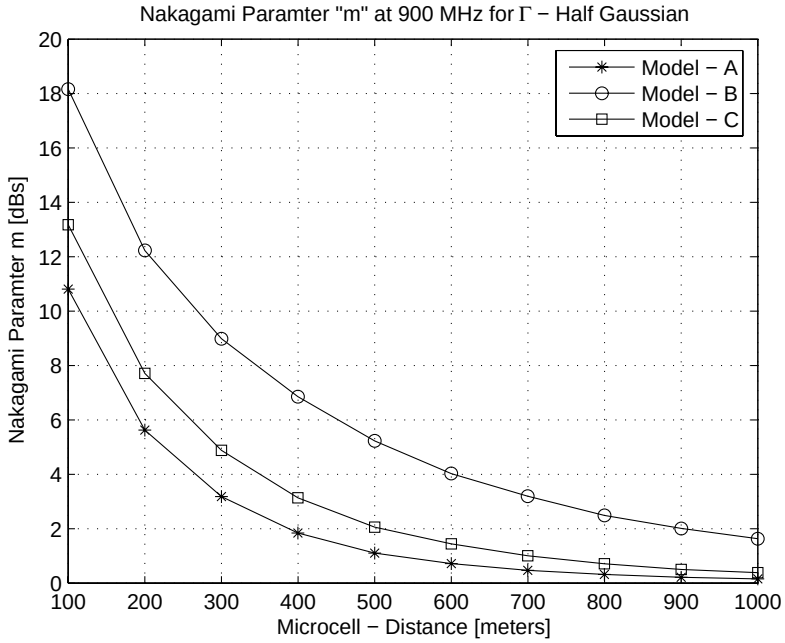

Figure 4.17: Nakagami m variations: Γ half gaussian, Microcell, 900 MHz

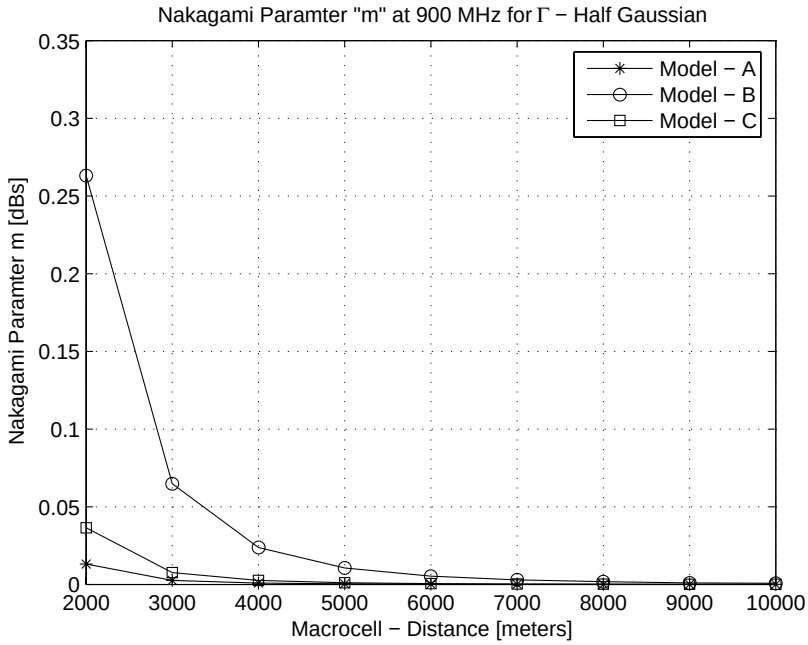

Figure 4.18: Nakagami m variations: Γ half gaussian, Macrocell, 900 MHz

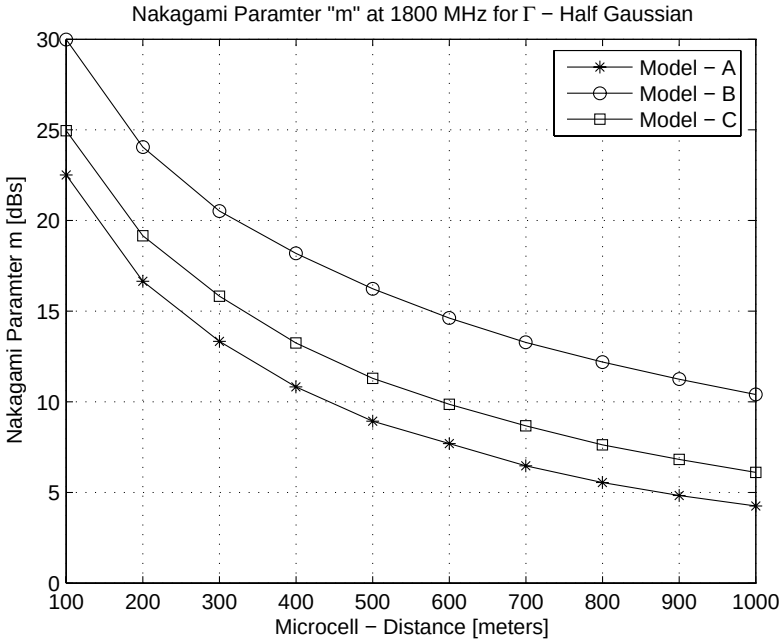

Figure 4.19: Nakagami m variations: Γ half gaussian, Microcell, 1800 MHz

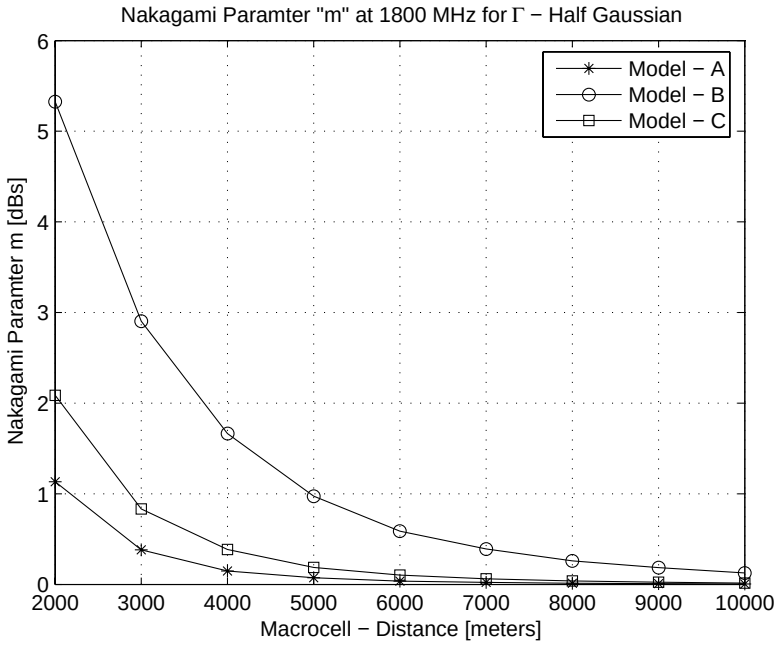

Figure 4.20: Nakagami m variations: Γ half gaussian, Macrocell, 1800 MHz

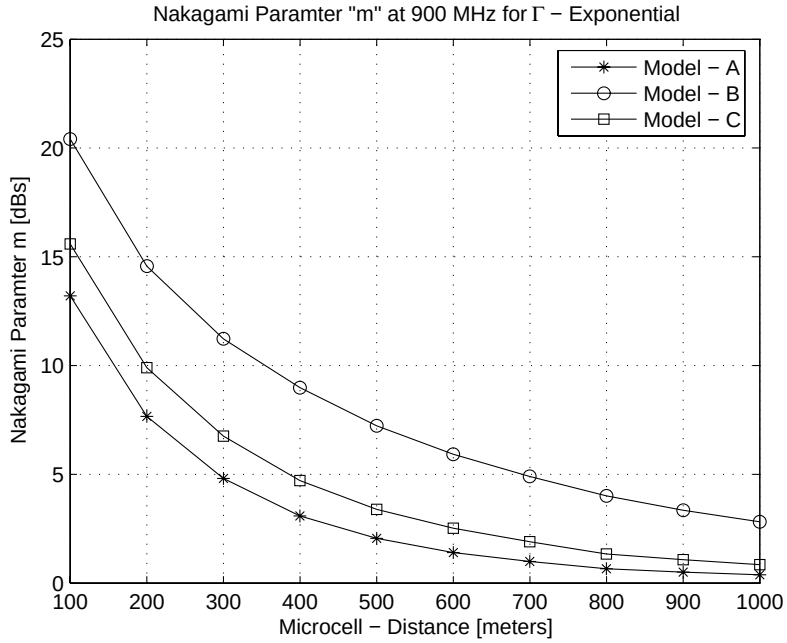

Figure 4.21: Nakagami m variations: Γ exponential, Microcell, 900 MHz

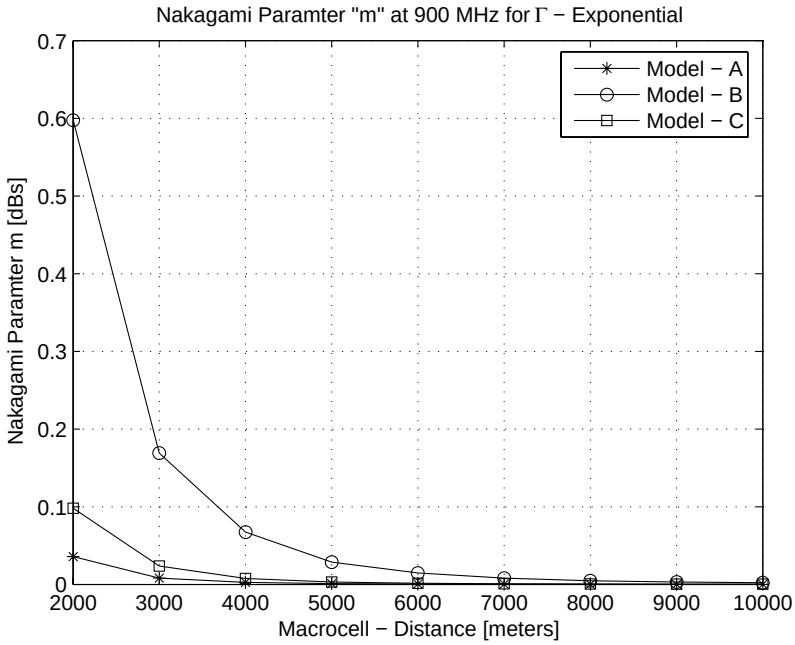

Figure 4.22: Nakagami m variations: Γ exponential, Macrocell, 900 MHz

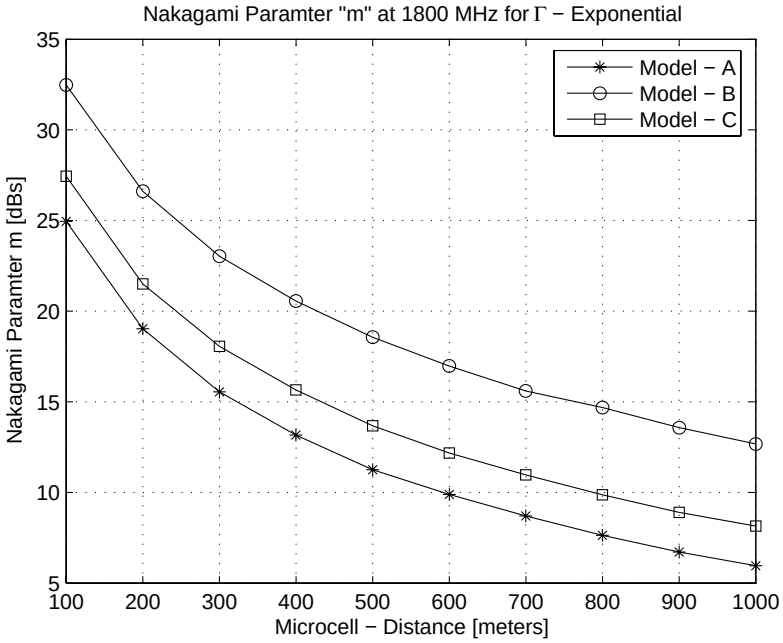

Figure 4.23: Nakagami m variations: Γ exponential, Microcell, 1800 MHz

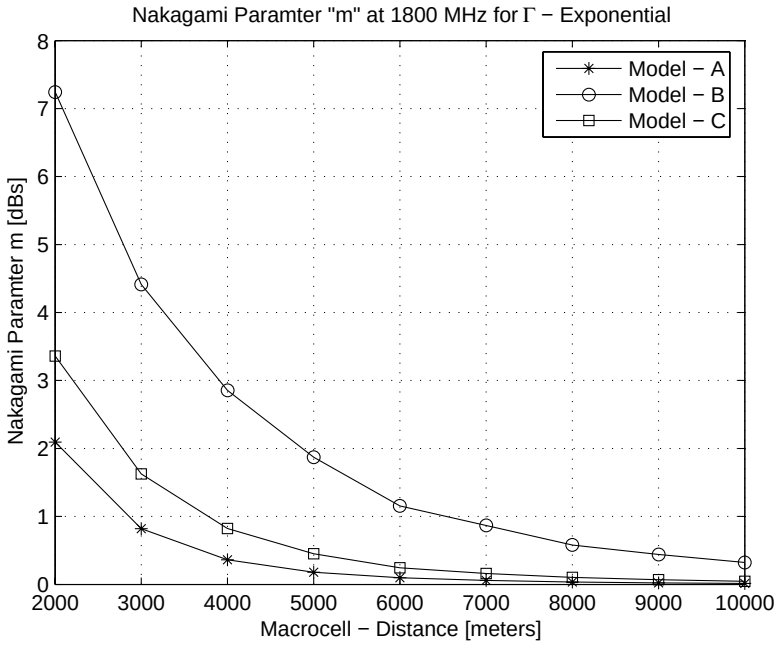

Figure 4.24: Nakagami m variations: Γ exponential, Macrocell, 1800 MHz

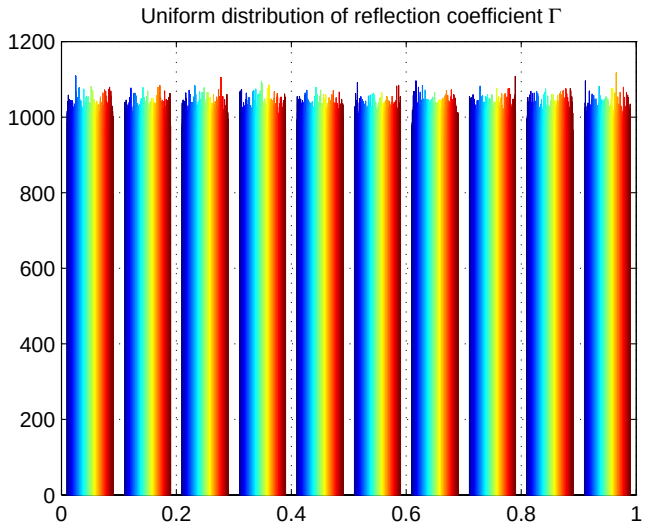

Figure 4.25: Uniformly distribution of reflection co-efficient Γ

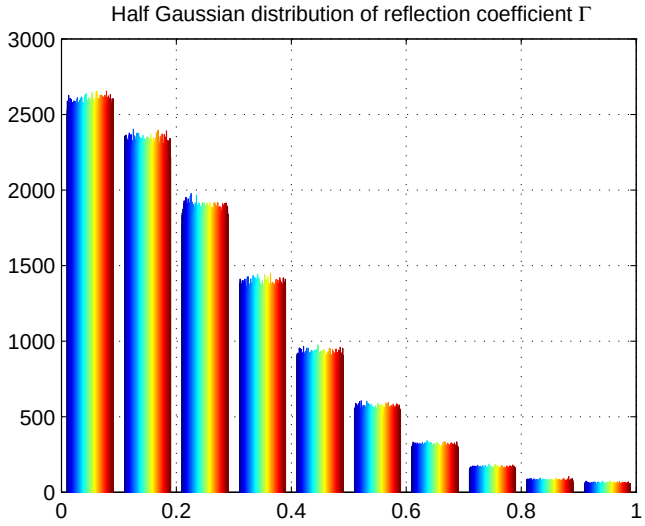

Figure 4.26: Half Gaussian distribution of reflection co-efficient Γ

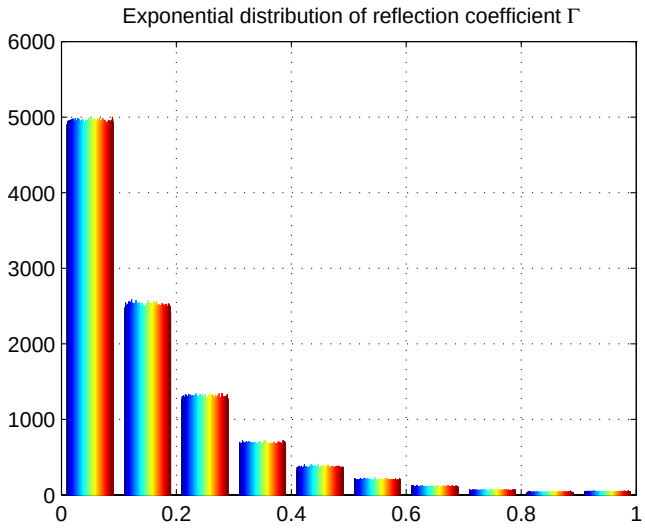

Figure 4.27: Exponential distribution of reflection co-efficient Γ

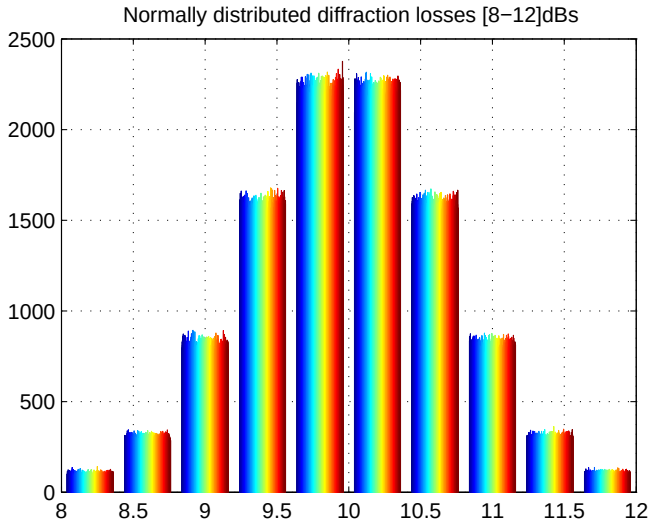

Figure 4.28: Normal distribution of diffraction losses with $10dB$ mean

Simulation Parameters:

Simulation Model: Model A

Distribution of reflection co-efficient: Uniform

Carrier Frequency: 900 MHz

Path Loss Exponent $\alpha_1 = 2$

Additional Path Loss Exponent $\alpha_2 = 4$

Tranmitter Antenna Height $h_t = 50$ m

Receiver Antenna Height $h_r = 3$ m

Average Distance between MS & Scatterers $d_2 = 12$ m

Microcell				
Distance (m)	**Direct Power** (dB)	**Scattered Power** (dB)	**Rician 'K'** (dB)	**Nakagami 'm'** (dB)
100	-26.48	-37.14	10.67	8.19
200	-38.52	-43.11	4.59	3.47
300	-45.56	-46.60	1.03	1.63
400	-50.56	-49.12	-1.44	0.84
500	-54.44	-51.21	-3.23	0.48
600	-57.60	-52.72	-4.88	0.27
700	-60.28	-53.98	-6.30	0.16
800	-62.60	-55.20	-7.40	0.10
900	-64.65	-56.24	-8.41	0.07
1000	-66.48	-57.18	-9.30	0.05
Macrocell				
2000	-78.52	-63.21	-15.31	3.57E-03
3000	-85.56	-66.63	-18.94	6.99E-04
4000	-90.56	-69.37	-21.19	2.51E-04
5000	-94.44	-71.12	-23.32	9.43E-05
6000	-97.60	-72.72	-24.88	4.60E-05
7000	-100.28	-74.11	-26.18	2.54E-05
8000	-102.60	-75.22	-27.39	1.47E-05
9000	-104.65	-76.23	-28.42	9.05E-06
10000	-106.48	-77.17	-29.31	6.01E-06

Table 4.1: Variations of Nakagami-m parameter with distance for Micro and Macrocells - Model A, Uniform distribution at 900 MHz

Simulation Parameters:

Simulation Model: Model A

Distribution of reflection co-efficient: Uniform

Carrier Frequency: 1800 MHz

Path Loss Exponent $\alpha_1 = 2$

Additional Path Loss Exponent $\alpha_2 = 4$

Tranmitter Antenna Height $h_t = 50$ m

Receiver Antenna Height $h_r = 3$ m

Average Distance between MS & Scatterers $d_2 = 12$ m

Microcell				
Distance (m)	**Direct Power** (dB)	**Scattered Power** (dB)	**Rician 'K'** (dB)	**Nakagami 'm'** (dB)
100	-26.48	-49.21	22.73	19.76
200	-38.52	-55.20	16.68	13.80
300	-45.56	-58.86	13.30	10.59
400	-50.56	-61.24	10.68	8.20
500	-54.44	-63.17	8.73	6.53
600	-57.60	-64.67	7.07	5.21
700	-60.28	-66.14	5.85	4.32
800	-62.60	-67.23	4.63	3.50
900	-64.65	-68.33	3.68	2.93
1000	-66.48	-69.20	2.72	2.40
Macrocell				
2000	-78.52	-75.26	-3.26	4.73E-01
3000	-85.56	-78.87	-6.70	1.39E-01
4000	-90.56	-81.31	-9.25	4.95E-02
5000	-94.44	-83.17	-11.26	2.13E-02
6000	-97.60	-84.78	-12.83	1.08E-02
7000	-100.28	-86.12	-14.16	6.00E-03
8000	-102.60	-87.21	-15.39	3.48E-03
9000	-104.65	-88.27	-16.37	2.24E-03
10000	-106.48	-89.15	-17.33	1.46E-03

Table 4.2: Variations of Nakagami-m parameter with distance for Micro and Macrocells - Model A, Uniform distribution at 1800 MHz

Simulation Parameters:

Simulation Model: Model A

Distribution of reflection co-efficient: Exponential

Carrier Frequency: 900 MHz

Path Loss Exponent $\alpha_1 = 2$

Additional Path Loss Exponent $\alpha_2 = 4$

Tranmitter Antenna Height $h_t = 50$ m

Receiver Antenna Height $h_r = 3$ m

Average Distance between MS & Scatterers $d_2 = 12$ m

Microcell				
Distance (m)	**Direct Power** (dB)	**Scattered Power** (dB)	**Rician 'K'** (dB)	**Nakagami 'm'** (dB)
100	-26.48	-42.53	16.05	13.20
200	-38.52	-48.59	10.07	7.67
300	-45.56	-52.10	6.54	4.81
400	-50.56	-54.51	3.95	3.09
500	-54.44	-56.43	2.00	2.05
600	-57.60	-58.05	0.44	1.40
700	-60.28	-59.45	-0.84	1.00
800	-62.60	-60.52	-2.08	0.69
900	-64.65	-61.57	-3.08	0.50
1000	-66.48	-62.55	-3.92	0.38
Macrocell				
2000	-78.52	-68.48	-10.04	3.57E-02
3000	-85.56	-72.07	-13.50	8.02E-03
4000	-90.56	-74.50	-16.06	2.57E-03
5000	-94.44	-76.57	-17.87	1.14E-03
6000	-97.60	-78.04	-19.57	5.22E-04
7000	-100.28	-79.33	-20.95	2.77E-04
8000	-102.60	-80.45	-22.15	1.61E-04
9000	-104.65	-81.48	-23.16	1.01E-04
10000	-106.48	-82.33	-24.15	6.45E-05

Table 4.3: Variations of Nakagami-m parameter with distance for Micro and Macrocells - Model A, Exponential distribution at 900 MHz

Simulation Parameters:

Simulation Model: Model A

Distribution of reflection co-efficient: Exponential

Carrier Frequency: 1800 MHz

Path Loss Exponent $\alpha_1 = 2$

Additional Path Loss Exponent $\alpha_2 = 4$

Tranmitter Antenna Height $h_t = 50$ m

Receiver Antenna Height $h_r = 3$ m

Average Distance between MS & Scatterers $d_2 = 12$ m

Microcell				
Distance (m)	**Direct Power** (dB)	**Scattered Power** (dB)	**Rician 'K'** (dB)	**Nakagami 'm'** (dB)
100	-26.48	-54.43	27.95	24.95
200	-38.52	-60.52	22.00	19.03
300	-45.56	-64.03	18.47	15.55
400	-50.56	-66.58	16.02	13.17
500	-54.44	-68.44	14.01	11.25
600	-57.60	-70.15	12.54	9.89
700	-60.28	-71.53	11.25	8.71
800	-62.60	-72.63	10.03	7.63
900	-64.65	-73.59	8.94	6.71
1000	-66.48	-74.50	8.02	5.96
Macrocell				
2000	-78.52	-80.60	2.08	2.09E+00
3000	-85.56	-84.06	-1.51	8.19E-01
4000	-90.56	-86.49	-4.07	3.61E-01
5000	-94.44	-88.42	-6.01	1.79E-01
6000	-97.60	-90.00	-7.60	9.69E-02
7000	-100.28	-91.45	-8.83	5.88E-02
8000	-102.60	-92.59	-10.01	3.63E-02
9000	-104.65	-93.60	-11.05	2.34E-02
10000	-106.48	-94.36	-12.12	1.46E-02

Table 4.4: Variations of Nakagami-m parameter with distance for Micro and Macro-cells - Model A, Exponential distribution at 1800 MHz

Simulation Parameters:

Simulation Model: Model A

Distribution of reflection co-efficient: Half Gaussian

Carrier Frequency: 900 MHz

Path Loss Exponent $\alpha_1 = 2$

Additional Path Loss Exponent $\alpha_2 = 4$

Tranmitter Antenna Height $h_t = 50$ m

Receiver Antenna Height $h_r = 3$ m

Average Distance between MS & Scatterers $d_2 = 12$ m

Microcell				
Distance (m)	**Direct Power** (dB)	**Scattered Power** (dB)	**Rician 'K'** (dB)	**Nakagami 'm'** (dB)
100	-26.48	-40.02	13.54	10.81
200	-38.52	-46.13	7.61	5.63
300	-45.56	-49.68	4.11	3.18
400	-50.56	-52.10	1.54	1.84
500	-54.44	-53.96	-0.48	1.10
600	-57.60	-55.65	-1.95	0.72
700	-60.28	-56.98	-3.30	0.47
800	-62.60	-58.15	-4.46	0.32
900	-64.65	-59.08	-5.57	0.21
1000	-66.48	-60.09	-6.39	0.15
Macrocell				
2000	-78.52	-66.15	-12.37	1.31E-02
3000	-85.56	-69.49	-16.07	2.56E-03
4000	-90.56	-71.97	-18.59	8.21E-04
5000	-94.44	-73.98	-20.46	3.49E-04
6000	-97.60	-75.44	-22.16	1.61E-04
7000	-100.28	-76.87	-23.41	9.03E-05
8000	-102.60	-78.00	-24.60	5.22E-05
9000	-104.65	-79.17	-25.47	3.51E-05
10000	-106.48	-80.00	-26.48	2.20E-05

Table 4.5: Variations of Nakagami-m parameter with distance for Micro and Macrocells - Model A, Half Gaussian distribution at 900 MHz

Simulation Parameters:

Simulation Model: Model A

Distribution of reflection co-efficient: Half Gaussian

Carrier Frequency: 1800 MHz

Path Loss Exponent $\alpha_1 = 2$

Additional Path Loss Exponent $\alpha_2 = 4$

Tranmitter Antenna Height $h_t = 50$ m

Receiver Antenna Height $h_r = 3$ m

Average Distance between MS & Scatterers $d_2 = 12$ m

Microcell				
Distance (m)	**Direct Power** (dB)	**Scattered Power** (dB)	**Rician 'K'** (dB)	**Nakagami 'm'** (dB)
100	-26.48	-51.98	25.50	22.51
200	-38.52	-58.11	19.59	16.65
300	-45.56	-61.75	16.19	13.34
400	-50.56	-64.11	13.55	10.82
500	-54.44	-65.93	11.50	8.93
600	-57.60	-67.70	10.09	7.69
700	-60.28	-68.93	8.65	6.47
800	-62.60	-70.11	7.51	5.55
900	-64.65	-71.20	6.55	4.83
1000	-66.48	-72.23	5.76	4.25
Macrocell				
2000	-78.52	-78.15	-0.37	1.13E+00
3000	-85.56	-81.66	-3.90	3.81E-01
4000	-90.56	-84.04	-6.52	1.48E-01
5000	-94.44	-86.13	-8.31	7.30E-02
6000	-97.60	-87.66	-9.95	3.70E-02
7000	-100.28	-89.11	-11.17	2.21E-02
8000	-102.60	-90.12	-12.48	1.25E-02
9000	-104.65	-91.15	-13.50	8.11E-03
10000	-106.48	-92.14	-14.34	5.52E-03

Table 4.6: Variations of Nakagami-m parameter with distance for Micro and Macrocells - Model A, Half Gaussian distribution at 1800 MHz

Simulation Parameters:

Simulation Model: Model B

Distribution of reflection co-efficient: Uniform

Carrier Frequency: 900 MHz

Path Loss Exponent $\alpha_1 = 2$

Additional Path Loss Exponent $\alpha_2 = 4$

Tranmitter Antenna Height $h_t = 50$ m

Receiver Antenna Height $h_r = 3$ m

Average Distance between MS & Scatterers $d_2 = 16$ m

Microcell				
Distance (m)	**Direct Power** (dB)	**Scattered Power** (dB)	**Rician 'K'** (dB)	**Nakagami 'm'** (dB)
100	-26.48	-44.72	18.24	15.33
200	-38.52	-50.78	12.26	9.63
300	-45.56	-54.24	8.67	6.49
400	-50.56	-56.80	6.24	4.60
500	-54.44	-58.63	4.19	3.23
600	-57.60	-60.24	2.63	2.36
700	-60.28	-61.52	1.24	1.71
800	-62.60	-62.80	0.20	1.32
900	-64.65	-63.78	-0.86	0.99
1000	-66.48	-64.65	-1.83	0.74
Macrocell				
2000	-78.52	-70.80	-7.72	9.25E-02
3000	-85.56	-74.13	-11.43	1.97E-02
4000	-90.56	-76.75	-13.81	6.99E-03
5000	-94.44	-78.58	-15.86	2.80E-03
6000	-97.60	-80.25	-17.35	1.44E-03
7000	-100.28	-81.59	-18.69	7.86E-04
8000	-102.60	-82.66	-19.94	4.41E-04
9000	-104.65	-83.67	-20.98	2.76E-04
10000	-106.48	-84.63	-21.85	1.86E-04

Table 4.7: Variations of Nakagami-m parameter with distance for Micro and Macrocells - Model B, Uniform distribution at 900 MHz

Simulation Parameters:

Simulation Model: Model B

Distribution of reflection co-efficient: Uniform

Carrier Frequency: 1800 MHz

Path Loss Exponent $\alpha_1 = 2$

Additional Path Loss Exponent $\alpha_2 = 4$

Tranmitter Antenna Height $h_t = 50$ m

Receiver Antenna Height $h_r = 3$ m

Average Distance between MS & Scatterers $d_2 = 16$ m

Microcell				
Distance (m)	**Direct Power** (dB)	**Scattered Power** (dB)	**Rician 'K'** (dB)	**Nakagami 'm'** (dB)
100	-26.48	-56.55	30.07	27.07
200	-38.52	-62.79	24.27	21.29
300	-45.56	-66.16	20.60	17.65
400	-50.56	-68.76	18.20	15.29
500	-54.44	-70.77	16.34	13.48
600	-57.60	-72.22	14.62	11.83
700	-60.28	-73.75	13.46	10.74
800	-62.60	-74.79	12.18	9.56
900	-64.65	-75.79	11.14	8.61
1000	-66.48	-76.64	10.17	7.75
Macrocell				
2000	-78.52	-82.67	4.15	3.20E+00
3000	-85.56	-86.32	0.76	1.52E+00
4000	-90.56	-88.70	-1.86	7.37E-01
5000	-94.44	-90.66	-3.78	3.98E-01
6000	-97.60	-92.29	-5.31	2.32E-01
7000	-100.28	-93.68	-6.60	1.44E-01
8000	-102.60	-94.89	-7.72	9.27E-02
9000	-104.65	-95.90	-8.75	6.09E-02
10000	-106.48	-96.65	-9.83	3.90E-02

Table 4.8: Variations of Nakagami-m parameter with distance for Micro and Macro-cells - Model B, Uniform distribution at 1800 MHz

Simulation Parameters:

Simulation Model: Model B

Distribution of reflection co-efficient: Exponential

Carrier Frequency: 900 MHz

Path Loss Exponent $\alpha_1 = 2$

Additional Path Loss Exponent $\alpha_2 = 4$

Tranmitter Antenna Height $h_t = 50$ m

Receiver Antenna Height $h_r = 3$ m

Average Distance between MS & Scatterers $d_2 = 16$ m

Microcell				
Distance (m)	**Direct Power** (dB)	**Scattered Power** (dB)	**Rician 'K'** (dB)	**Nakagami 'm'** (dB)
100	-26.48	-49.87	23.39	20.41
200	-38.52	-55.99	17.47	14.57
300	-45.56	-59.55	13.98	11.23
400	-50.56	-62.12	11.56	8.99
500	-54.44	-64.00	9.56	7.23
600	-57.60	-65.58	7.98	5.92
700	-60.28	-66.94	6.65	4.90
800	-62.60	-68.01	5.40	4.01
900	-64.65	-69.02	4.38	3.34
1000	-66.48	-69.95	3.47	2.81
Macrocell				
2000	-78.52	-75.97	-2.55	5.98E-01
3000	-85.56	-79.40	-6.16	1.69E-01
4000	-90.56	-82.06	-8.50	6.75E-02
5000	-94.44	-83.87	-10.56	2.86E-02
6000	-97.60	-85.50	-12.11	1.48E-02
7000	-100.28	-86.83	-13.46	8.17E-03
8000	-102.60	-87.84	-14.76	4.58E-03
9000	-104.65	-88.97	-15.68	3.05E-03
10000	-106.48	-90.03	-16.45	2.16E-03

Table 4.9: Variations of Nakagami-m parameter with distance for Micro and Macro-cells - Model B, Exponential distribution at 900 MHz

Simulation Parameters:

Simulation Model: Model B

Distribution of reflection co-efficient: Exponential

Carrier Frequency: 1800 MHz

Path Loss Exponent $\alpha_1 = 2$

Additional Path Loss Exponent $\alpha_2 = 4$

Tranmitter Antenna Height $h_t = 50$ m

Receiver Antenna Height $h_r = 3$ m

Average Distance between MS & Scatterers $d_2 = 16$ m

Microcell				
Distance (m)	**Direct Power** (dB)	**Scattered Power** (dB)	**Rician 'K'** (dB)	**Nakagami 'm'** (dB)
100	-26.48	-61.96	35.49	32.48
200	-38.52	-68.13	29.61	26.61
300	-45.56	-71.58	26.02	23.03
400	-50.56	-74.10	23.54	20.56
500	-54.44	-75.96	21.52	18.56
600	-57.60	-77.52	19.92	16.97
700	-60.28	-78.80	18.52	15.60
800	-62.60	-80.18	17.58	14.68
900	-64.65	-81.09	16.44	13.58
1000	-66.48	-81.98	15.51	12.68
Macrocell				
2000	-78.52	-88.09	9.57	7.24E+00
3000	-85.56	-91.55	5.98	4.41E+00
4000	-90.56	-94.11	3.55	2.85E+00
5000	-94.44	-96.04	1.60	1.87E+00
6000	-97.60	-97.49	-0.11	1.22E+00
7000	-100.28	-98.96	-1.32	8.66E-01
8000	-102.60	-99.97	-2.63	5.80E-01
9000	-104.65	-101.17	-3.48	4.42E-01
10000	-106.48	-102.10	-4.37	3.24E-01

Table 4.10: Variations of Nakagami-m parameter with distance for Micro and Macrocells - Model B, Exponential distribution at 1800 MHz

Simulation Parameters:

Simulation Model: Model B

Distribution of reflection co-efficient: Half Gaussian

Carrier Frequency: 900 MHz

Path Loss Exponent $\alpha_1 = 2$

Additional Path Loss Exponent $\alpha_2 = 4$

Tranmitter Antenna Height $h_t = 50$ m

Receiver Antenna Height $h_r = 3$ m

Average Distance between MS & Scatterers $d_2 = 16$ m

Microcell				
Distance (m)	**Direct Power** (dB)	**Scattered Power** (dB)	**Rician 'K'** (dB)	**Nakagami 'm'** (dB)
100	-26.48	-47.60	21.13	18.16
200	-38.52	-53.56	15.04	12.23
300	-45.56	-57.12	11.56	8.98
400	-50.56	-59.68	9.12	6.85
500	-54.44	-61.52	7.09	5.22
600	-57.60	-63.03	5.42	4.02
700	-60.28	-64.41	4.13	3.19
800	-62.60	-65.49	2.88	2.49
900	-64.65	-66.56	1.91	2.01
1000	-66.48	-67.51	1.03	1.63
Macrocell				
2000	-78.52	-73.56	-4.96	2.63E-01
3000	-85.56	-77.09	-8.47	6.82E-02
4000	-90.56	-79.56	-11.01	2.37E-02
5000	-94.44	-81.56	-12.87	1.05E-02
6000	-97.60	-83.19	-14.41	5.38E-03
7000	-100.28	-84.51	-15.77	2.91E-03
8000	-102.60	-85.65	-16.95	1.73E-03
9000	-104.65	-86.50	-18.15	9.98E-04
10000	-106.48	-87.59	-18.89	7.09E-04

Table 4.11: Variations of Nakagami-m parameter with distance for Micro and Macrocells - Model B, Half Gaussian distribution at 900 MHz

Simulation Parameters:

Simulation Model: Model B

Distribution of reflection co-efficient: Half Gaussian

Carrier Frequency: 1800 MHz

Path Loss Exponent $\alpha_1 = 2$

Additional Path Loss Exponent $\alpha_2 = 4$

Tranmitter Antenna Height $h_t = 50$ m

Receiver Antenna Height $h_r = 3$ m

Average Distance between MS & Scatterers $d_2 = 16$ m

Microcell				
Distance (m)	**Direct Power** (dB)	**Scattered Power** (dB)	**Rician 'K'** (dB)	**Nakagami 'm'** (dB)
100	-26.48	-59.47	32.99	29.99
200	-38.52	-65.57	27.05	24.05
300	-45.56	-69.06	23.50	20.52
400	-50.56	-71.71	21.15	18.19
500	-54.44	-73.60	19.17	16.23
600	-57.60	-75.11	17.51	14.61
700	-60.28	-76.41	16.13	13.27
800	-62.60	-77.61	15.00	12.20
900	-64.65	-78.64	14.00	11.24
1000	-66.48	-79.58	13.10	10.40
Macrocell				
2000	-78.52	-85.74	7.22	5.32E+00
3000	-85.56	-89.20	3.64	2.90E+00
4000	-90.56	-91.67	1.11	1.66E+00
5000	-94.44	-93.51	-0.92	9.74E-01
6000	-97.60	-95.01	-2.59	5.88E-01
7000	-100.28	-96.44	-3.84	3.90E-01
8000	-102.60	-97.62	-4.98	2.61E-01
9000	-104.65	-98.73	-5.92	1.85E-01
10000	-106.48	-99.55	-6.93	1.27E-01

Table 4.12: Variations of Nakagami-m parameter with distance for Micro and Macrocells - Model B, Half Gaussian distribution at 1800 MHz

Simulation Parameters:

Simulation Model: Model C

Distribution of reflection co-efficient: Uniform

Carrier Frequency: 900 MHz

Path Loss Exponent $\alpha_1 = 2$

Additional Path Loss Exponent $\alpha_2 = 4$

Tranmitter Antenna Height $h_t = 40$ m

Receiver Antenna Height $h_r = 5$ m

Average Distance between MS & Scatterers $d_2 = 12$ m

Microcell				
Distance (m)	**Direct Power** (dB)	**Scattered Power** (dB)	**Rician 'K'** (dB)	**Nakagami 'm'** (dB)
100	-23.98	-37.15	13.17	10.46
200	-36.02	-43.12	7.10	5.23
300	-43.06	-46.56	3.49	2.82
400	-48.06	-49.12	1.06	1.64
500	-51.94	-51.25	-0.69	1.04
600	-55.11	-52.72	-2.38	0.63
700	-57.78	-54.07	-3.72	0.41
800	-60.10	-55.17	-4.93	0.27
900	-62.15	-56.21	-5.94	0.18
1000	-63.98	-57.30	-6.68	0.14
Macrocell				
2000	-76.02	-63.20	-12.82	1.08E-02
3000	-83.06	-66.71	-16.36	2.24E-03
4000	-88.06	-69.14	-18.93	7.06E-04
5000	-91.94	-71.08	-20.86	2.89E-04
6000	-95.11	-72.74	-22.36	1.46E-04
7000	-97.78	-74.10	-23.68	7.96E-05
8000	-100.10	-75.18	-24.92	4.52E-05
9000	-102.15	-76.30	-25.85	2.95E-05
10000	-103.98	-77.15	-26.83	1.88E-05

Table 4.13: Variations of Nakagami-m parameter with distance for Micro and Macrocells - Model C, Uniform distribution at 900 MHz

Simulation Parameters:

Simulation Model: Model C

Distribution of reflection co-efficient: Uniform

Carrier Frequency: 1800 MHz

Path Loss Exponent $\alpha_1 = 2$

Additional Path Loss Exponent $\alpha_2 = 4$

Tranmitter Antenna Height $h_t = 40$ m

Receiver Antenna Height $h_r = 5$ m

Average Distance between MS & Scatterers $d_2 = 12$ m

Microcell				
Distance (m)	**Direct Power** (dB)	**Scattered Power** (dB)	**Rician 'K'** (dB)	**Nakagami 'm'** (dB)
100	-23.98	-49.32	25.34	22.35
200	-36.02	-55.28	19.26	16.33
300	-43.06	-58.82	15.75	12.91
400	-48.06	-61.22	13.16	10.45
500	-51.94	-63.15	11.21	8.67
600	-55.11	-64.68	9.57	7.24
700	-57.78	-66.12	8.34	6.21
800	-60.10	-67.32	7.21	5.32
900	-62.15	-68.29	6.14	4.53
1000	-63.98	-69.21	5.23	3.89
Macrocell				
2000	-76.02	-75.23	-0.79	1.01E+00
3000	-83.06	-78.72	-4.34	3.28E-01
4000	-88.06	-81.26	-6.81	1.33E-01
5000	-91.94	-83.11	-8.83	5.91E-02
6000	-95.11	-84.77	-10.33	3.18E-02
7000	-97.78	-86.15	-11.63	1.82E-02
8000	-100.10	-87.26	-12.84	1.07E-02
9000	-102.15	-88.40	-13.75	7.16E-03
10000	-103.98	-89.21	-14.77	4.57E-03

Table 4.14: Variations of Nakagami-m parameter with distance for Micro and Macrocells - Model C, Uniform distribution at 1800 MHz

Simulation Parameters:

Simulation Model: Model C

Distribution of reflection co-efficient: Exponential

Carrier Frequency: 900 MHz

Path Loss Exponent $\alpha_1 = 2$

Additional Path Loss Exponent $\alpha_2 = 4$

Tranmitter Antenna Height $h_t = 40$ m

Receiver Antenna Height $h_r = 5$ m

Average Distance between MS & Scatterers $d_2 = 12$ m

Microcell				
Distance (m)	**Direct Power** (dB)	**Scattered Power** (dB)	**Rician 'K'** (dB)	**Nakagami 'm'** (dB)
100	-23.98	-42.49	18.51	15.59
200	-36.02	-48.58	12.56	9.90
300	-43.06	-52.07	9.00	6.76
400	-48.06	-54.46	6.40	4.71
500	-51.94	-56.38	4.44	3.39
600	-55.11	-58.06	2.95	2.52
700	-57.78	-59.46	1.67	1.90
800	-60.10	-60.54	0.44	1.33
900	-62.15	-61.58	-0.57	1.07
1000	-63.98	-62.57	-1.41	0.84
Macrocell				
2000	-76.02	-68.45	-7.57	9.79E-02
3000	-83.06	-72.06	-11.00	2.37E-02
4000	-88.06	-74.48	-13.58	7.75E-03
5000	-91.94	-76.35	-15.59	3.16E-03
6000	-95.11	-77.89	-17.22	1.52E-03
7000	-97.78	-79.26	-18.53	8.39E-04
8000	-100.10	-80.52	-19.59	5.19E-04
9000	-102.15	-81.45	-20.70	3.12E-04
10000	-103.98	-82.61	-21.37	2.31E-04

Table 4.15: Variations of Nakagami-m parameter with distance for Micro and Macrocells - Model C, Exponential distribution at 900 MHz

Simulation Parameters:

Simulation Model: Model C

Distribution of reflection co-efficient: Exponential

Carrier Frequency: 1800 MHz

Path Loss Exponent $\alpha_1 = 2$

Additional Path Loss Exponent $\alpha_2 = 4$

Tranmitter Antenna Height $h_t = 40$ m

Receiver Antenna Height $h_r = 5$ m

Average Distance between MS & Scatterers $d_2 = 12$ m

Microcell				
Distance (m)	**Direct Power** (dB)	**Scattered Power** (dB)	**Rician 'K'** (dB)	**Nakagami 'm'** (dB)
100	-23.98	-54.43	30.45	27.44
200	-36.02	-60.51	24.49	21.51
300	-43.06	-64.08	21.02	18.06
400	-48.06	-66.64	18.58	15.66
500	-51.94	-68.48	16.54	13.67
600	-55.11	-70.09	14.99	12.18
700	-57.78	-71.49	13.71	10.97
800	-60.10	-72.63	12.53	9.87
900	-62.15	-73.61	11.46	8.90
1000	-63.98	-74.59	10.61	8.14
Macrocell				
2000	-76.02	-80.42	4.40	3.36E+00
3000	-83.06	-84.08	1.02	1.62E+00
4000	-88.06	-86.57	-1.50	8.24E-01
5000	-91.94	-88.53	-3.41	4.50E-01
6000	-95.11	-89.95	-5.16	2.45E-01
7000	-97.78	-91.48	-6.31	1.61E-01
8000	-100.10	-92.65	-7.45	1.03E-01
9000	-102.15	-93.66	-8.49	6.81E-02
10000	-103.98	-94.54	-9.44	4.60E-02

Table 4.16: Variations of Nakagami-m parameter with distance for Micro and Macrocells - Model C, Exponential distribution at 1800 MHz

Simulation Parameters:

Simulation Model: Model C

Distribution of reflection co-efficient: Half Gaussian

Carrier Frequency: 900 MHz

Path Loss Exponent $\alpha_1 = 2$

Additional Path Loss Exponent $\alpha_2 = 4$

Tranmitter Antenna Height $h_t = 40$ m

Receiver Antenna Height $h_r = 5$ m

Average Distance between MS & Scatterers $d_2 = 12$ m

Microcell				
Distance (m)	**Direct Power** (dB)	**Scattered Power** (dB)	**Rician 'K'** (dB)	**Nakagami 'm'** (dB)
100	-23.98	-40.01	16.03	13.18
200	-36.02	-46.14	10.12	7.71
300	-43.06	-49.70	6.63	4.88
400	-48.06	-52.10	4.03	3.13
500	-51.94	-53.94	2.00	2.05
600	-55.11	-55.64	0.54	1.44
700	-57.78	-56.98	-0.81	1.00
800	-60.10	-58.13	-1.98	0.71
900	-62.15	-59.07	-3.08	0.50
1000	-63.98	-60.06	-3.92	0.38
Macrocell				
2000	-76.02	-66.02	-10.00	3.64E-02
3000	-83.06	-69.43	-13.63	7.58E-03
4000	-88.06	-72.00	-16.06	2.57E-03
5000	-91.94	-73.95	-17.99	1.07E-03
6000	-95.11	-75.65	-19.46	5.51E-04
7000	-97.78	-76.88	-20.91	2.83E-04
8000	-100.10	-78.16	-21.94	1.76E-04
9000	-102.15	-79.06	-23.09	1.05E-04
10000	-103.98	-79.98	-24.00	6.93E-05

Table 4.17: Variations of Nakagami-m parameter with distance for Micro and Macrocells - Model C, Half Gaussian distribution at 900 MHz

Simulation Parameters:

Simulation Model: Model C

Distribution of reflection co-efficient: Half Gaussian

Carrier Frequency: 1800 MHz

Path Loss Exponent $\alpha_1 = 2$

Additional Path Loss Exponent $\alpha_2 = 4$

Tranmitter Antenna Height $h_t = 40$ m

Receiver Antenna Height $h_r = 5$ m

Average Distance between MS & Scatterers $d_2 = 12$ m

Microcell				
Distance (m)	**Direct Power** (dB)	**Scattered Power** (dB)	**Rician 'K'** (dB)	**Nakagami 'm'** (dB)
100	-23.98	-51.94	27.96	24.96
200	-36.02	-58.15	22.13	19.16
300	-43.06	-61.81	18.75	15.83
400	-48.06	-64.15	16.09	13.24
500	-51.94	-65.99	14.05	11.29
600	-55.11	-67.63	12.52	9.87
700	-57.78	-68.99	11.21	8.67
800	-60.10	-70.13	10.02	7.63
900	-62.15	-71.23	9.08	6.82
1000	-63.98	-72.19	8.21	6.11
Macrocell				
2000	-76.02	-78.09	2.07	2.09E+00
3000	-83.06	-81.62	-1.45	8.33E-01
4000	-88.06	-84.19	-3.88	3.85E-01
5000	-91.94	-86.05	-5.89	1.87E-01
6000	-95.11	-87.64	-7.47	1.03E-01
7000	-97.78	-89.07	-8.71	6.18E-02
8000	-100.10	-90.22	-9.88	3.83E-02
9000	-102.15	-91.24	-10.91	2.47E-02
10000	-103.98	-91.95	-12.03	1.53E-02

Table 4.18: Variations of Nakagami-m parameter with distance for Micro and Macrocells - Model C, Half Gaussian distribution at 1800 MHz

4.5 Comparison of different modulation schemes over Flat Fading Nakagami-m channel with known m at different distances

In this section, the performance of different modulation schemes over flat fading Nakagami-m channel is studied. For simulation purposes, we considered *QPSK*, *8PSK* and *16QAM*, operating at two different frequencies $900MHz$ and $1800MHz$ with 3 distributions of the reflection coefficient Γ described earlier (i.e. Unifrom, Exponential and Half Gaussian). From here on, we will study the error performance of different MPSK and QAM modulation schemes only for Model A at the specified distances both for micro and macrocellular structures. The behavior of model B and model C can be derived by looking at the tabular representation of m variations with distance (see tables (4.7 to 4.18)). The microcellular structure is divided into $200m$, $500m$ and $800m$ while the macrocellular structure is divided into $2km$, $5km$ and $8km$. It is observed from figures (4.29 to 4.43) that at shorter distances and larger values of m, the error rate is reduced considerably while as the mobile station moves away from the base station and the distance between them increases, the values of m get close to $1(0dB)$ and each modulation scheme gets closer to its performance in Rayleigh environment.

It is of importance to know that m changes by how many dBs as we move from

one operating frequency to another in a cellular environment for a particular description of the reflection co-efficient (Uniform, Exponential or Half Gaussian). The value of m decays almost exponentially as the distance increases, so how quickly this value gets close to $0dB$ should effect the performance of the communication system significantly. When Γ is exponentially distributed, it can be seen from figures (4.1 to 4.4) that the value of m gets close to $0dB$ quicker than any other distribution of the reflection co-efficient. So, a particular error rate for any modulation scheme is acheived at lower value of SNR, if exponentially distributed reflection co-efficient Γ is used.

This is shown with the help of figures (4.31), (4.36) and (4.41). In order to achieve an error rate of 10^{-4} for QPSK at $d = 800m$ for $f = 1800MHz$, the exponential distribution of the reflection co-efficient gives this BER at almost $10dB$ SNR, while the uniform distribution gives this error rate at $19dB$.

From the performance of different modulation schemes in microcell environment ($200m$, $500m$, and $800m$), the difference between the Nakagami parameter m at $900MHz$ and at $1800MHz$ is quite large ($> 2dB$) thereby acheiving the desired error rate at lower values of SNR. However, if we move to macrocellular distances ($2km$, $5km$ and $8km$), this difference in the value of m decreases thereby providing no considerable improvement in the error rate while operating at higher frequency. Therefore, it is inferred that the parameter Δm (rate of change of m) is of paramount importance in order to study the performance of any digital communication system.

It is observed from figure (4.32) that at $d = 2km$, as we move from $900MHz$ to $1800MHz$, the difference in Nakagami-m parameter is very small ($0.47dBs$) for uniform distribution of reflection co-efficient and there is no considerable improvement in the error rate for any modulation scheme if we operate at a higher frequency. But if we look at the same distance of $d = 2km$, the exponential distribution of the reflection co-efficient (see figure (4.37)), we observe that a particular bit error rate for the desired modulation scheme is acheived at a lower SNR at a higher frequency than at a lower frequency, since the parameter Δm has a value of $2.0543dB$. Similar behavior can be observed from figure (4.42) in which the distribution of the reflection coefficient is half Gaussian and Δm is approximately $1.1169dB$. Similarly, at higher distances where the difference in parameter Δm is lower than $2dB$, there is no considerable improvement in the bit error rate of a particular modulation scheme if we move from lower to higher frequency.

So, there exist a relationship between the system performance parameter BER and the difference in the Nakagami-m parameter Δm for operating at a particular frequency at a certain distance in a cell. And this relationship depends on four parameters:

- the distribution of reflection co-efficient
- the transmitter antenna height
- the receiver antenna height

- the distance between the mobile and the scatterers

Other parameters such as the path loss exponent also effects the performance of the system depending on the terrain type and material surfaces.

For microcellular structure, figures (4.29, 4.34, and 4.39) represent a comparison between different modulation schemes while operating at different frequencies. It also describes the SNR penalty given while moving from one modulation scheme to another at a particular link distance d defined by Nakagami parameter m. It is observed that 8PSK need $5-7dB$ more signal power as compared to QPSK and $1-2dB$ less signal power than 16QAM to acheive the same value of BER depending on the distribution of the reflection co-efficient.

Figures (4.44 to 4.61) gives 3D representation of the error performance of different modulation schemes with the increase in distance. The x-axis represents the distance in log scale, the y-axis represents the SNR and the z-axis represents the Average BER. It is observed from the set of figures that for shorter distances and higher values of m, operating at higher frequencies with Γ exponentially distributed gives better error rates for a specified modulation scheme.

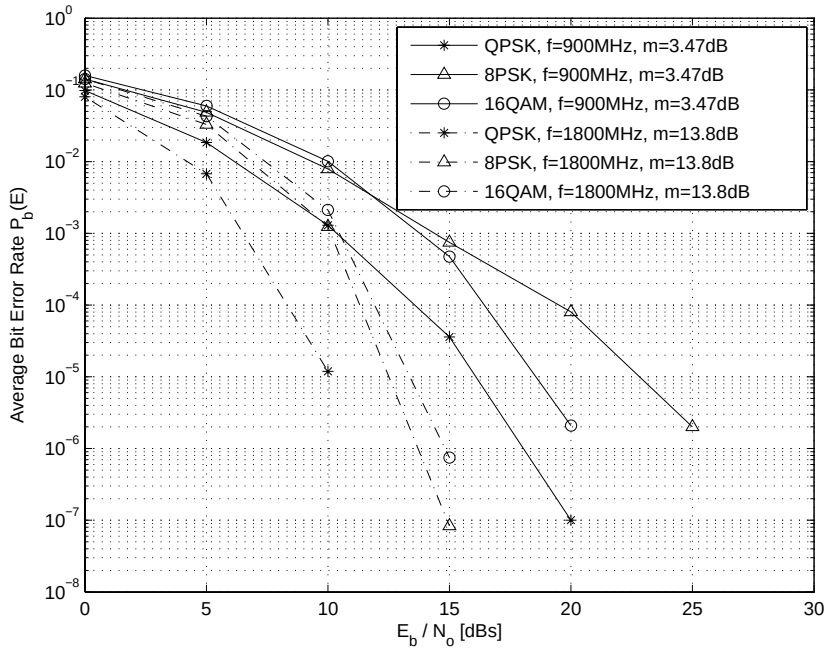

Figure 4.29: Comparison of different modulation schemes over Flat Fading Nakagami-m channel, $d = 200m$, Γ Uniform

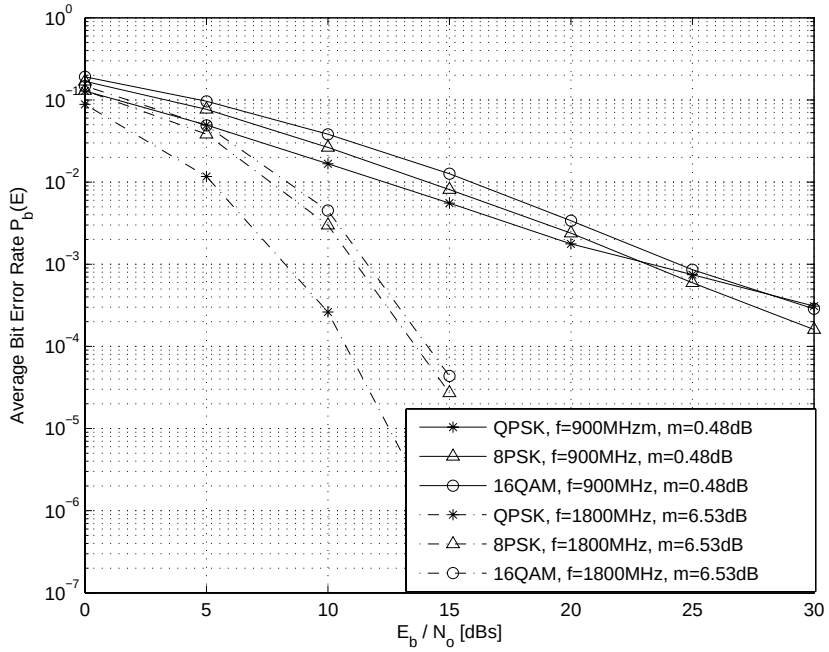

Figure 4.30: Comparison of different modulation schemes over Flat Fading Nakagami-m channel, $d = 500m$, Γ Uniform

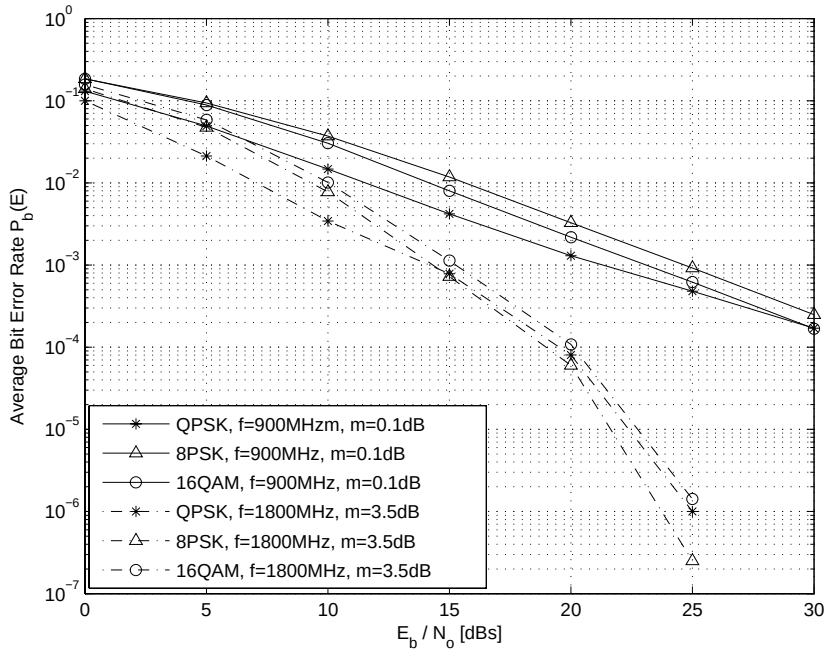

Figure 4.31: Comparison of different modulation schemes over Flat Fading Nakagami-m channel, $d = 800m$, Γ Uniform

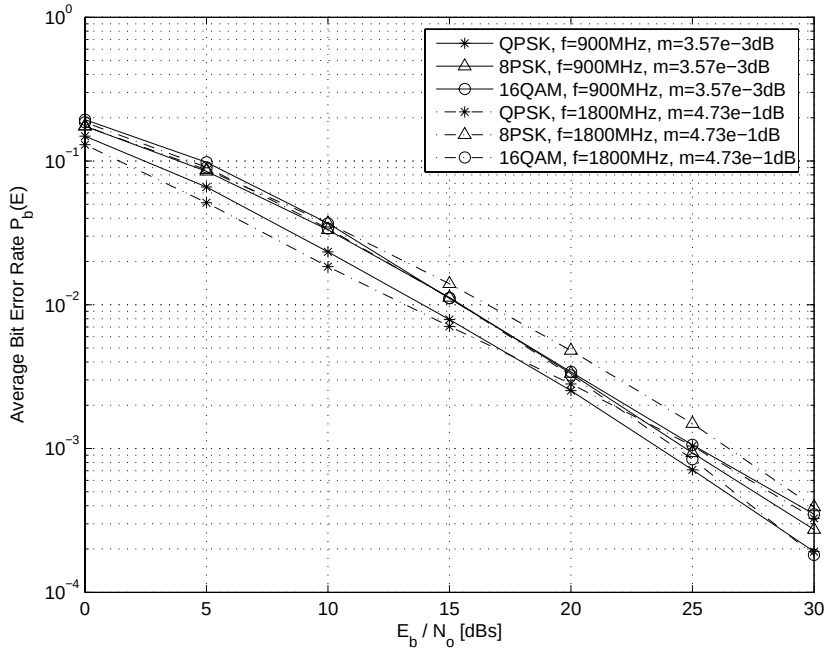

Figure 4.32: Comparison of different modulation schemes over Flat Fading Nakagami-m channel, $d = 2km$, Γ Uniform

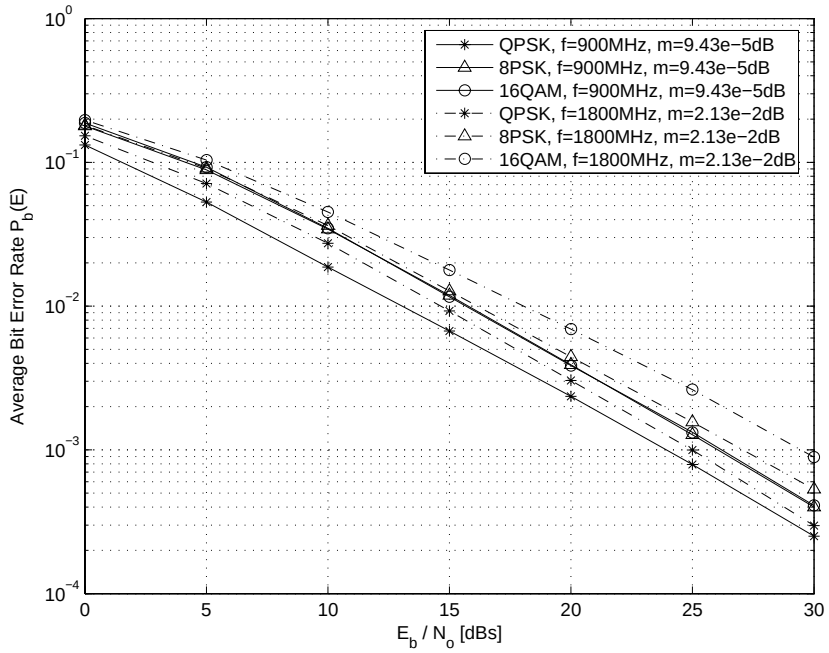

Figure 4.33: Comparison of different modulation schemes over Flat Fading Nakagami-m channel, $d = 5km$, Γ Uniform

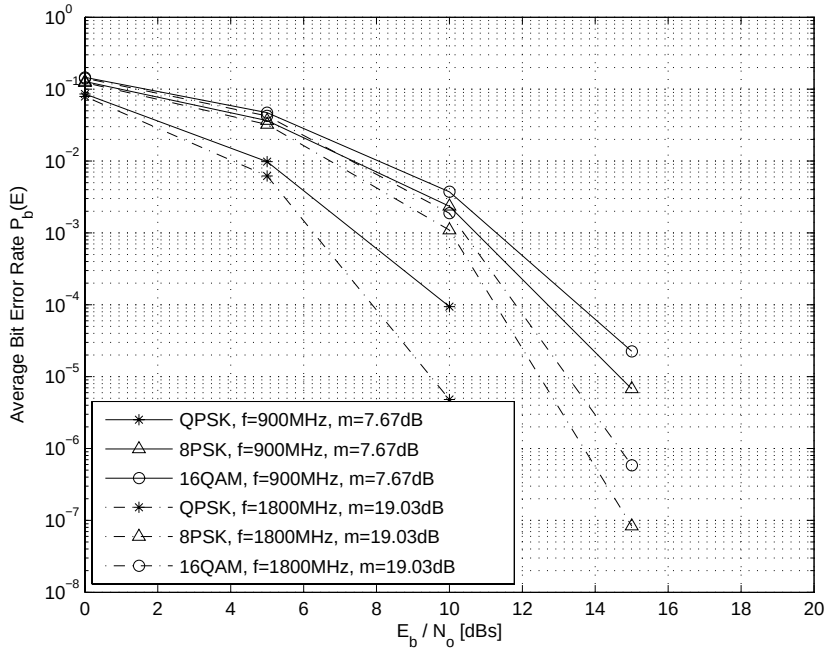

Figure 4.34: Comparison of different modulation schemes over Flat Fading Nakagami-m channel, $d = 200m$, Γ Exponential

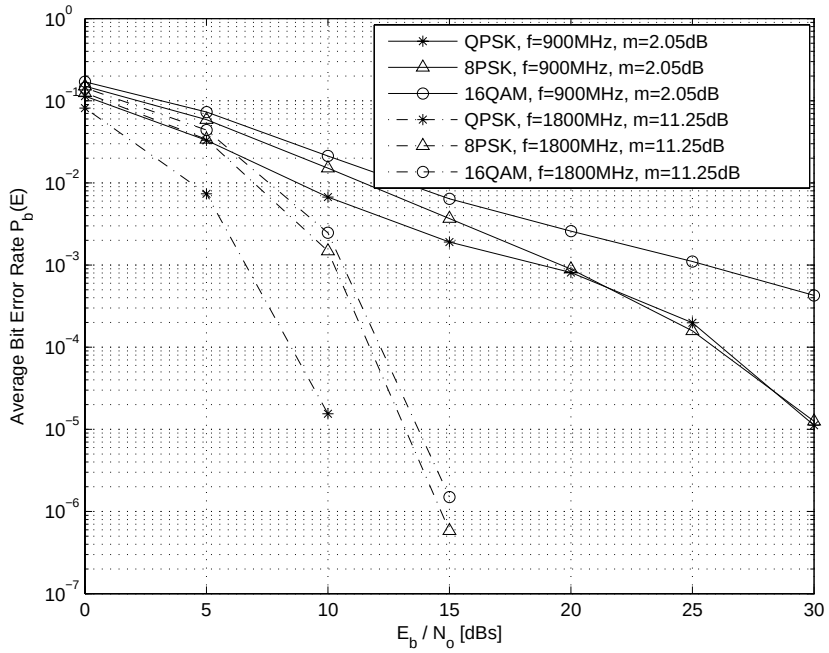

Figure 4.35: Comparison of different modulation schemes over Flat Fading Nakagami-m channel, $d = 500m$, Γ Exponential

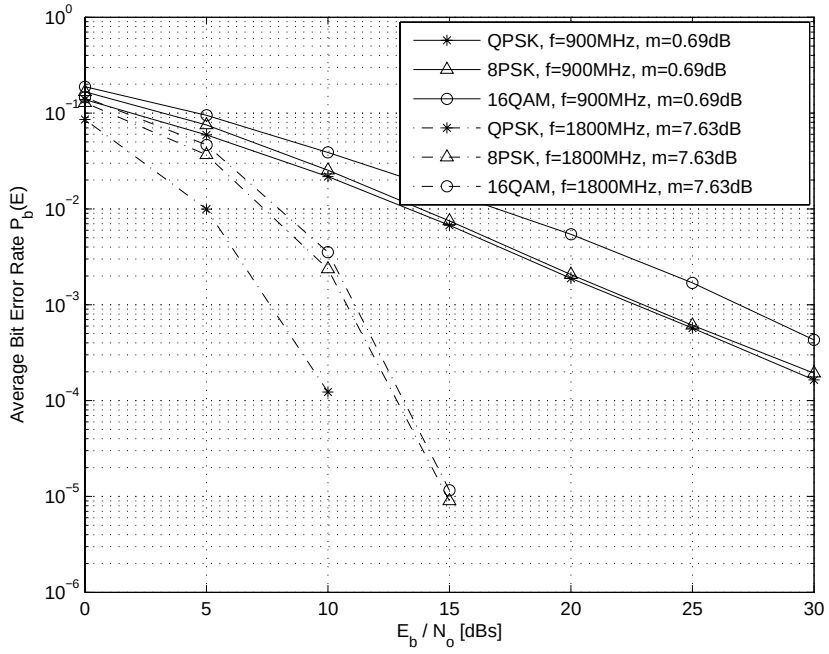

Figure 4.36: Comparison of different modulation schemes over Flat Fading Nakagami-m channel, $d = 800m$, Γ Exponential

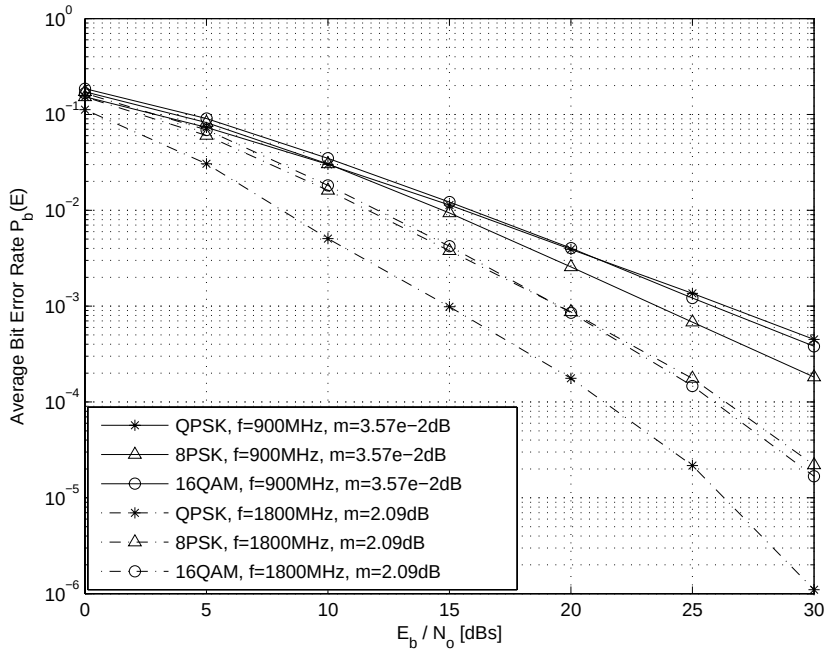

Figure 4.37: Comparison of different modulation schemes over Flat Fading Nakagami-m channel, $d = 2km$, Γ Exponential

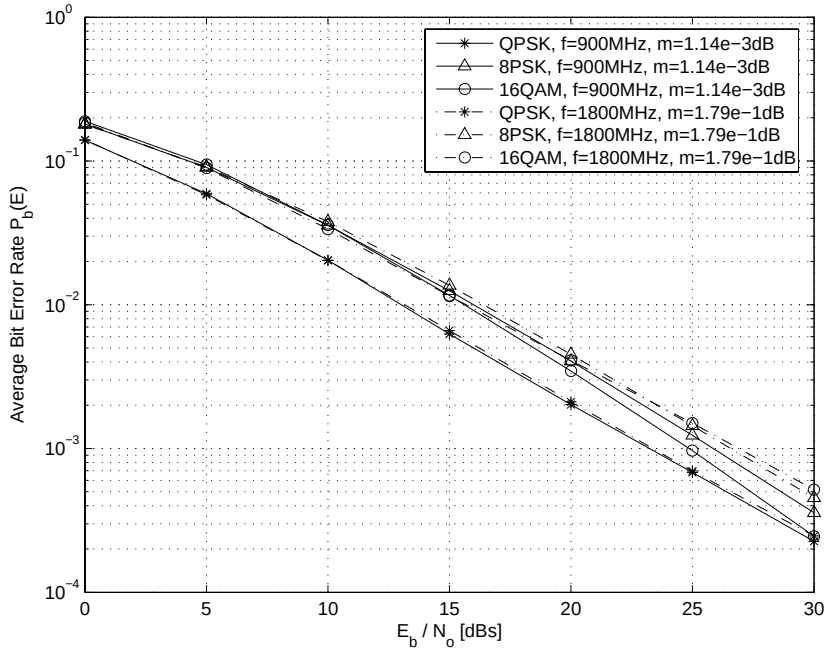

Figure 4.38: Comparison of different modulation schemes over Flat Fading Nakagami-m channel, $d = 5km$, Γ Exponential

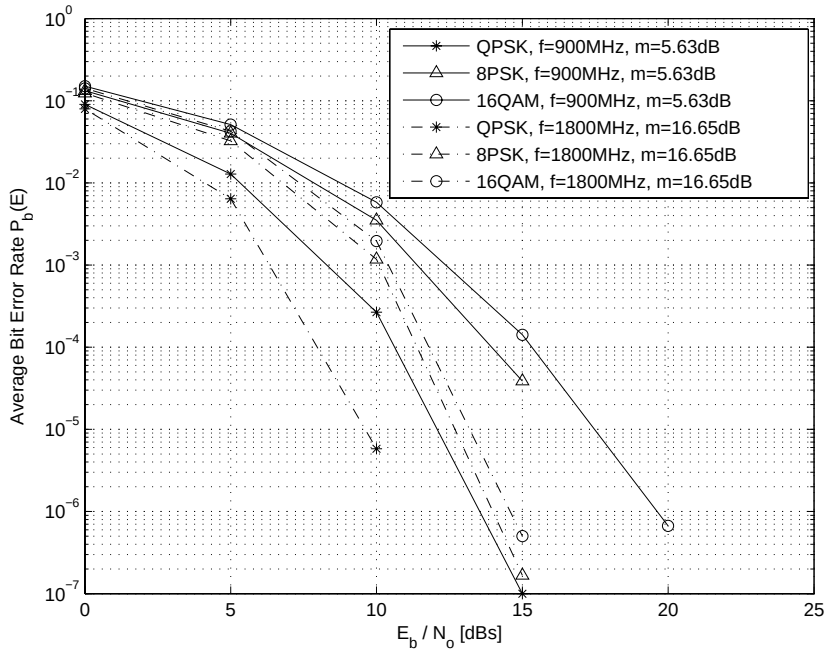

Figure 4.39: Comparison of different modulation schemes over Flat Fading Nakagami-m channel, $d = 200m$, Γ Half Gaussian

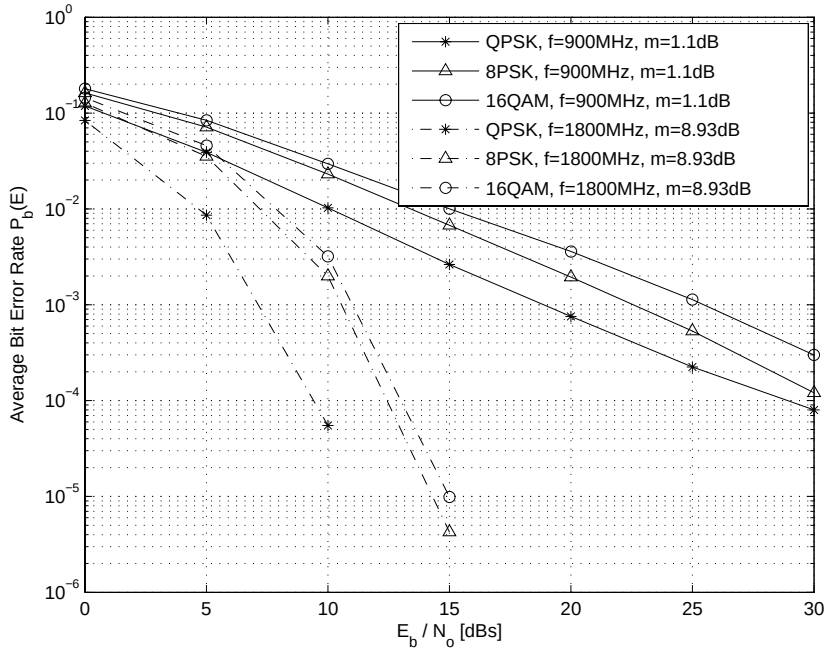

Figure 4.40: Comparison of different modulation schemes over Flat Fading Nakagami-m channel, $d = 500m$, Γ Half Gaussian

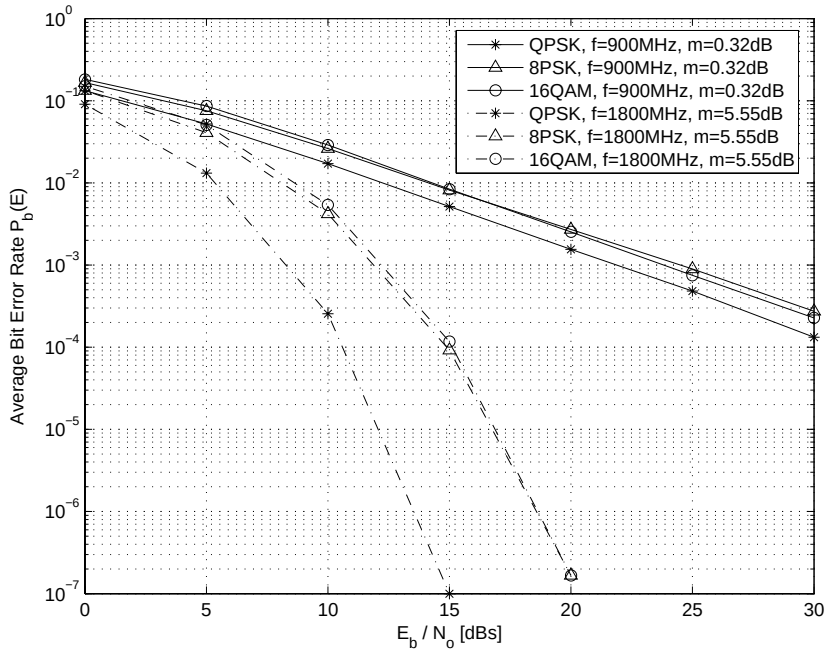

Figure 4.41: Comparison of different modulation schemes over Flat Fading Nakagami-m channel, $d = 800m$, Γ Half Gaussian

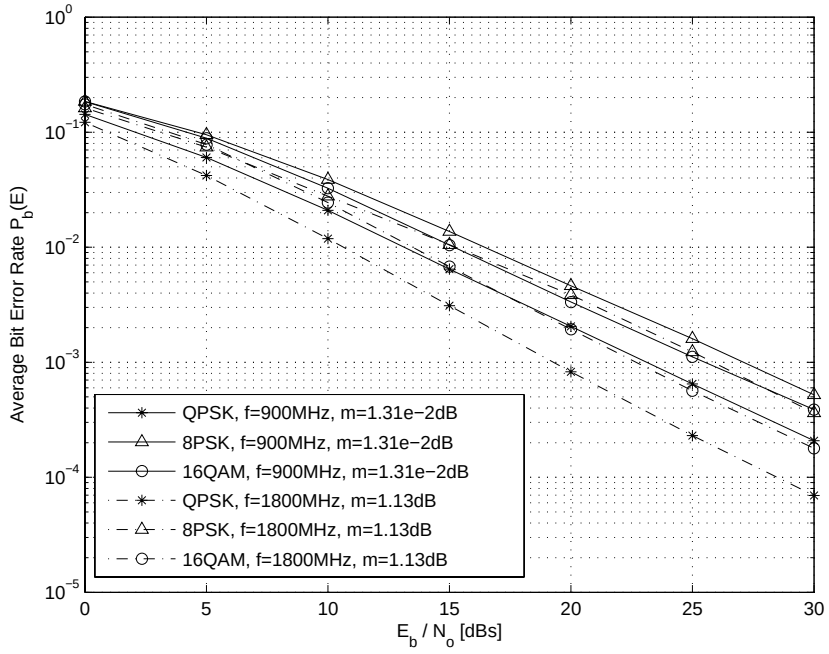

Figure 4.42: Comparison of different modulation schemes over Flat Fading Nakagami-m channel, $d = 2km$, Γ Half Gaussian

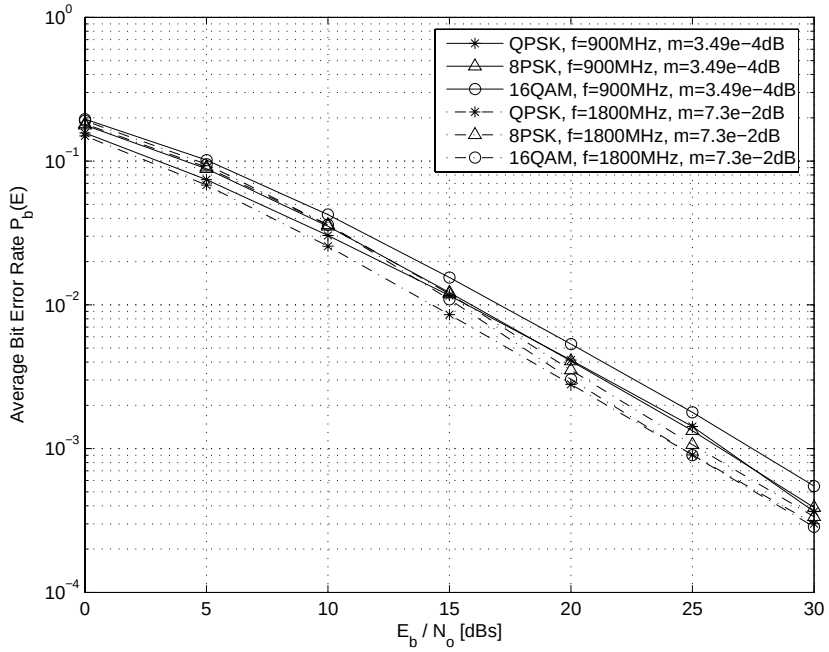

Figure 4.43: Comparison of different modulation schemes over Flat Fading Nakagami-m channel, $d = 5km$, Γ Half Gaussian

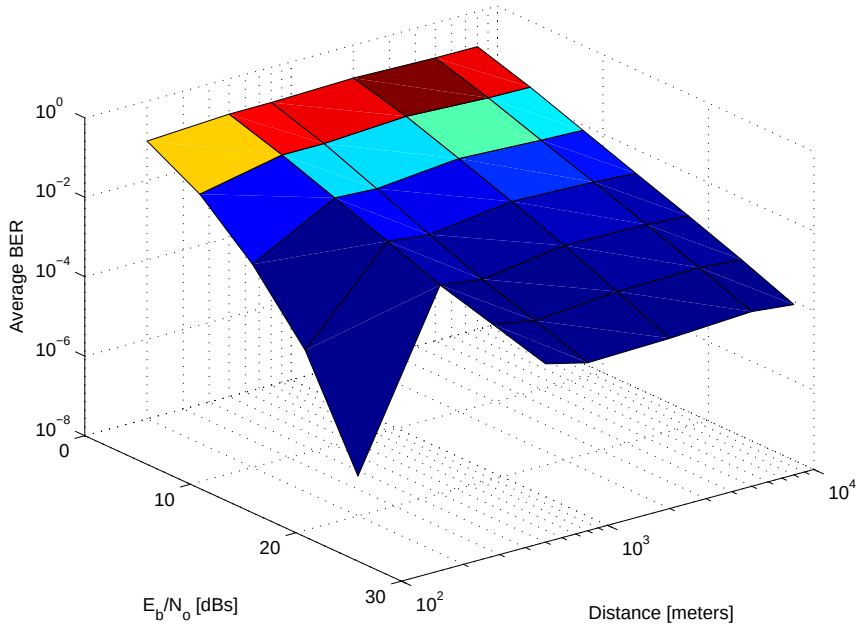

Figure 4.44: QPSK over Flat Fading Nakagami-m channel with distance variations, $f = 900MHz$, Γ Uniform

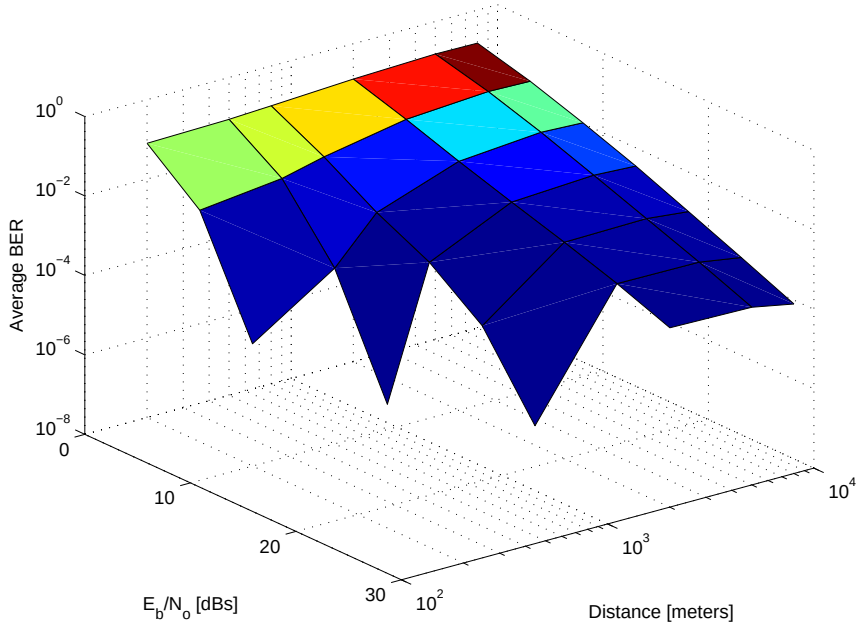

Figure 4.45: QPSK over Flat Fading Nakagami-m channel with distance variations, $f = 1800MHz$, Γ Uniform

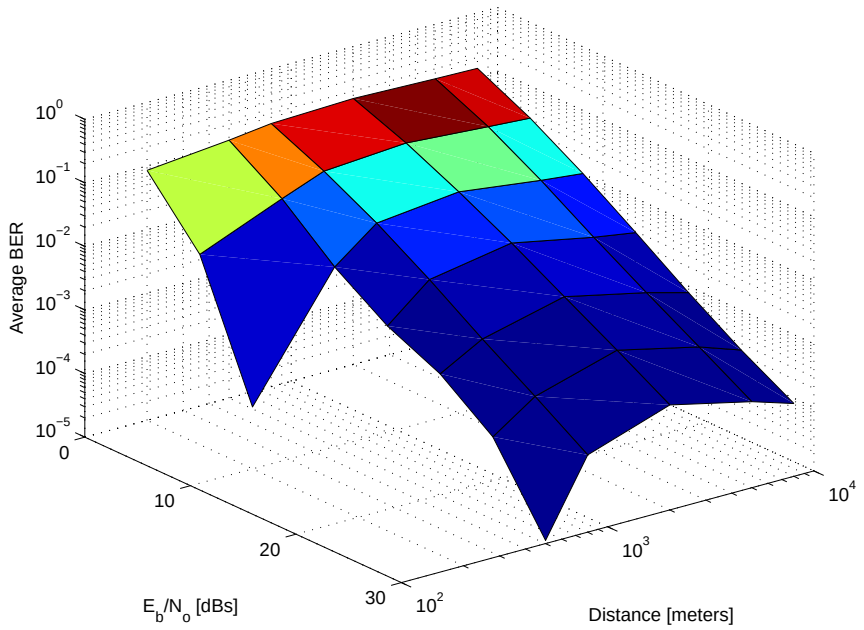

Figure 4.46: QPSK over Flat Fading Nakagami-m channel with distance variations, $f = 900MHz$, Γ Exponential

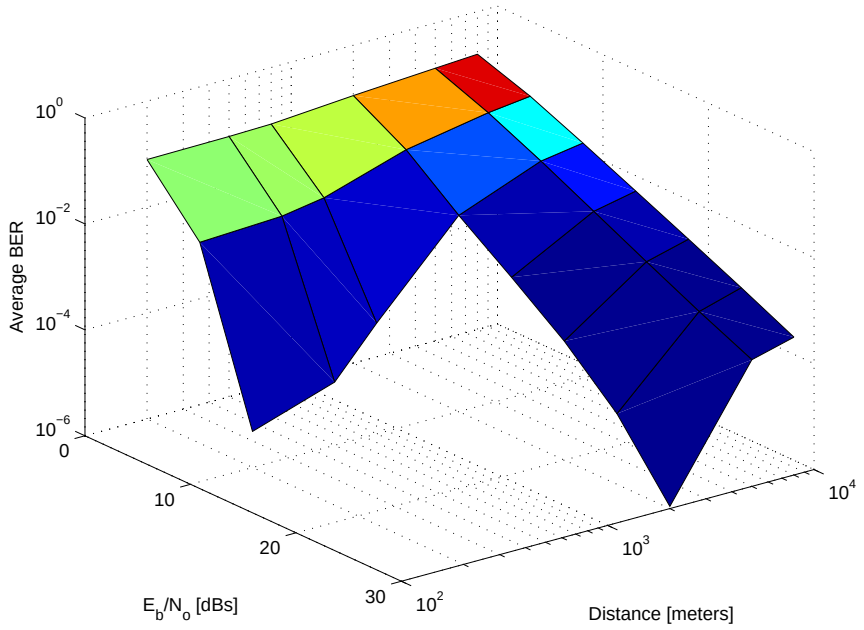

Figure 4.47: QPSK over Flat Fading Nakagami-m channel with distance variations, $f = 1800MHz$, Γ Exponential

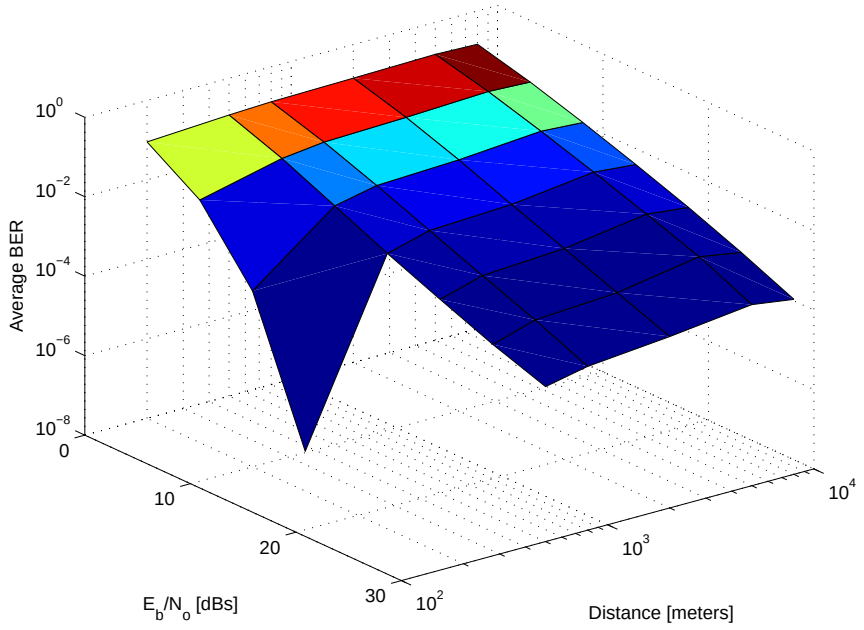

Figure 4.48: QPSK over Flat Fading Nakagami-m channel with distance variations, $f = 900MHz$, Γ Half Gaussian

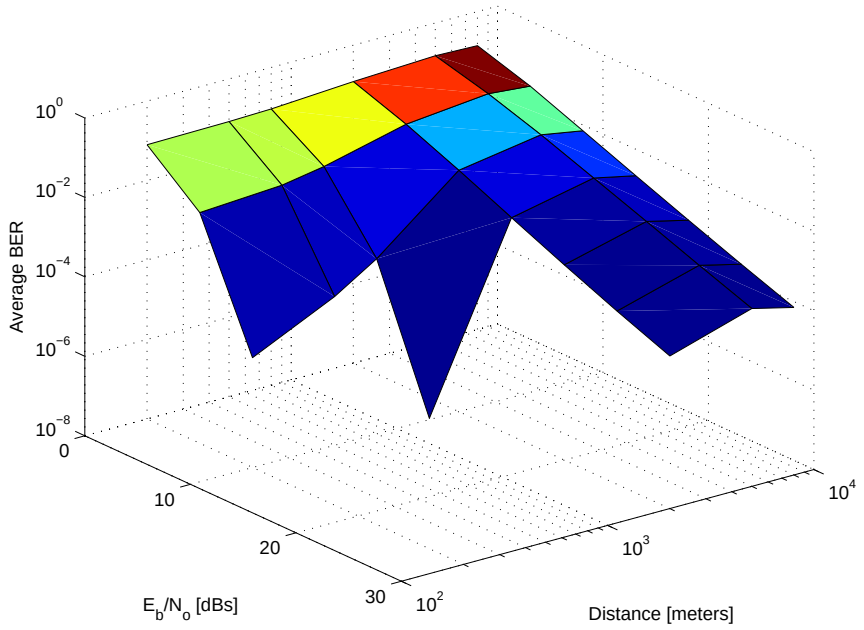

Figure 4.49: QPSK over Flat Fading Nakagami-m channel with distance variations, $f = 1800MHz$, Γ Half Gaussian

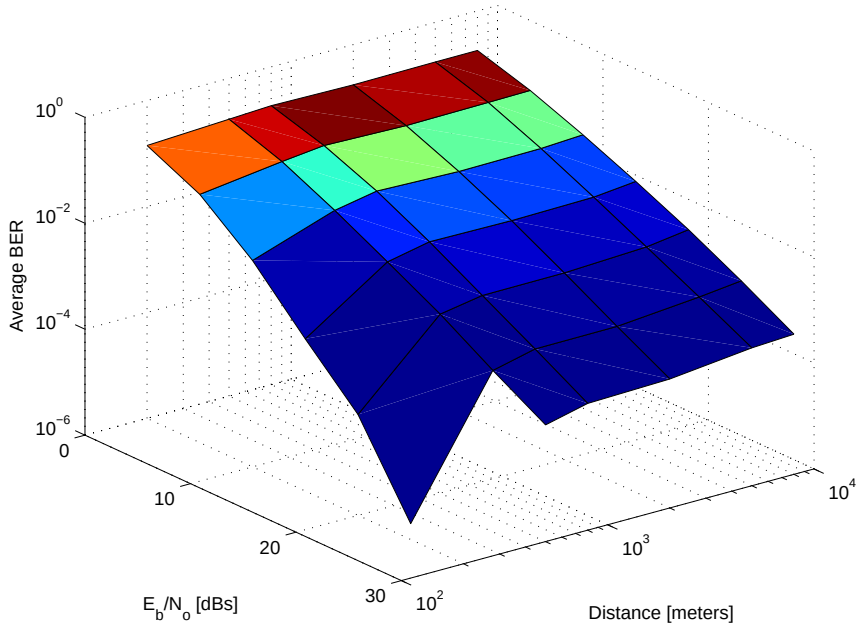

Figure 4.50: 8PSK over Flat Fading Nakagami-m channel with distance variations, $f = 900MHz$, Γ Uniform

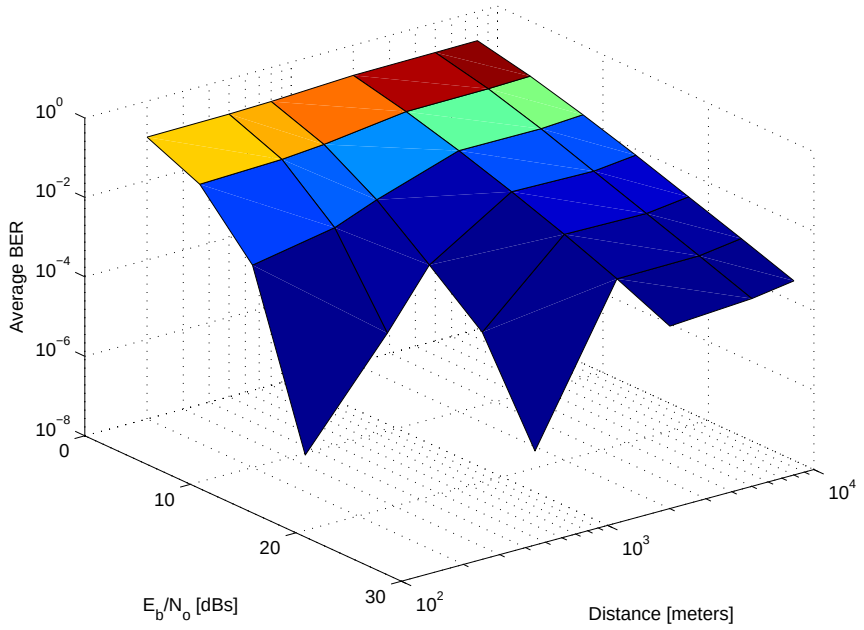

Figure 4.51: 8PSK over Flat Fading Nakagami-m channel with distance variations, $f = 1800MHz$, Γ Uniform

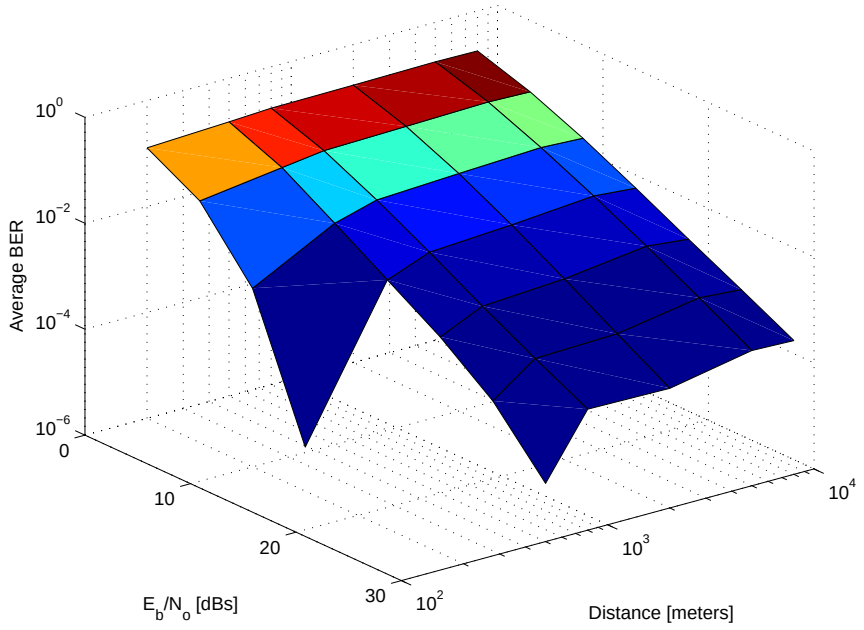

Figure 4.52: 8PSK over Flat Fading Nakagami-m channel with distance variations, $f = 900MHz$, Γ Exponential

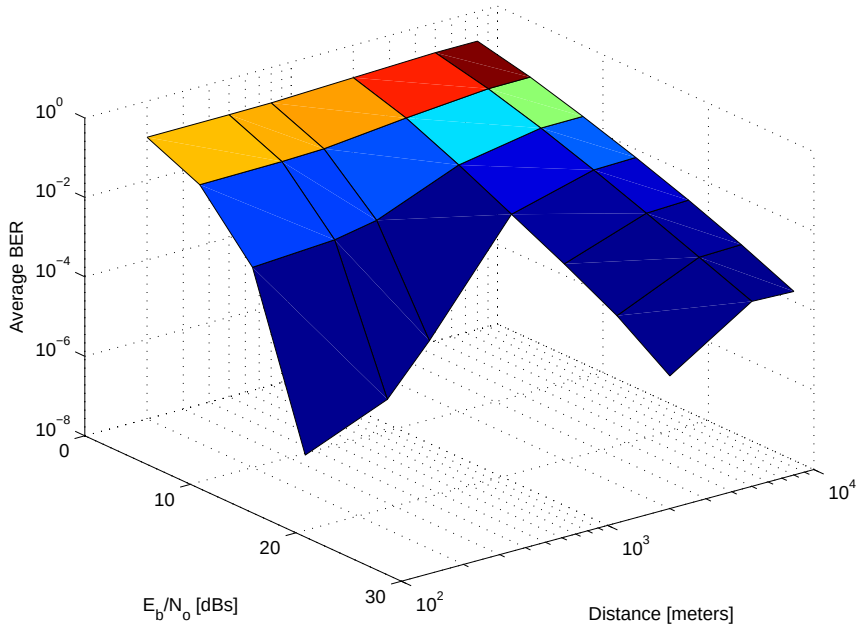

Figure 4.53: 8PSK over Flat Fading Nakagami-m channel with distance variations, $f = 1800MHz$, Γ Exponential

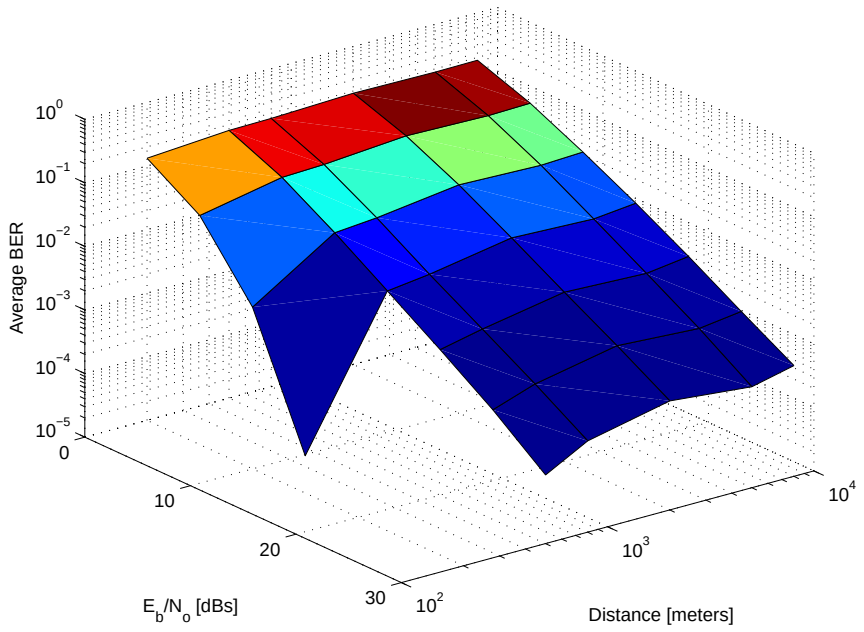

Figure 4.54: 8PSK over Flat Fading Nakagami-m channel with distance variations, $f = 900MHz$, Γ Half Gaussian

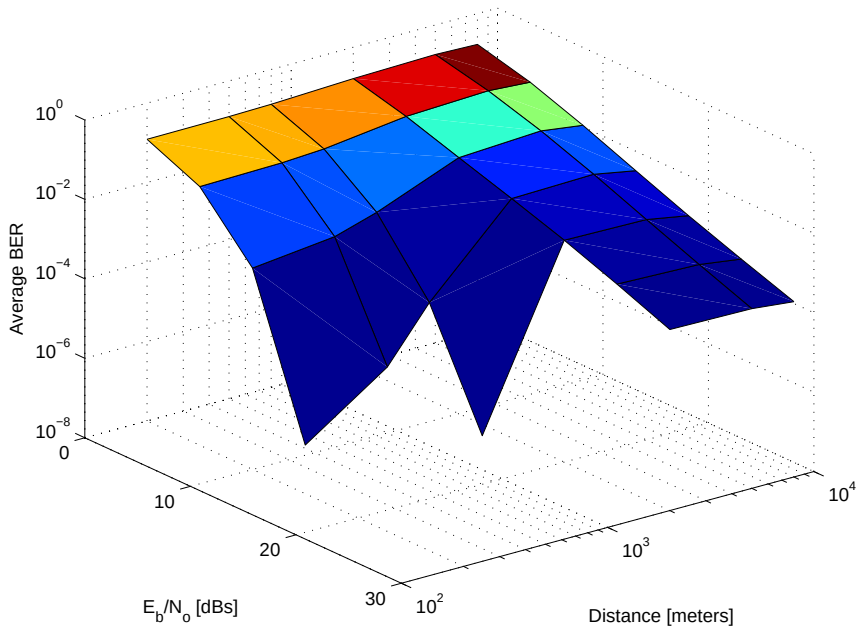

Figure 4.55: 8PSK over Flat Fading Nakagami-m channel with distance variations, $f = 1800MHz$, Γ Half Gaussian

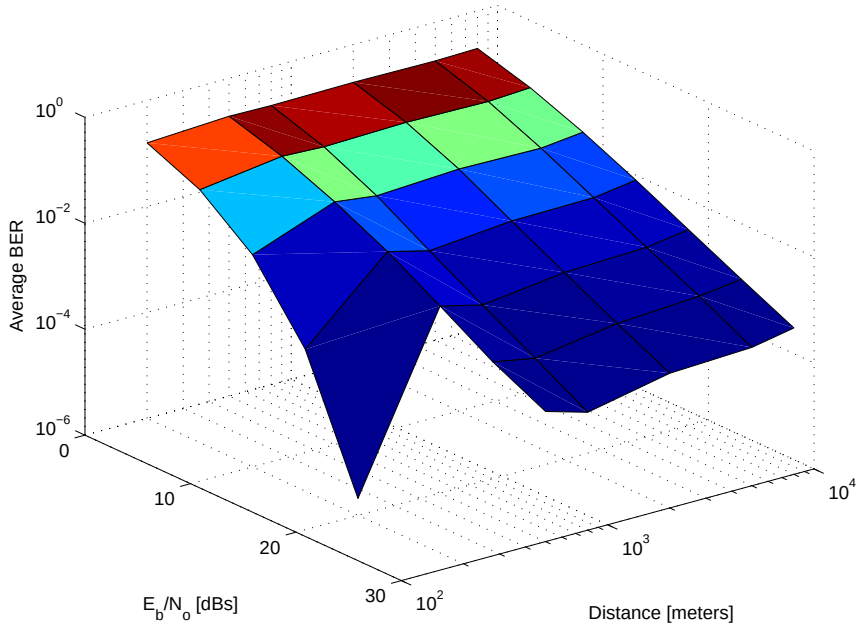

Figure 4.56: 16QAM over Flat Fading Nakagami-m channel with distance variations, $f = 900MHz$, Γ Uniform

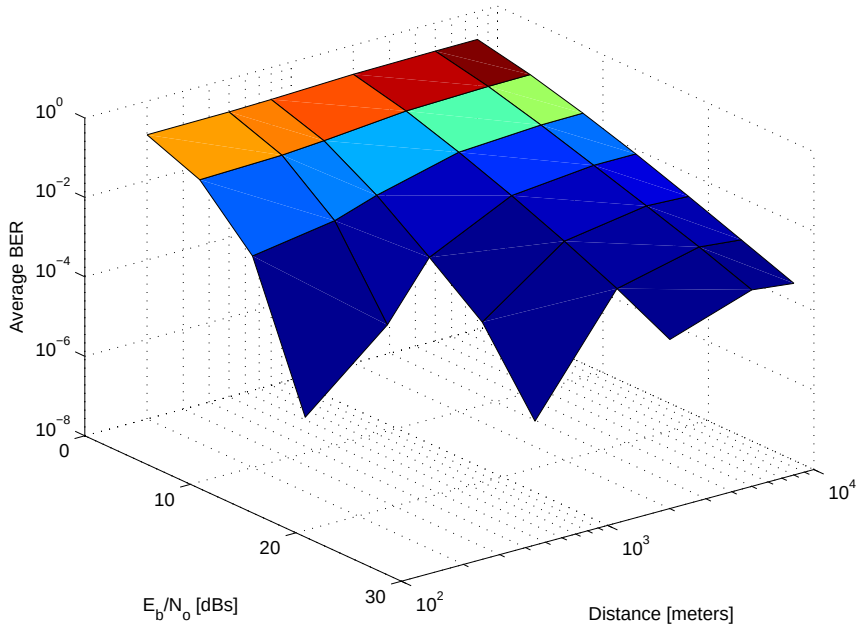

Figure 4.57: 16QAM over Flat Fading Nakagami-m channel with distance variations, $f = 1800MHz$, Γ Uniform

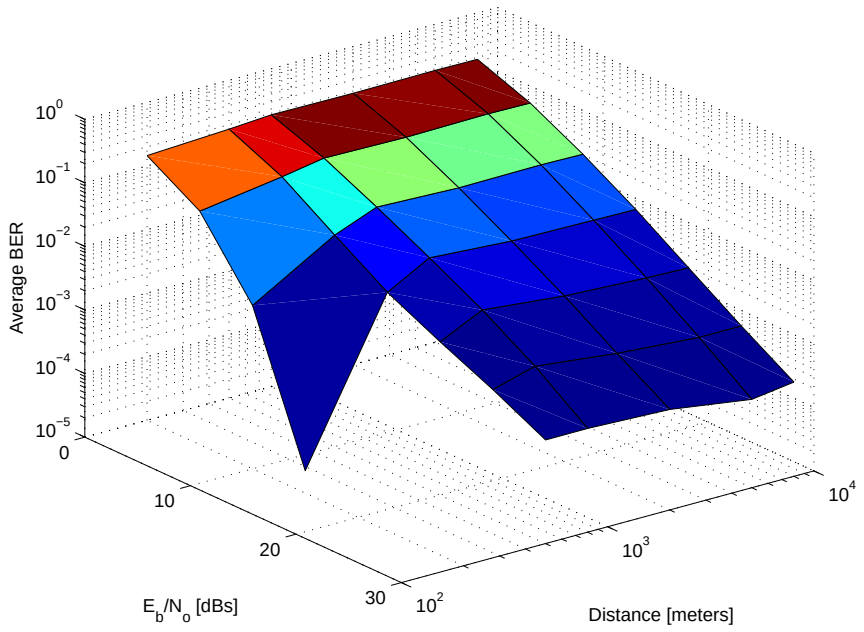

Figure 4.58: 16QAM over Flat Fading Nakagami-m channel with distance variations, $f = 900MHz$, Γ Exponential

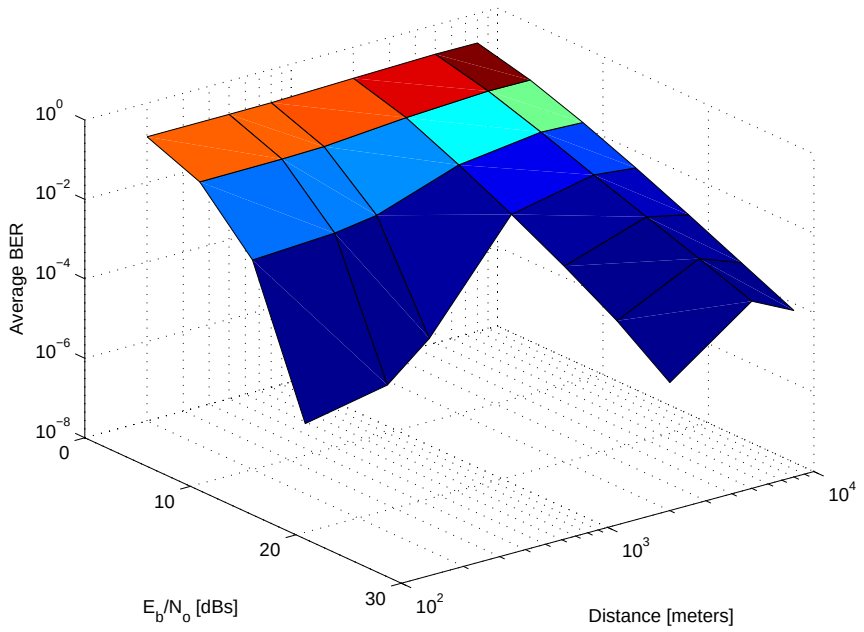

Figure 4.59: 16QAM over Flat Fading Nakagami-m channel with distance variations, $f = 1800MHz$, Γ Exponential

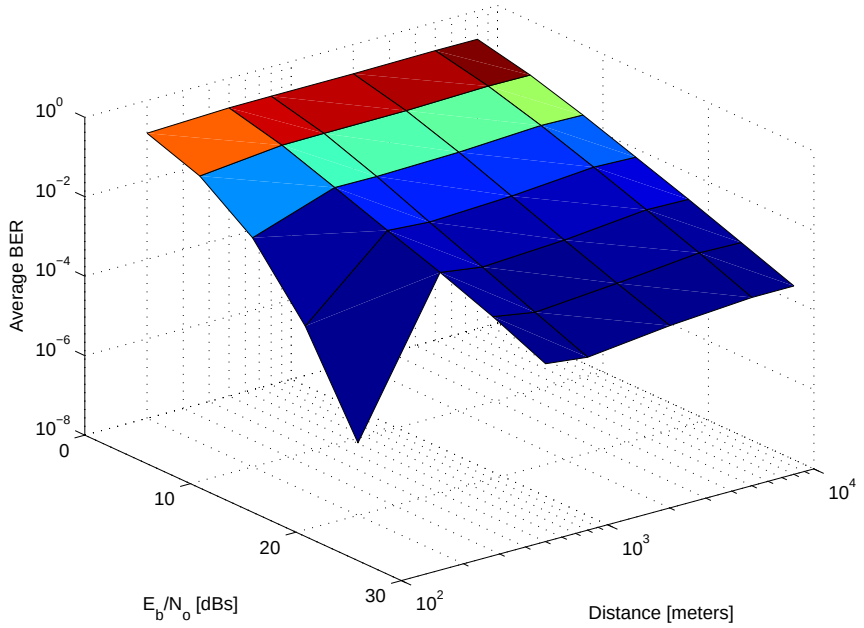

Figure 4.60: 16QAM over Flat Fading Nakagami-m channel with distance variations, $f = 900MHz$, Γ Half Gaussian

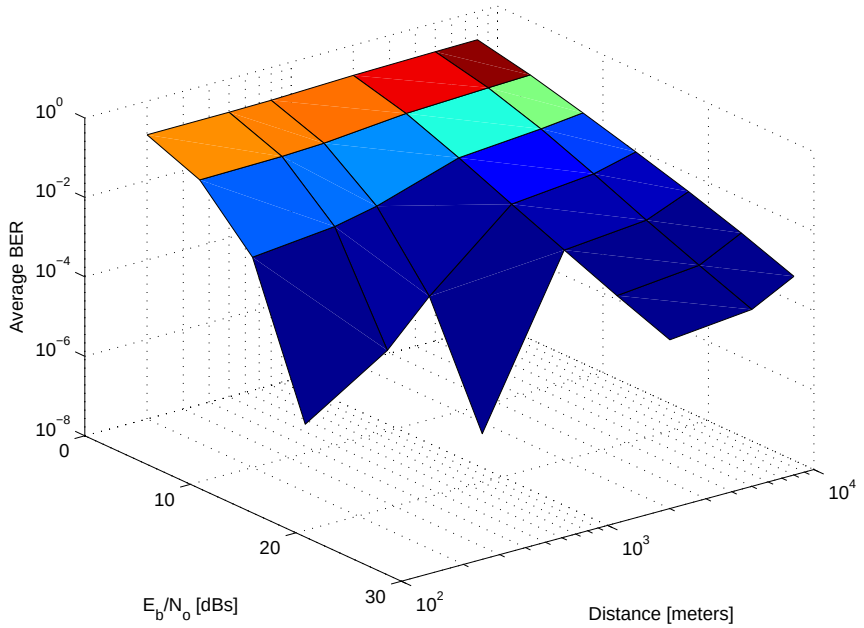

Figure 4.61: 16QAM over Flat Fading Nakagami-m channel with distance variations, $f = 1800MHz$, Γ Half Gaussian

4.6 Performance of MPSK over Frequency Selective Nakagami-m channel with Rake Receiver

This section compares QPSK and 8PSK modulation schemes over frequency selective Nakagami-m channels. Three cases are considered:

- Case 1: MPSK over Flat Fading Nakagami-m channel without Diversity.
- Case 2: MPSK over Flat Fading Nakagami-m channel with Equal Gain Combining (L=3).
- Case 3: MPSK over Frequency Selective Nakagami-m channel with Rake Receiver (L=3).

The variation of Nakagami-m parameter with distances is considered in comparing the error performance of the two modulation schemes. Figures (4.62 to 4.79) show a considerable improvement in the error performance of both QPSK and 8PSK with Equal Gain Combining (L=3) as compared to without diversity. Further, a three fingers Rake Receiver is employed to get the error performance over slowly varying frequency selective Nakagami-m channel.

As described earlier in section (4.5), the exponential distribution of the reflection co-efficient gives improved results as compared to other distributions. In this section, we considered only the macrocellular structure ($d = 2km$, $d = 5km$, and $d = 8km$), since at higher distances, performance degradation occurs and we are employing

rake diversity technique to improve the bit error rate. The effect of distribution of reflection co-efficient Γ is studied at different distances for particular values of m. e.g. If we take the case of QPSK with L=3 order diversity over flat fading channel at $900MHz$ and $d = 5km$, with Γ uniform and half Gaussian distributed, figure (4.64) and figure (4.76) shows that a BER of 10^{-3} is acheived at $10db$ SNR and $9dB$ SNR respectively for corresponding values of $m = 9.43e^{-5}dB$ and $m = 3.49e^{-4}dB$. At the same value of distance and frequency, the same BER can be acheived at lower value of SNR $7.5 - 8dB$ if exponential distribution is used. Similar behavior can be observed for both the modulation schemes for different cases (case 1, case 2, and case 3) discussed earlier.

Now consider case 3, i.e. MPSK over Frequency Selective Nakagami-m fading channel with Rake Receiver (L=3). If we consider 8PSK modulation scheme at distance $d = 2km$ and $f = 1800MHz$, figures (4.63, 4.69, and 4.75) represent that at a particular value of SNR let's say $20dB$, the exponential distribution of the reflection co-efficient gives lower error rate i.e. 10^{-2} while the other distributions (uniform and half Gaussian) give degraded performance and higher error rates. Same behavior is also observed for QPSK at higher distances with $f = 900MHz$.

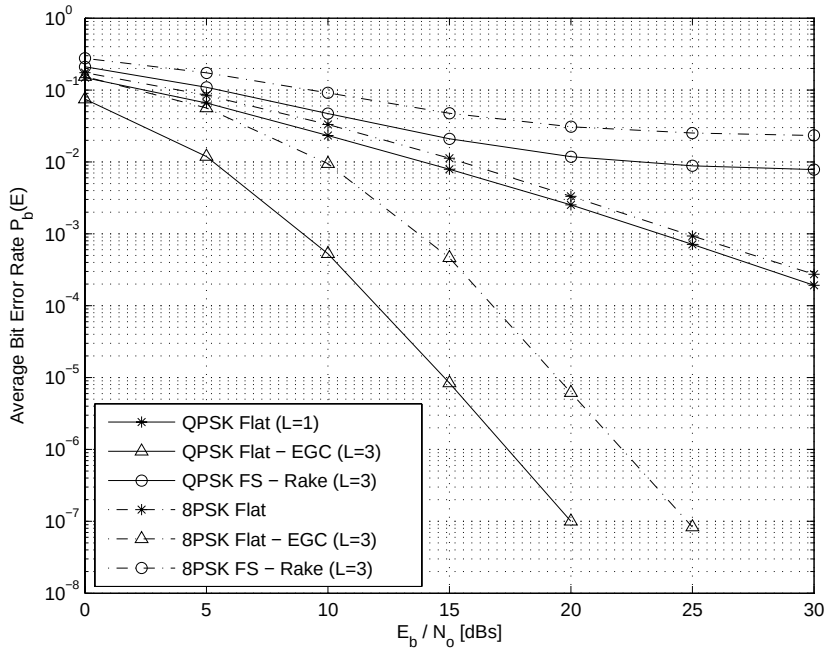

Figure 4.62: MPSK System:Flat fading with EGC and Frequency Selective fading with Rake reception over slowly fading channel, $f = 900MHz$, $d = 2km$, Γ Uniform

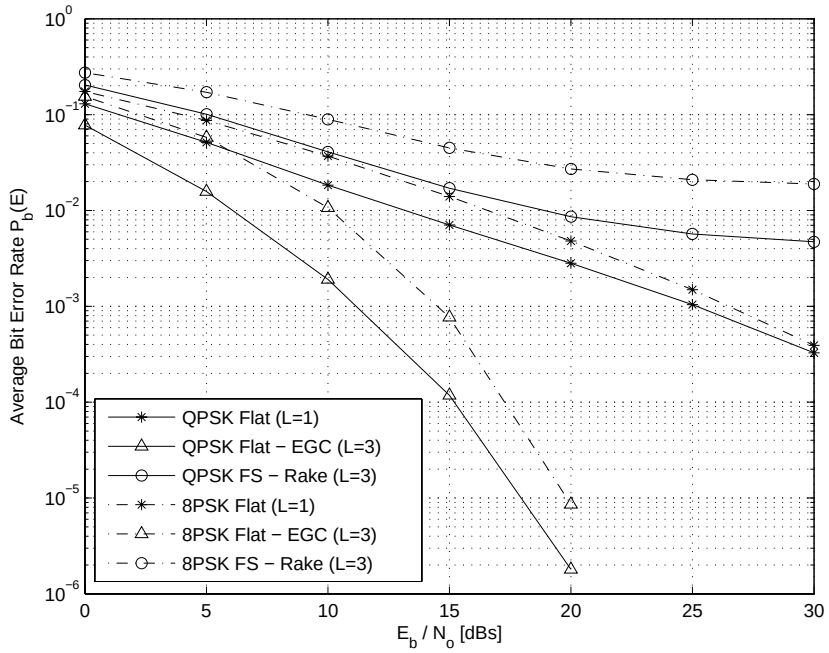

Figure 4.63: MPSK System:Flat fading with EGC and Frequency Selective fading with Rake reception over slowly fading channel, $f = 1800MHz$, $d = 2km$, Γ Uniform

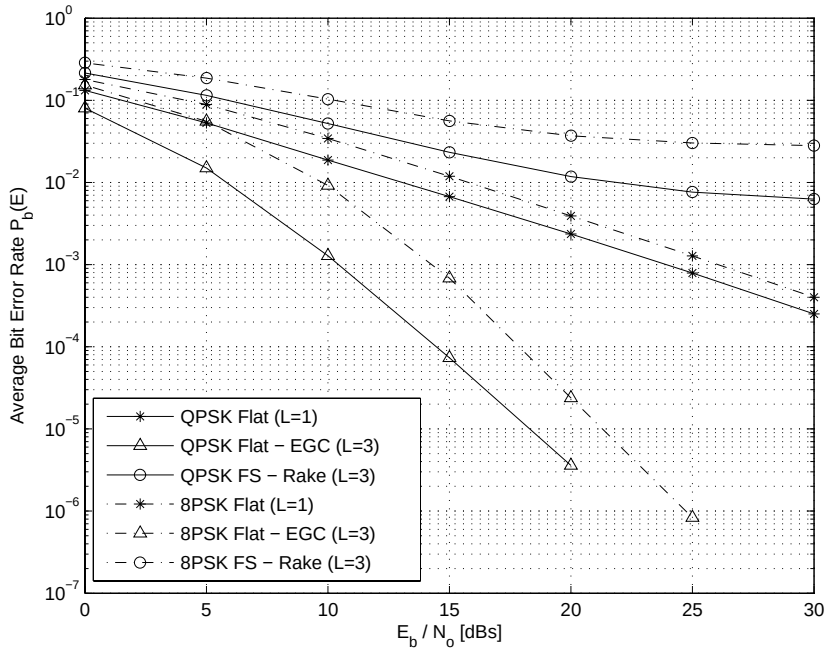

Figure 4.64: MPSK System:Flat fading with EGC and Frequency Selective fading with Rake reception over slowly fading channel, $f = 900MHz$, $d = 5km$, Γ Uniform

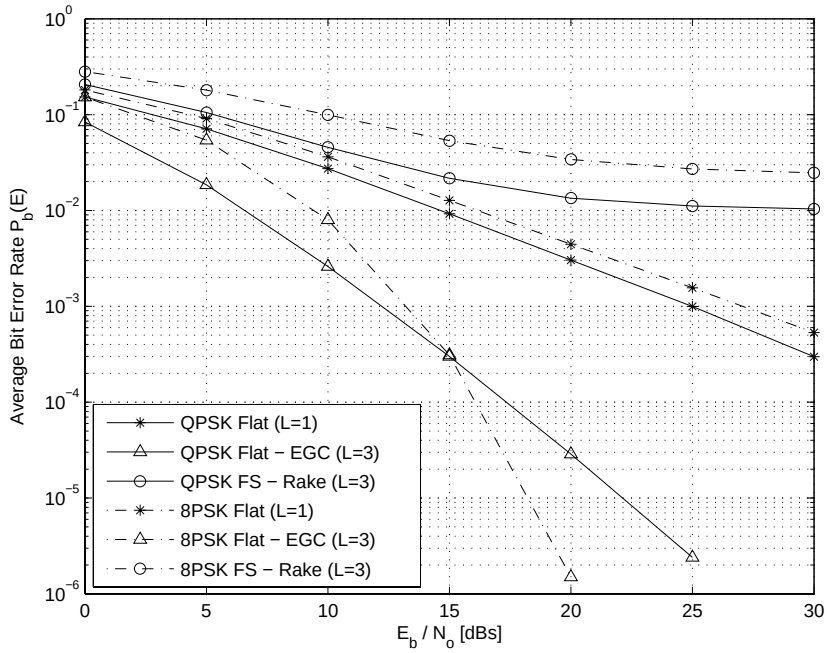

Figure 4.65: MPSK System:Flat fading with EGC and Frequency Selective fading with Rake reception over slowly fading channel, $f = 1800MHz$, $d = 5km$, Γ Uniform

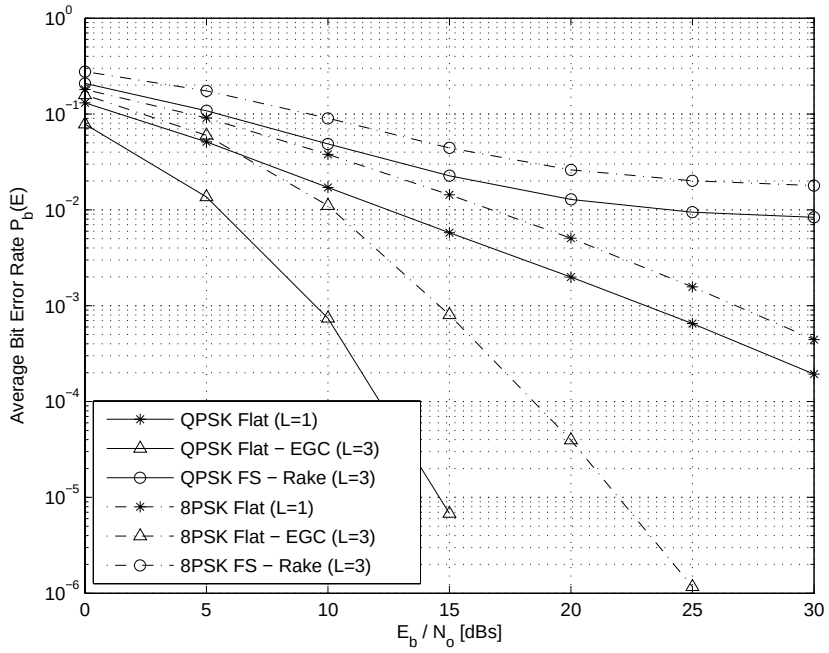

Figure 4.66: MPSK System:Flat fading with EGC and Frequency Selective fading with Rake reception over slowly fading channel, $f = 900MHz$, $d = 8km$, Γ Uniform

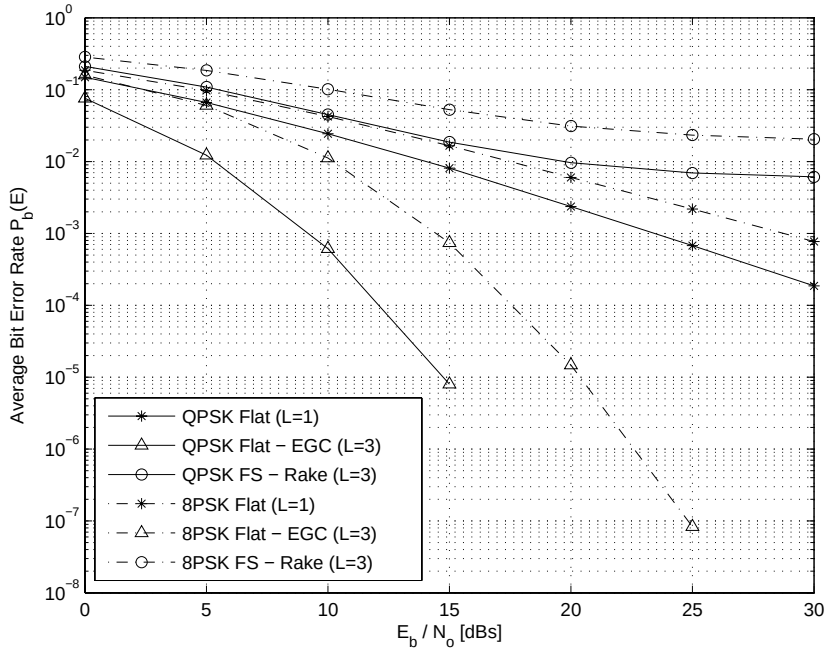

Figure 4.67: MPSK System:Flat fading with EGC and Frequency Selective fading with Rake reception over slowly fading channel, $f = 1800MHz$, $d = 8km$, Γ Uniform

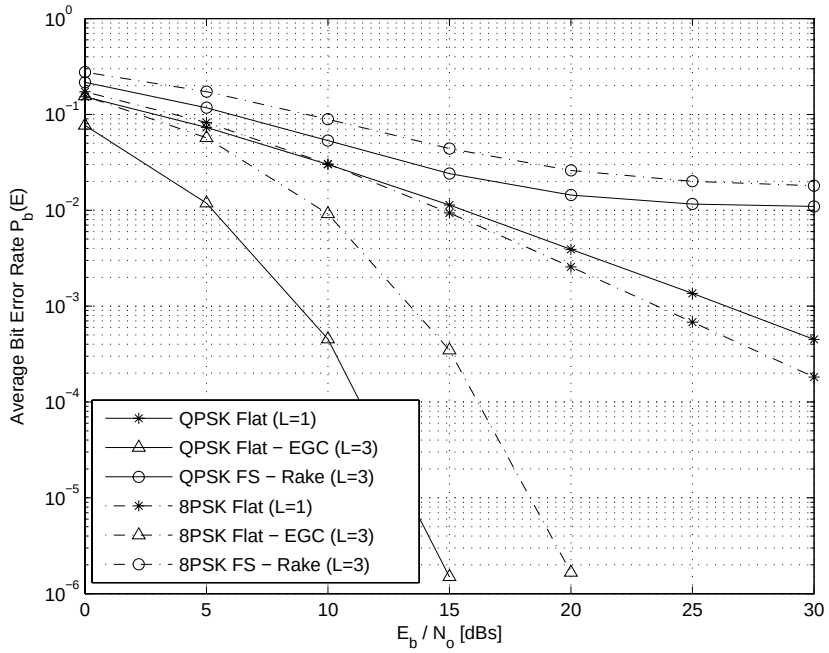

Figure 4.68: MPSK System:Flat fading with EGC and Frequency Selective fading with Rake reception over slowly fading channel, $f = 900MHz$, $d = 2km$, Γ Exponential

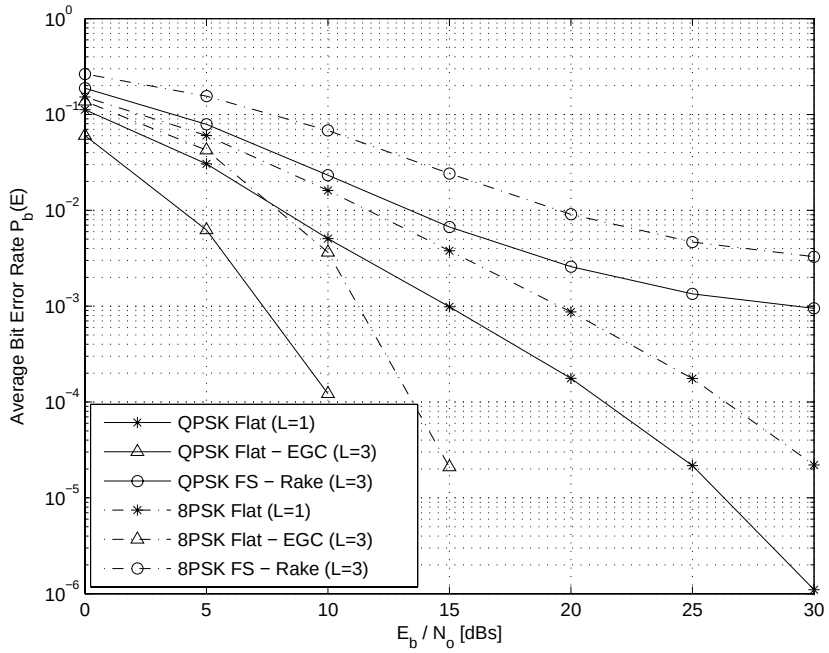

Figure 4.69: MPSK System:Flat fading with EGC and Frequency Selective fading with Rake reception over slowly fading channel, $f = 1800MHz$, $d = 2km$, Γ Exponential

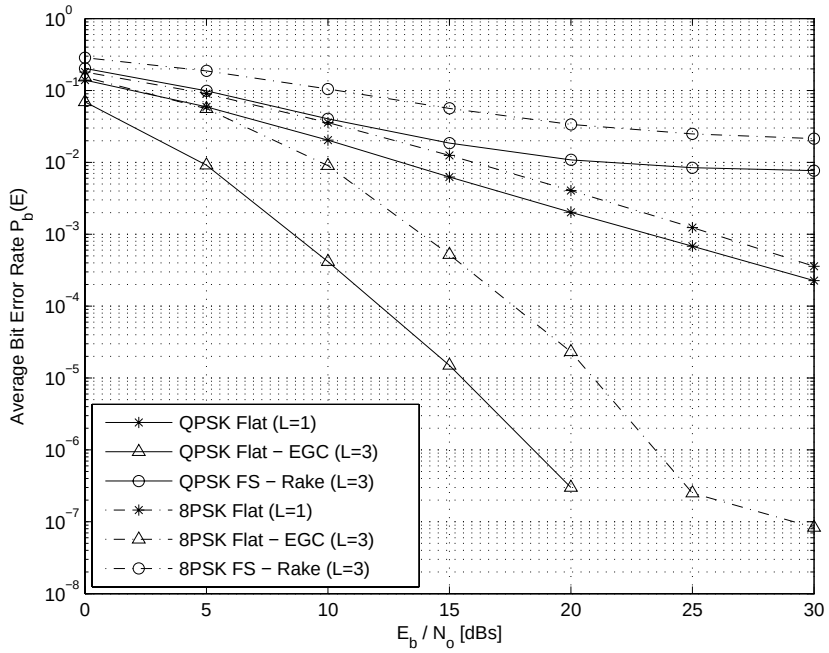

Figure 4.70: MPSK System:Flat fading with EGC and Frequency Selective fading with Rake reception over slowly fading channel, $f = 900MHz$, $d = 5km$, Γ Exponential

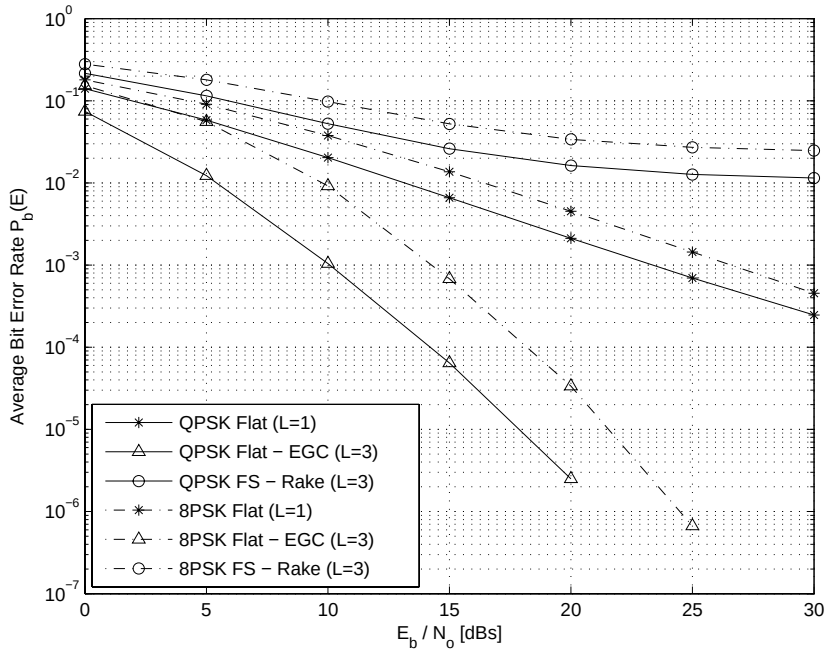

Figure 4.71: MPSK System:Flat fading with EGC and Frequency Selective fading with Rake reception over slowly fading channel, $f = 1800MHz$, $d = 5km$, Γ Exponential

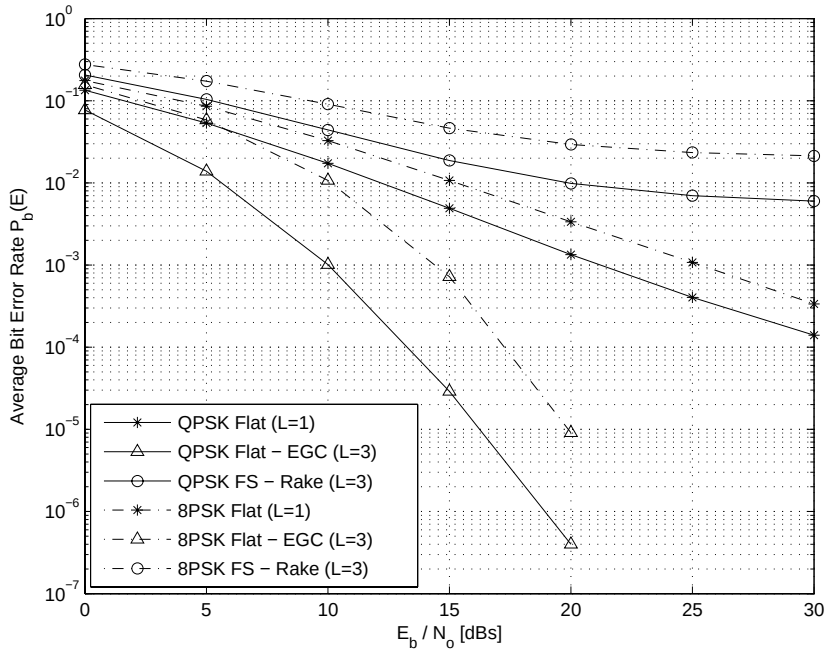

Figure 4.72: MPSK System:Flat fading with EGC and Frequency Selective fading with Rake reception over slowly fading channel, $f = 900MHz$, $d = 8km$, Γ Exponential

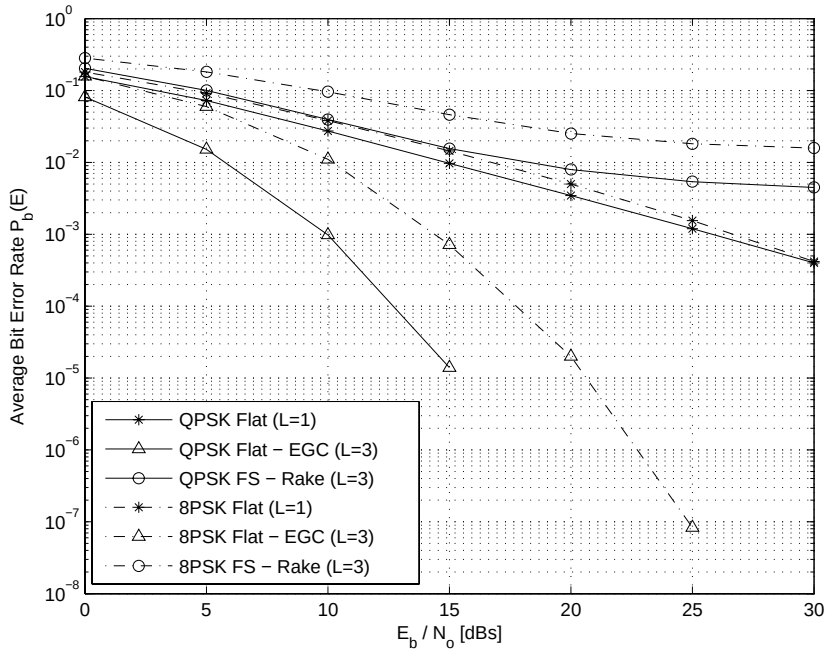

Figure 4.73: MPSK System:Flat fading with EGC and Frequency Selective fading with Rake reception over slowly fading channel, $f = 1800MHz$, $d = 8km$, Γ Exponential

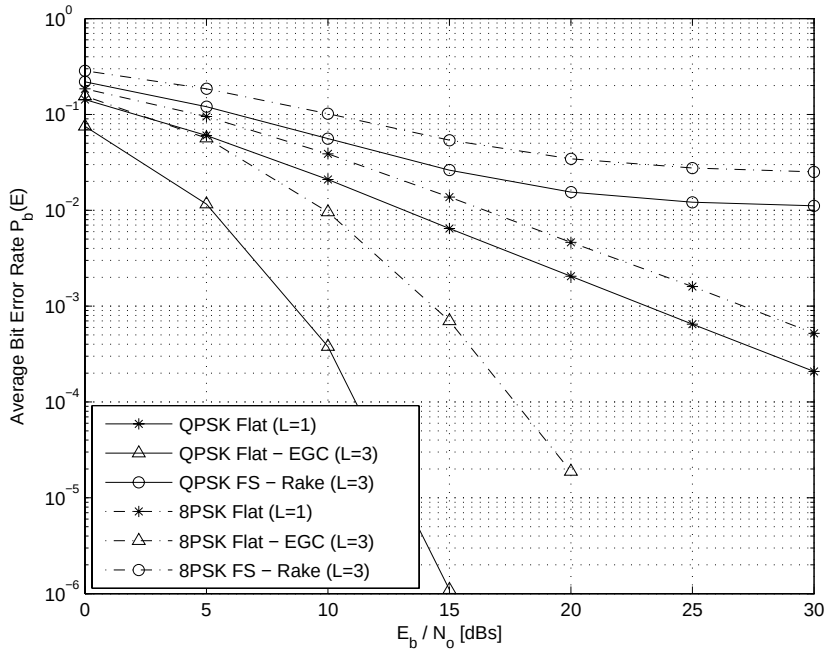

Figure 4.74: MPSK System:Flat fading with EGC and Frequency Selective fading with Rake reception over slowly fading channel, $f = 900MHz$, $d = 2km$, Γ Half Gaussian

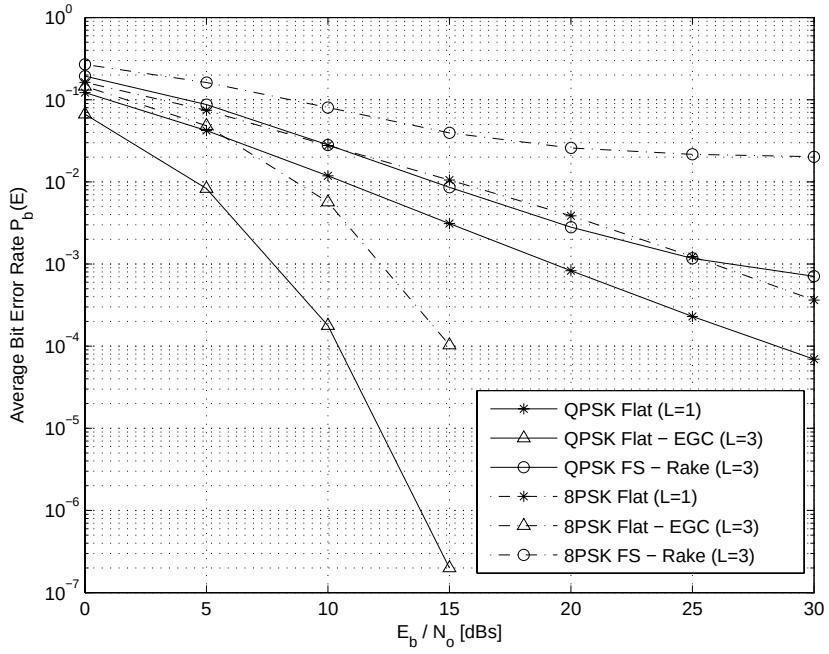

Figure 4.75: MPSK System:Flat fading with EGC and Frequency Selective fading with Rake reception over slowly fading channel, $f = 1800MHz$, $d = 2km$, Γ Half Gaussian

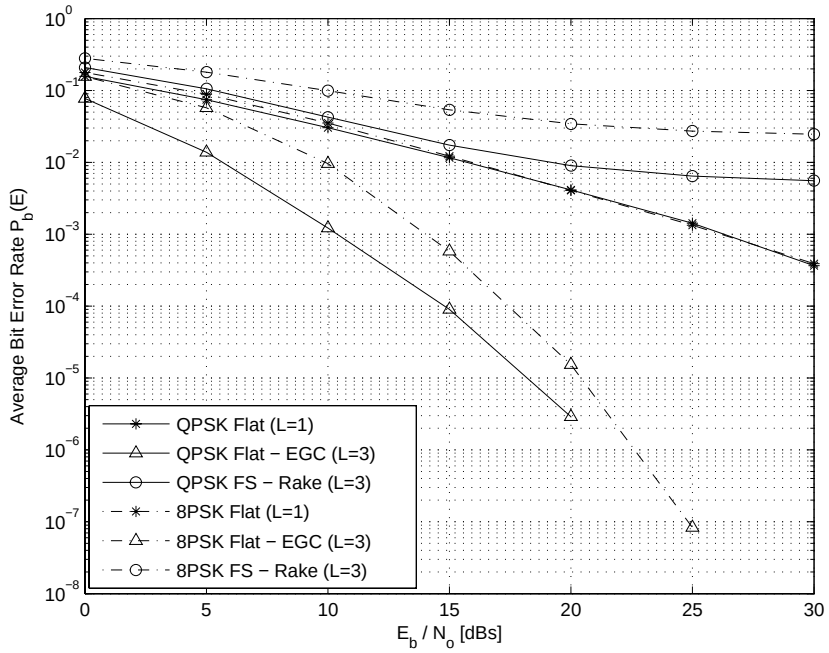

Figure 4.76: MPSK System:Flat fading with EGC and Frequency Selective fading with Rake reception over slowly fading channel, $f = 900MHz$, $d = 5km$, Γ Half Gaussian

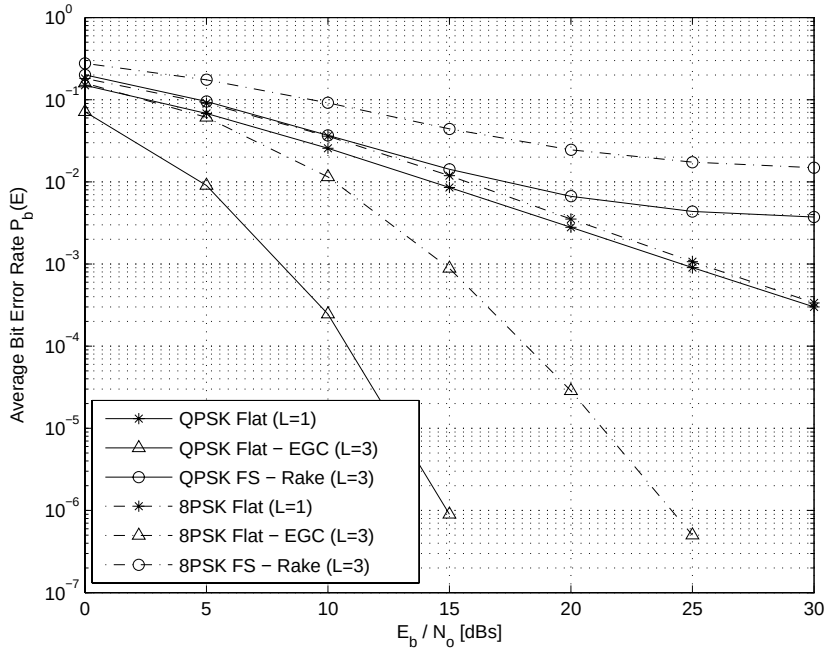

Figure 4.77: MPSK System:Flat fading with EGC and Frequency Selective fading with Rake reception over slowly fading channel, $f = 1800MHz$, $d = 5km$, Γ Half Gaussian

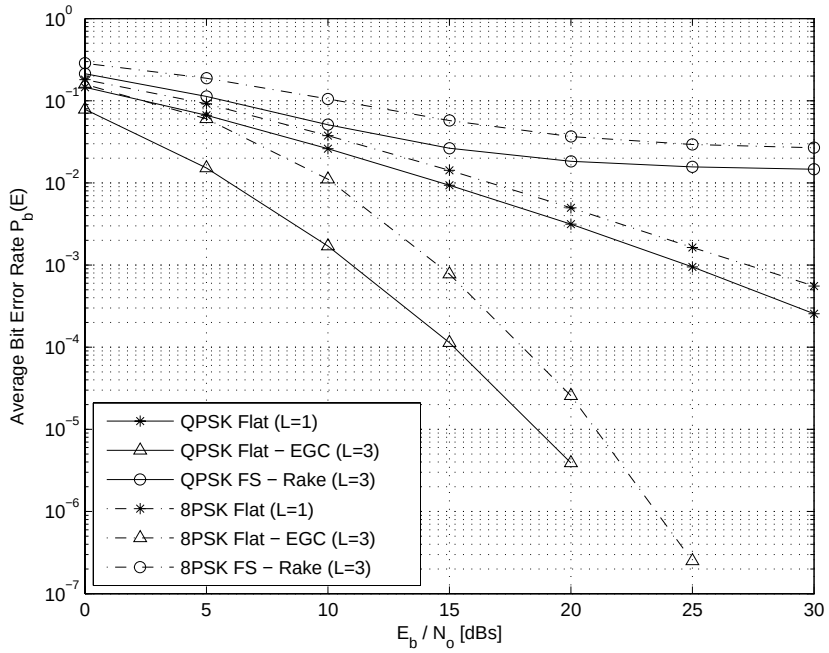

Figure 4.78: MPSK System:Flat fading with EGC and Frequency Selective fading with Rake reception over slowly fading channel, $f = 900MHz$, $d = 8km$, Γ Half Gaussian

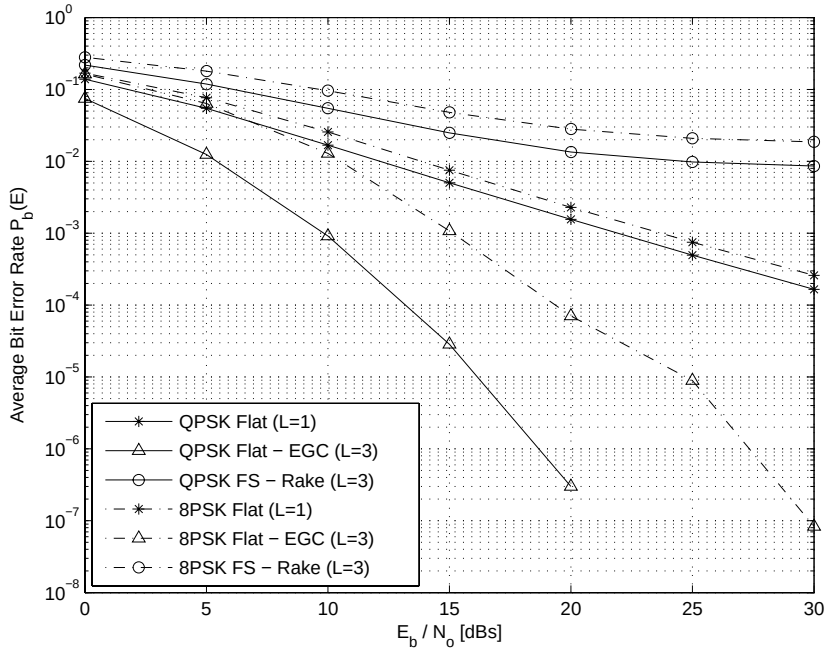

Figure 4.79: MPSK System:Flat fading with EGC and Frequency Selective fading with Rake reception over slowly fading channel, $f = 1800MHz$, $d = 8km$, Γ Half Gaussian

4.6.1 Effect of Frequency

As discussed in section (4.5) that frequency does not have a considerable impact on the error performance of the modulation scheme because the received power and the path loss becomes independent of the frequency at higher distances. But for shorter distances and higher frequencies, it is shown that the error performance is improved. Figures (4.80 to 4.85) represent this behavior for microcellular structure (short distances) for different distribution of reflection co-efficients for MPSK systems over frequency selective Nakagami-m channel with Rake reception.

It is observed that there is a significant amount of change in the performance of the system for short distances if we operate at higher frequencies. This behavior is explained with the help of figure (4.85). While operating at $900MHz$, at $SNR = 20dB$, the bit error rate is almost 2x10^{-2} for 8PSK. However, at the same signal to noise ratio, we acheive an improved BER of 10^{-3} at $1800MHz$.

On the other hand, we can also look into the change in Nakagami-m parameter i.e. Δm. As described earlier in section (4.3) that at lower distances, the decay rate of parameter Δm is high for exponential distribution of the reflection co-efficient Γ as compared to other distributions. This behavior is shown in the set of figures (4.80, 4.81, 4.82, 4.83, 4.84, and 4.85). It is observed that at $d = 200m$, the parameter Δm is $10.33dB$ if we switch from $900MHz$ to $1800MHz$ for uniform distribution of the reflection co-efficient. While at the same distance $d = 200m$, the parameter

Δm is $11.36dB$ if we switch from $900MHz$ to $1800MHz$ for exponential distribution of the reflection co-efficient. So, it is observed that the larger the parameter Δm, the better performance can be acheived. Similarly, if we look at $d = 500m$, the corresponding values of Δm for uniform, exponential and half Gaussian distributions of the reflection co-effiicents are $6.05dB$, $9.2dB$, and $7.83dB$ respectively while switching from $900MHz$ to $1800MHz$. The corresponding changes in the parameter Δm while moving $300m$ from the base station will be $4.28dB$, $2.16dB$, and $3.19dB$ accordingly. So, it is seen that the less this change will be, more stable will be the performance of the communication link. And, we have got the least value for the exponential distribution of the reflection co-efficient, hence describing the better performance of exponential type of distribution. Finding these values of Δm is useful in making the performance of digital communication link uniform over the interval of distances.

The same behavior is observed for 8PSK modulation scheme at different distances for varying distributions of the reflection co-efficients from figures (4.81, 4.83, and 4.85).

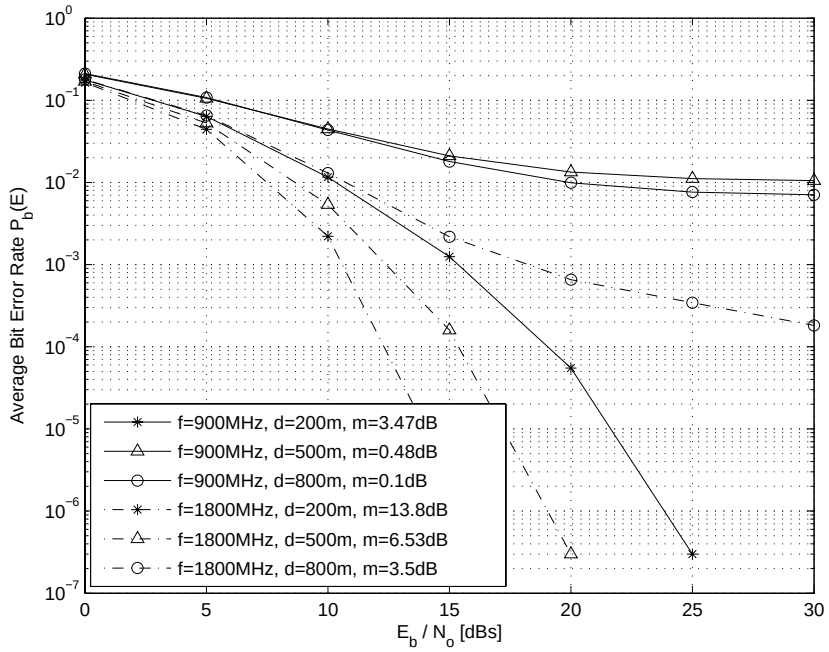

Figure 4.80: Microcell $d = 100m - 1km$ variations of QPSK in microcell over Nakagami-m channel with Rake reception, Γ Uniform

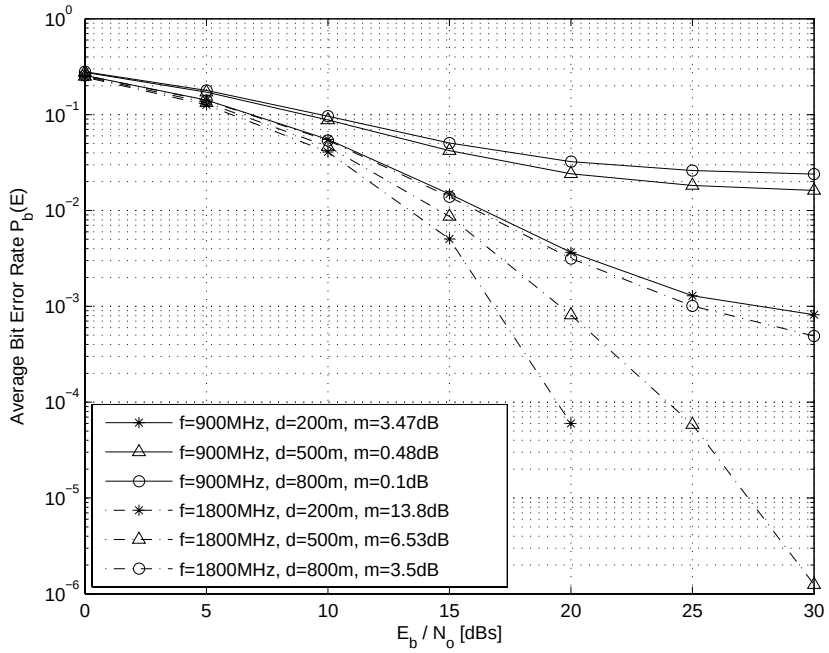

Figure 4.81: Microcell $d = 100m - 1km$ variations of 8PSK in microcell over Nakagami-m channel with Rake reception, Γ Uniform

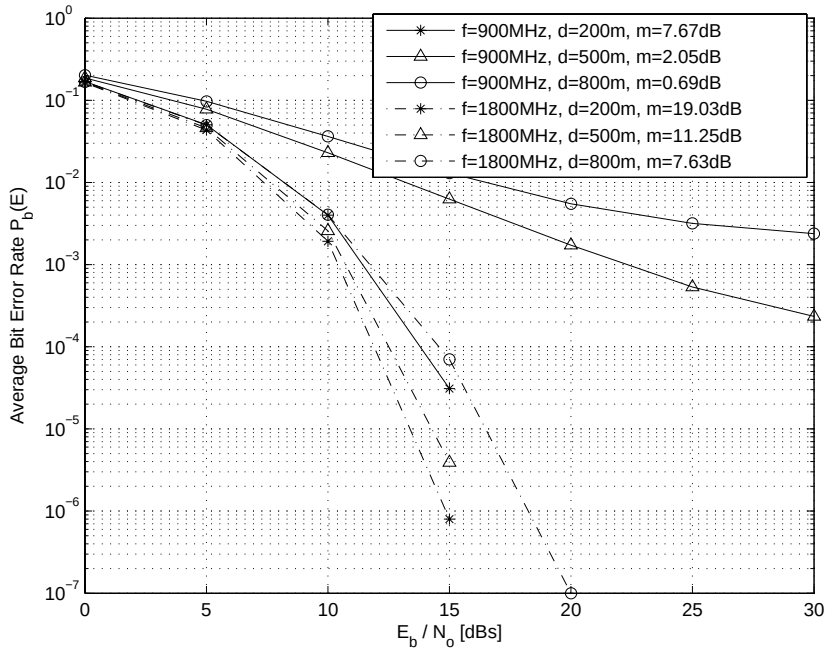

Figure 4.82: Microcell $d = 100m - 1km$ variations of QPSK in microcell over Nakagami-m channel with Rake reception, Γ Exponential

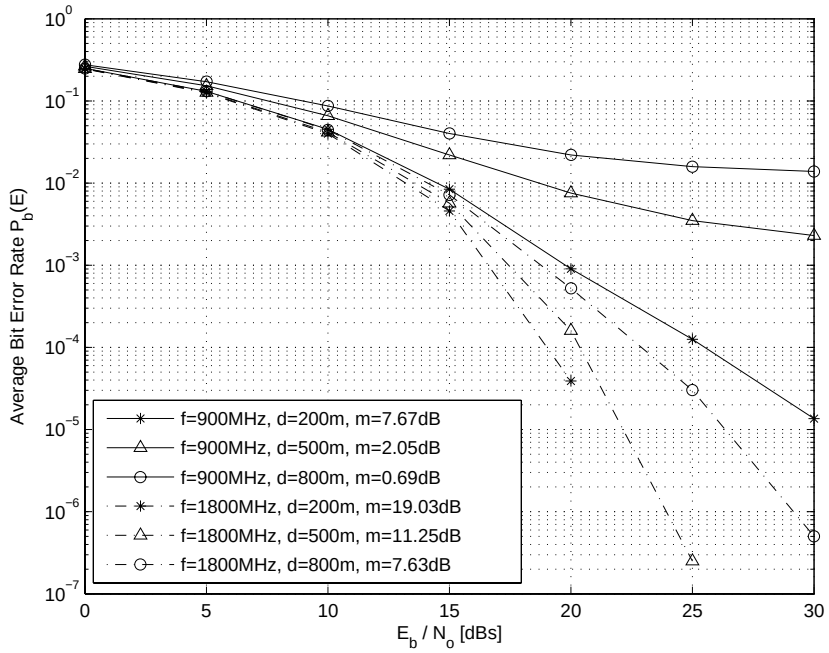

Figure 4.83: Microcell $d = 100m - 1km$ variations of 8PSK in microcell over Nakagami-m channel with Rake reception, Γ Exponential

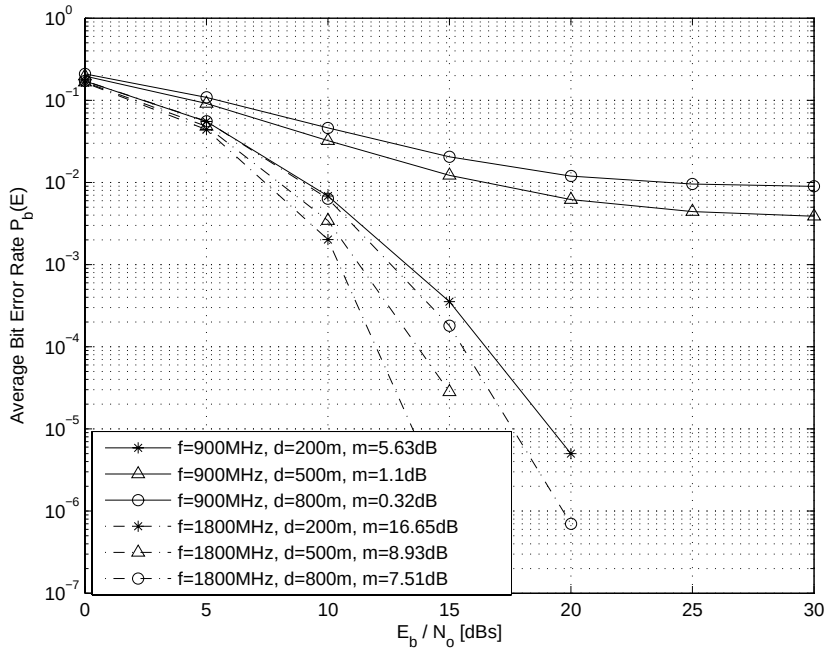

Figure 4.84: Microcell $d = 100m - 1km$ variations of QPSK in microcell over Nakagami-m channel with Rake reception, Γ Half Gaussian

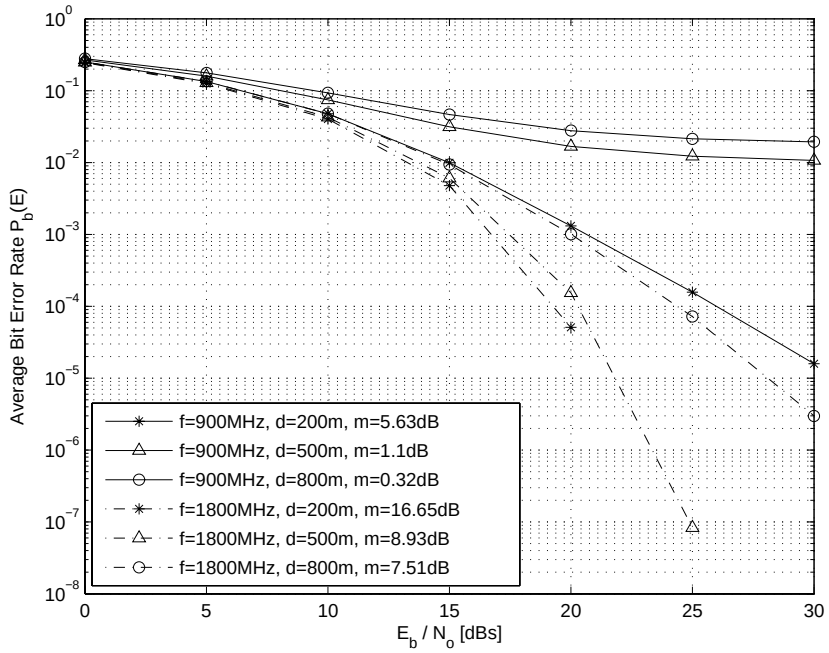

Figure 4.85: Microcell $d = 100m - 1km$ variations of 8PSK in microcell over Nakagami-m channel with Rake reception, Γ Half Gaussian

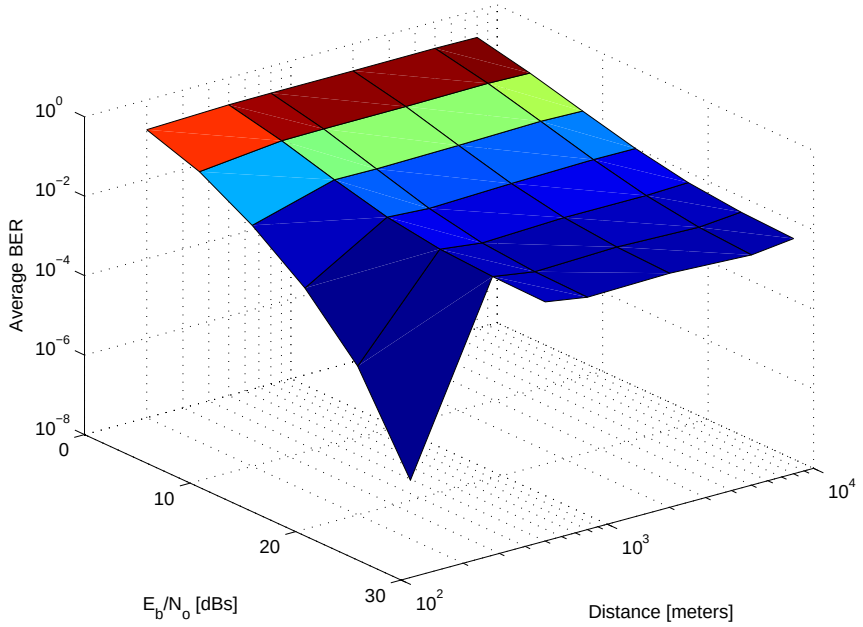

Figure 4.86: Impact of distance variations on Average BEP of QPSK with Rake receiver (L=3), $f = 900MHz$, Γ Uniform

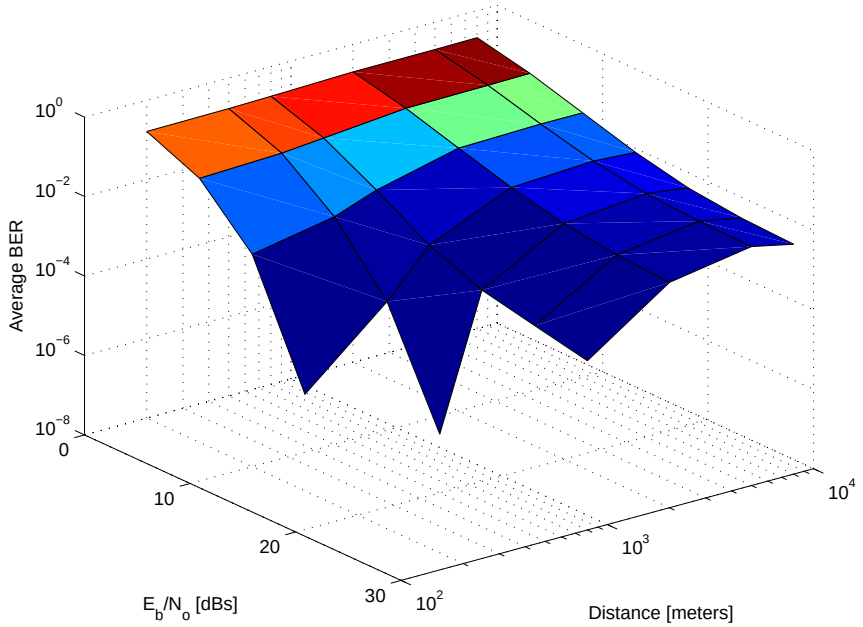

Figure 4.87: Impact of distance variations on Average BEP of QPSK with Rake receiver (L=3), $f = 1800MHz$, Γ Uniform

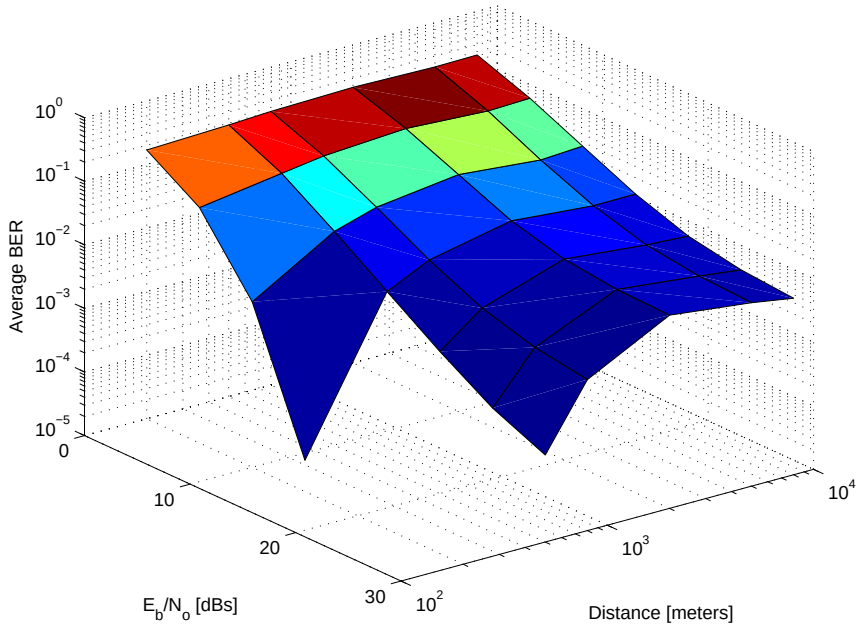

Figure 4.88: Impact of distance variations on Average BEP of QPSK with Rake receiver (L=3), $f = 900MHz$, Γ Exponential

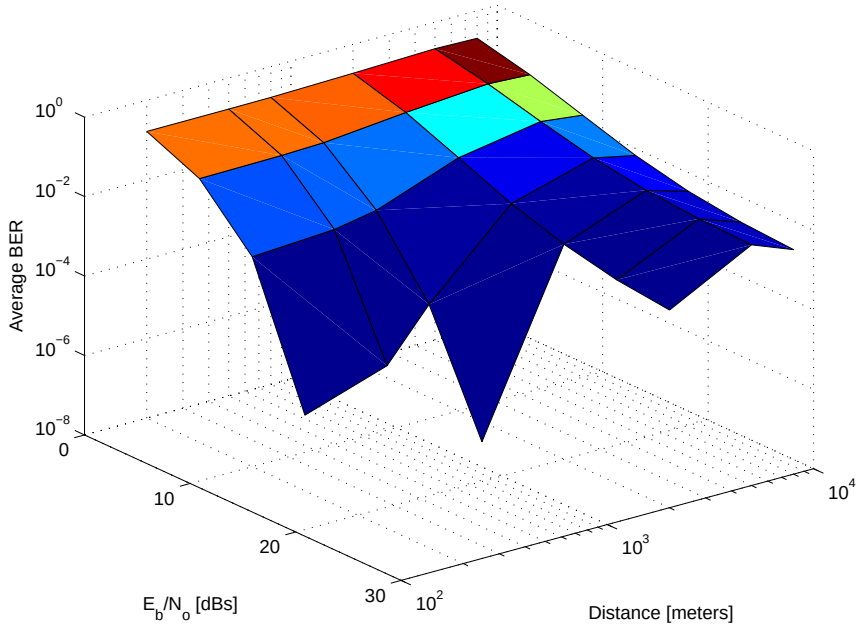

Figure 4.89: Impact of distance variations on Average BEP of QPSK with Rake receiver (L=3), $f = 1800MHz$, Γ Exponential

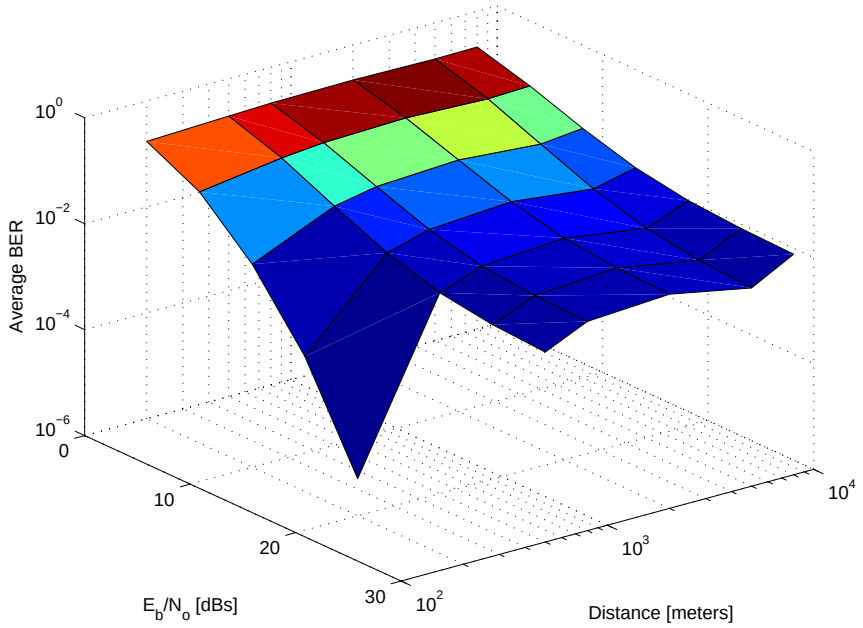

Figure 4.90: Impact of distance variations on Average BEP of QPSK with Rake receiver (L=3), $f = 900MHz$, Γ Half Gaussian

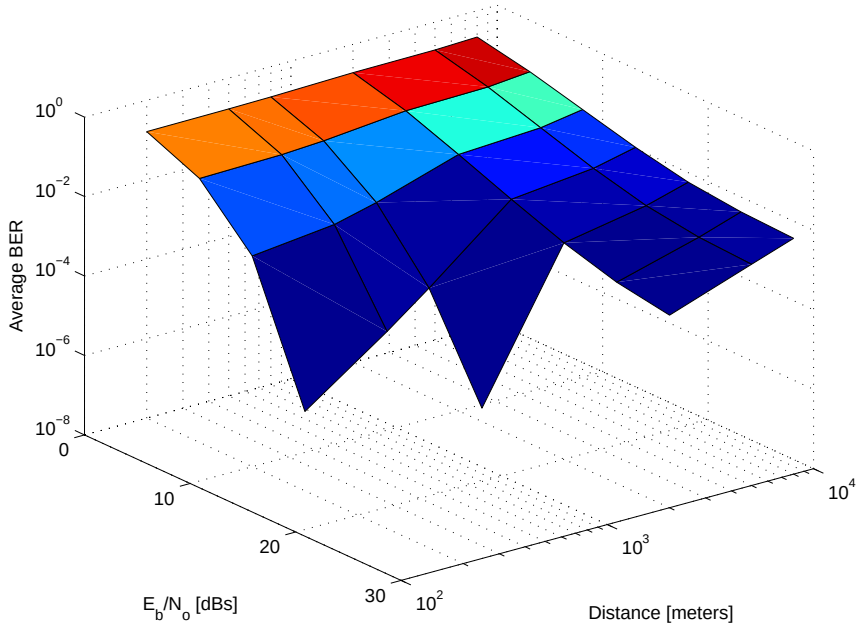

Figure 4.91: Impact of distance variations on Average BEP of QPSK with Rake receiver (L=3), $f = 1800MHz$, Γ Half Gaussian

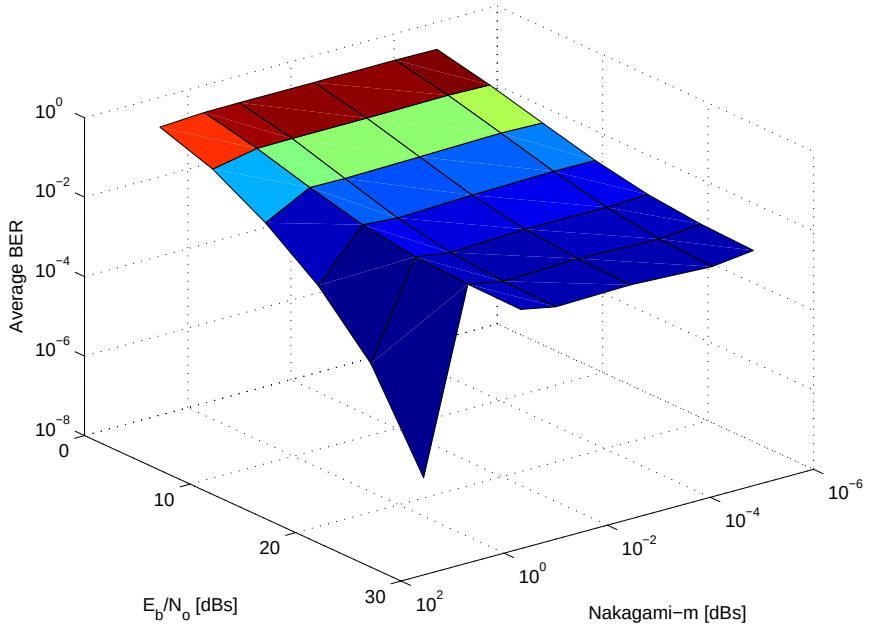

Figure 4.92: Impact of Nakagami-m variations on Average BEP of QPSK with Rake receiver (L=3), $f = 900MHz$, Γ Uniform

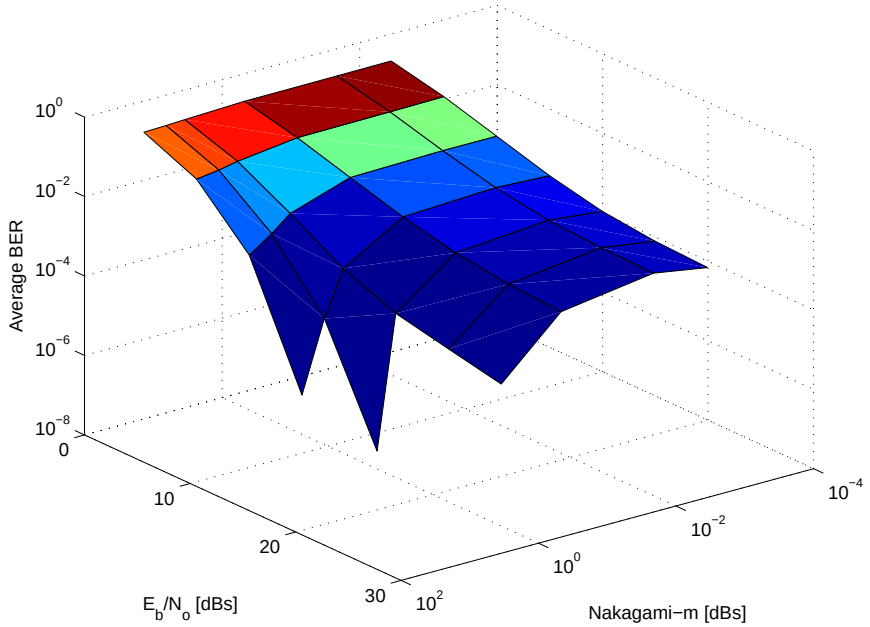

Figure 4.93: Impact of Nakagami-m variations on Average BEP of QPSK with Rake receiver (L=3), $f = 1800MHz$, Γ Uniform

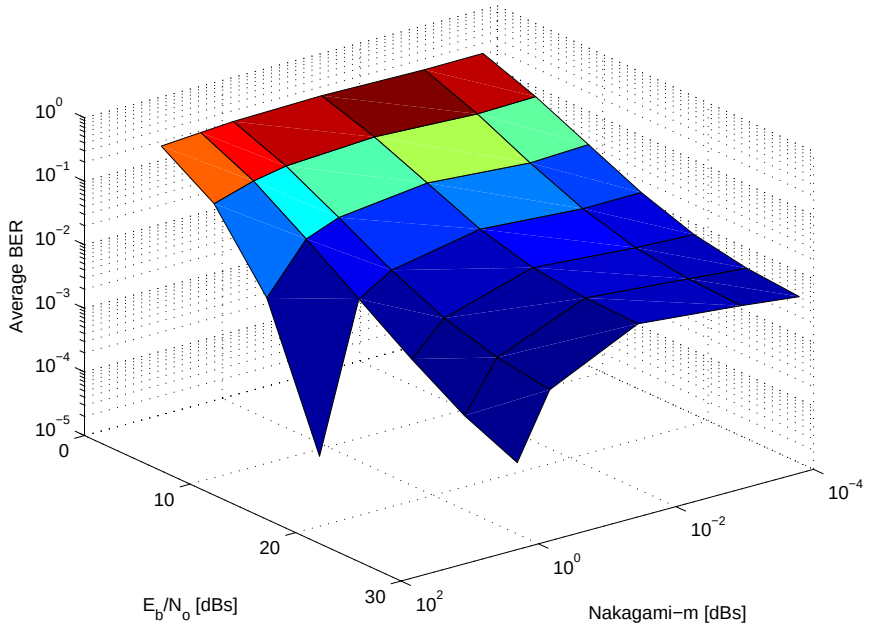

Figure 4.94: Impact of Nakagami-m variations on Average BEP of QPSK with Rake receiver (L=3), $f = 900MHz$, Γ Exponential

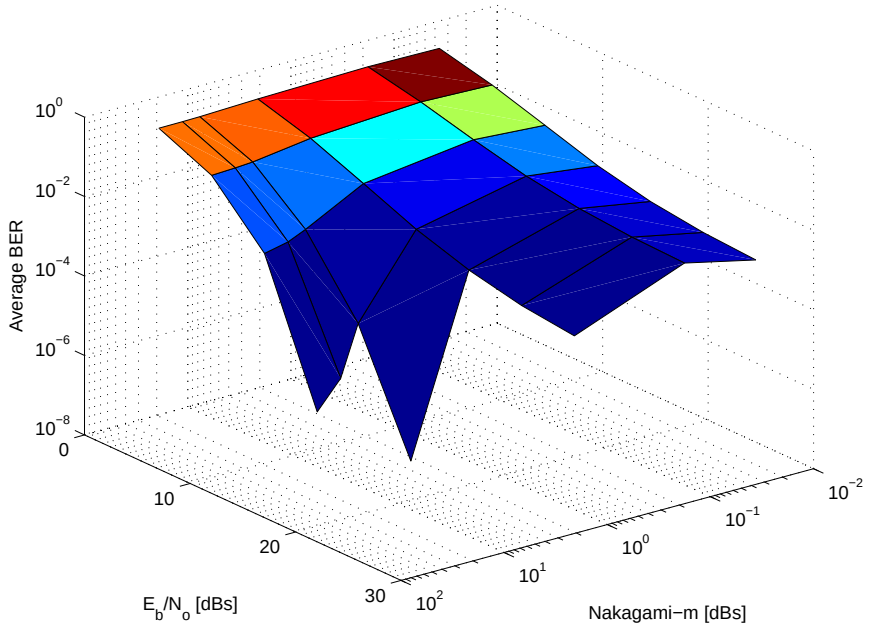

Figure 4.95: Impact of Nakagami-m variations on Average BEP of QPSK with Rake receiver (L=3), $f = 1800MHz$, Γ Exponential

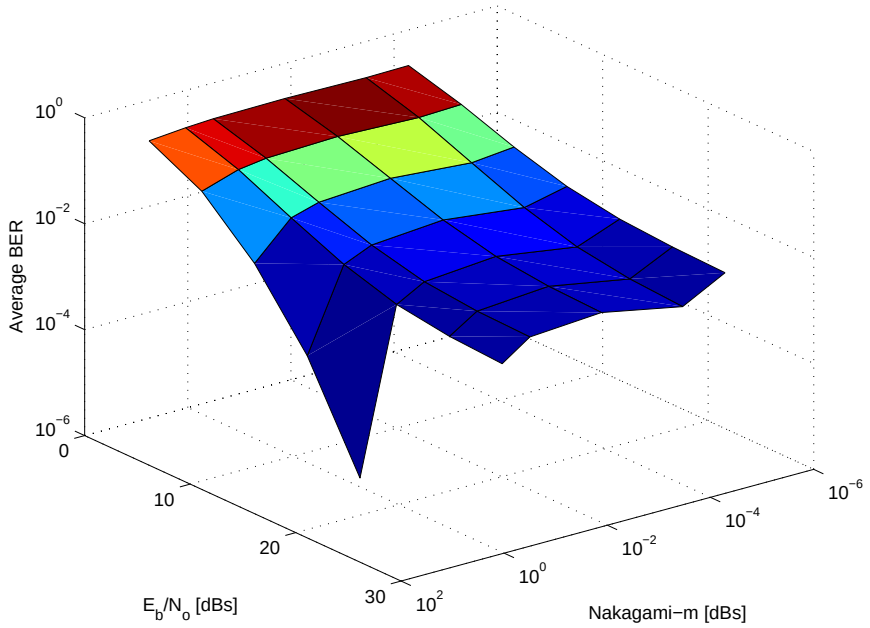

Figure 4.96: Impact of Nakagami-m variations on Average BEP of QPSK with Rake receiver (L=3), $f = 900MHz$, Γ Half Gaussian

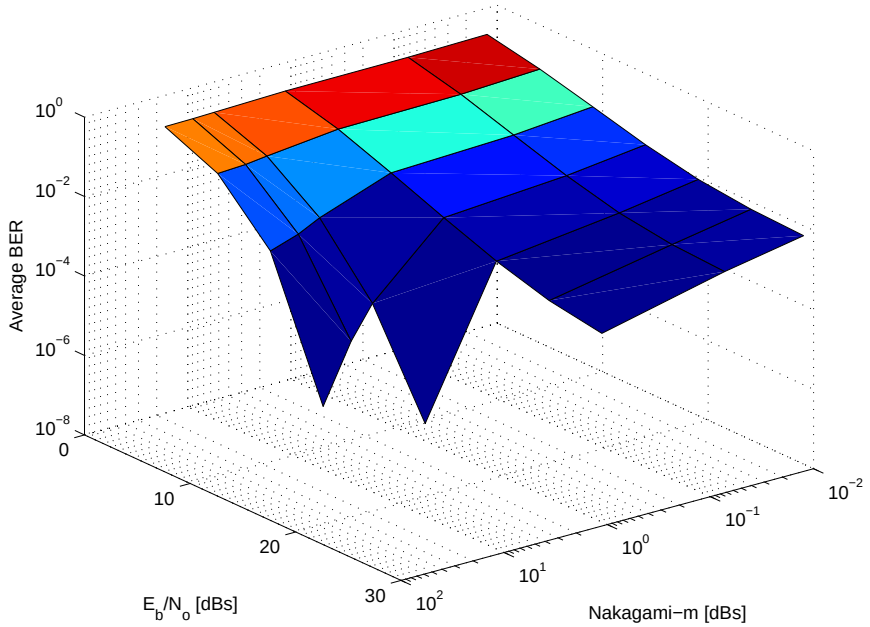

Figure 4.97: Impact of Nakagami-m variations on Average BEP of QPSK with Rake receiver (L=3), $f = 1800MHz$, Γ Half Gaussian

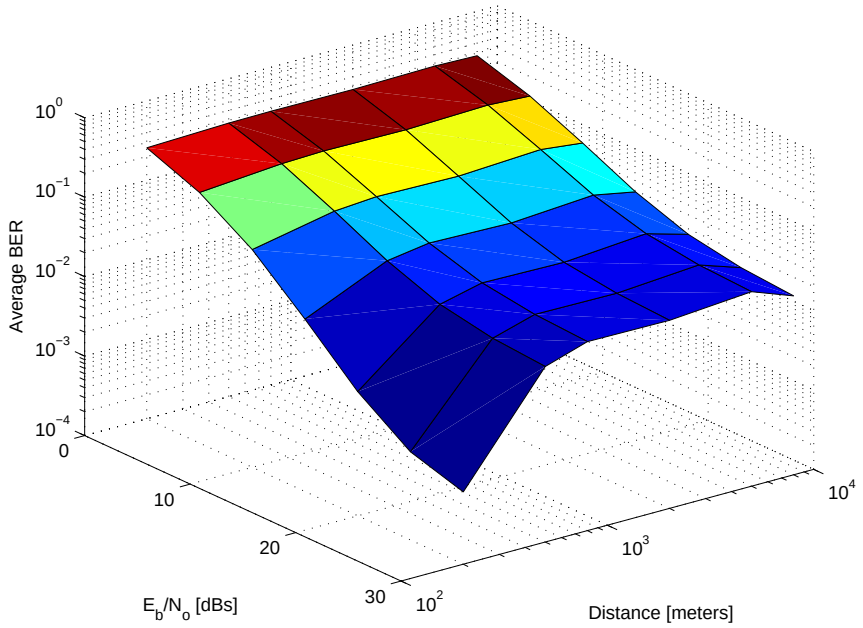

Figure 4.98: Impact of distance variations on Average BEP of 8PSK with Rake receiver (L=3), $f = 900MHz$, Γ Uniform

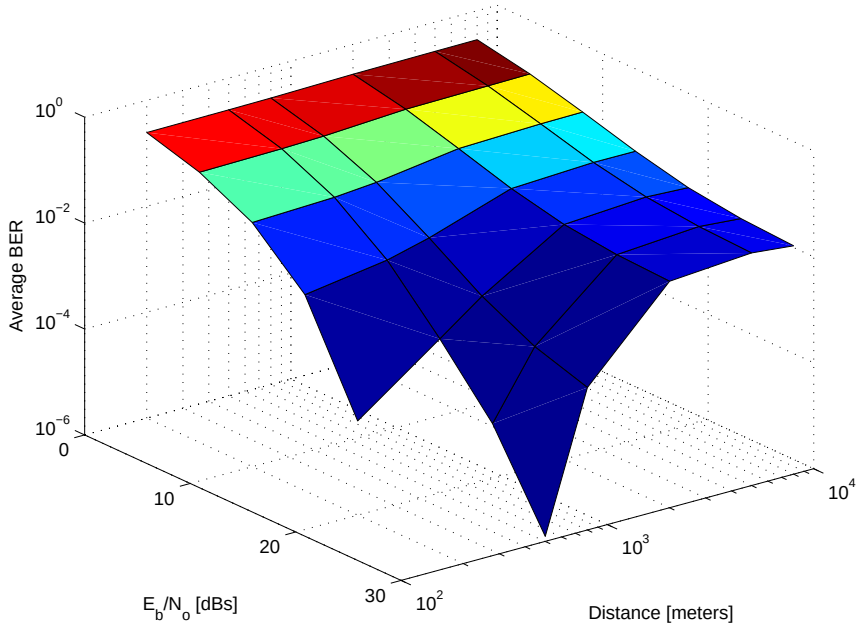

Figure 4.99: Impact of distance variations on Average BEP of 8PSK with Rake receiver (L=3), $f = 1800MHz$, Γ Uniform

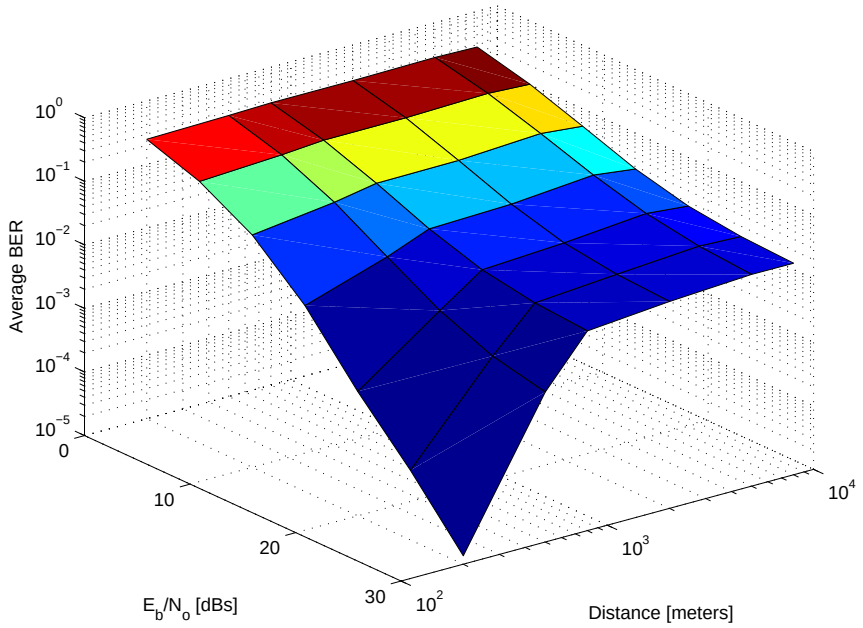

Figure 4.100: Impact of distance variations on Average BEP of 8PSK with Rake receiver (L=3), $f = 900MHz$, Γ Exponential

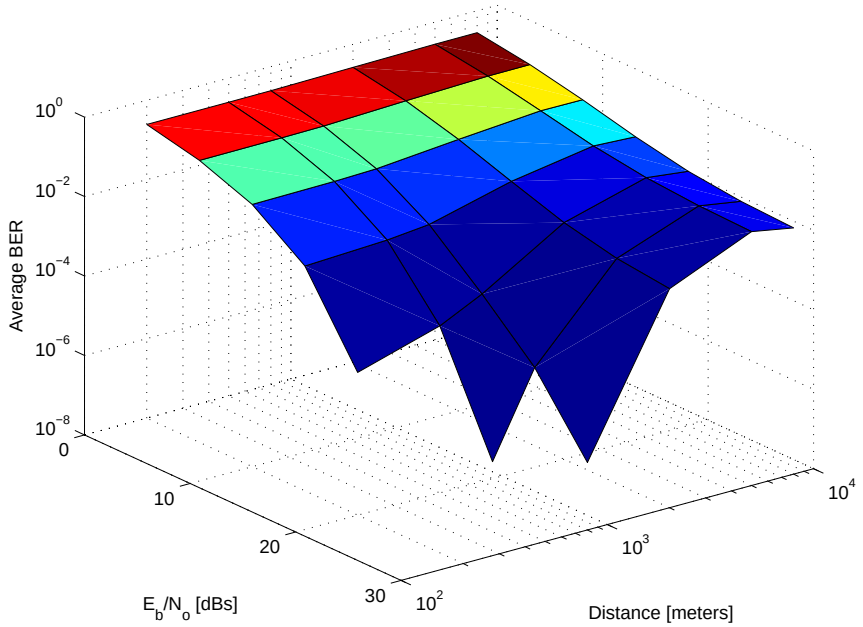

Figure 4.101: Impact of distance variations on Average BEP of 8PSK with Rake receiver (L=3), $f = 1800MHz$, Γ Exponential

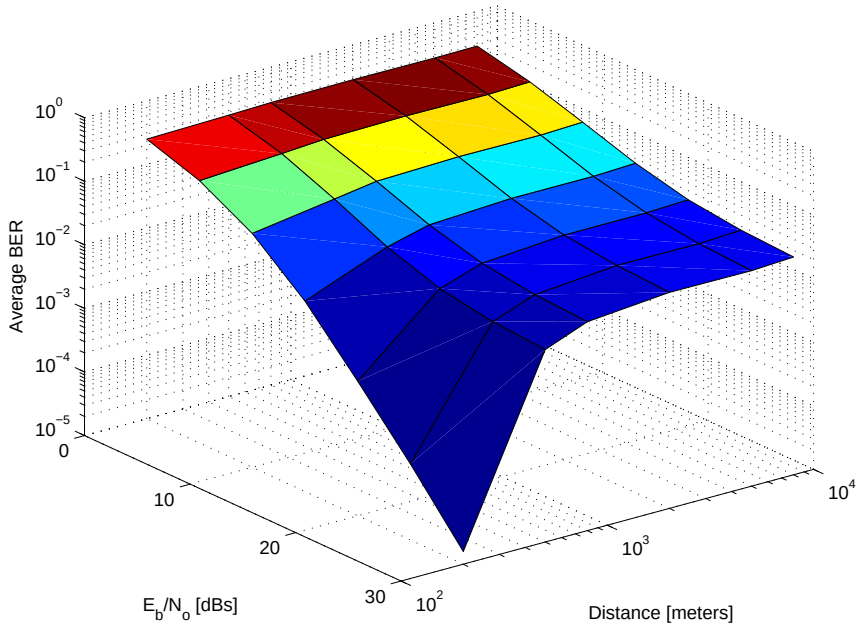

Figure 4.102: Impact of distance variations on Average BEP of 8PSK with Rake receiver (L=3), $f = 900MHz$, Γ Half Gaussian

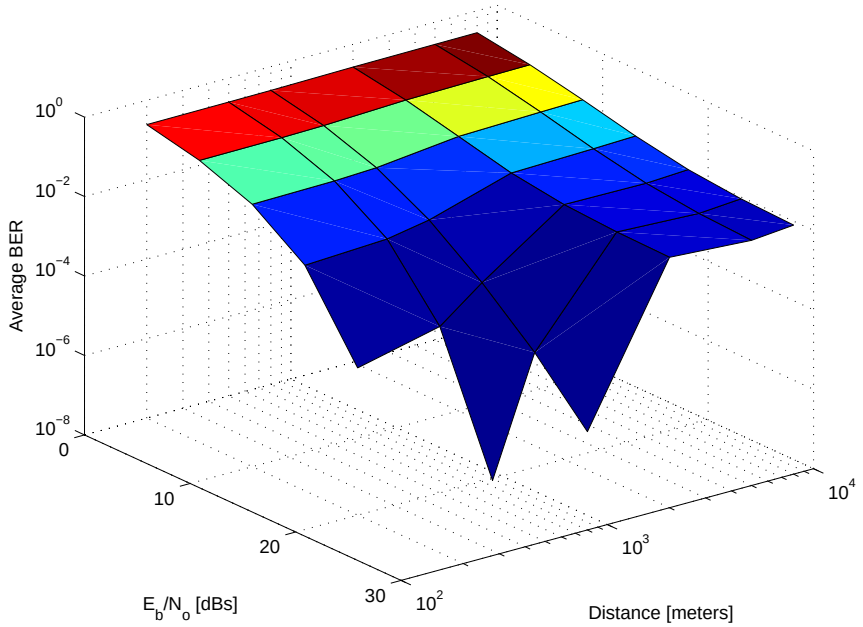

Figure 4.103: Impact of distance variations on Average BEP of 8PSK with Rake receiver (L=3), $f = 1800MHz$, Γ Half Gaussian

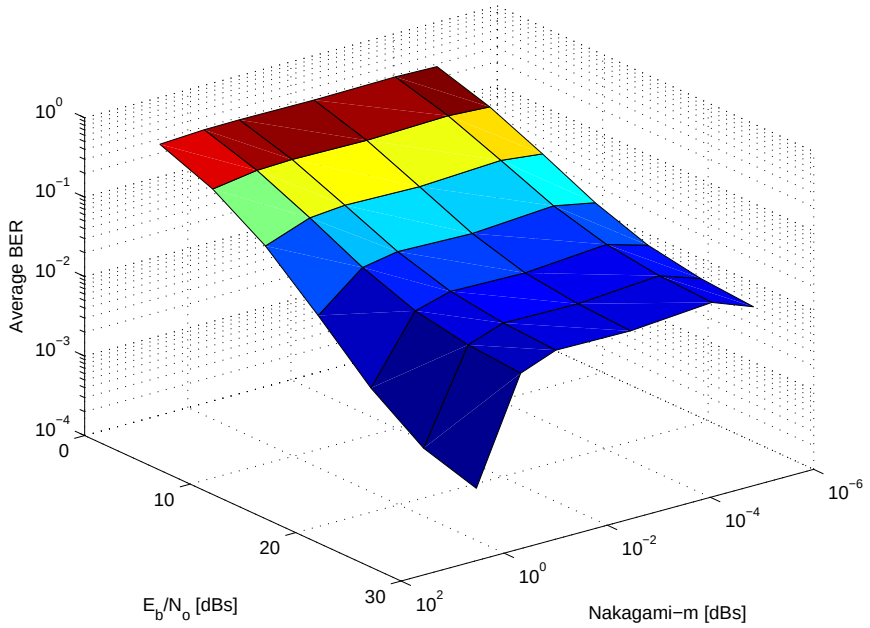

Figure 4.104: Impact of Nakagami-m variations on Average BEP of 8PSK with Rake receiver (L=3), $f = 900MHz$, Γ Uniform

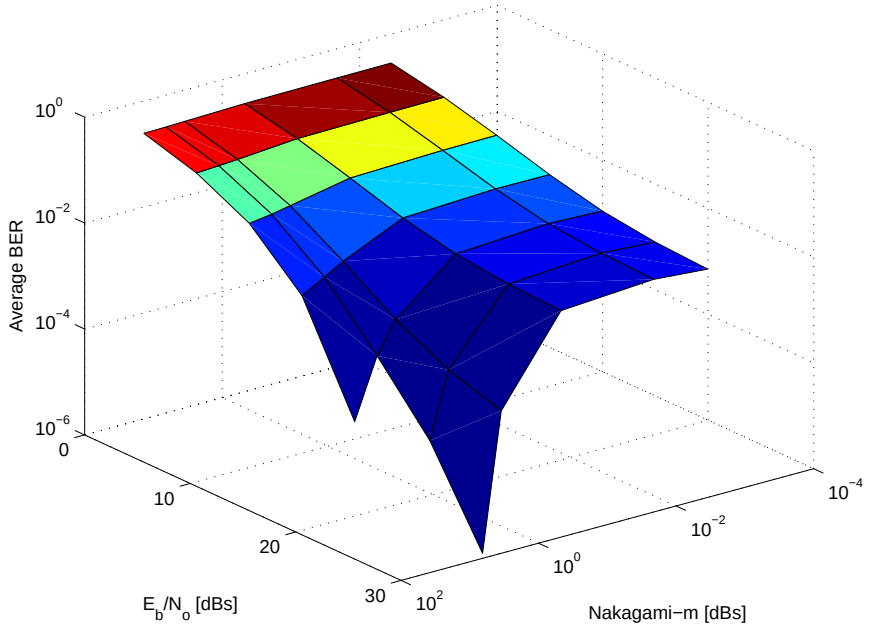

Figure 4.105: Impact of Nakagami-m variations on Average BEP of 8PSK with Rake receiver (L=3), $f = 1800MHz$, Γ Uniform

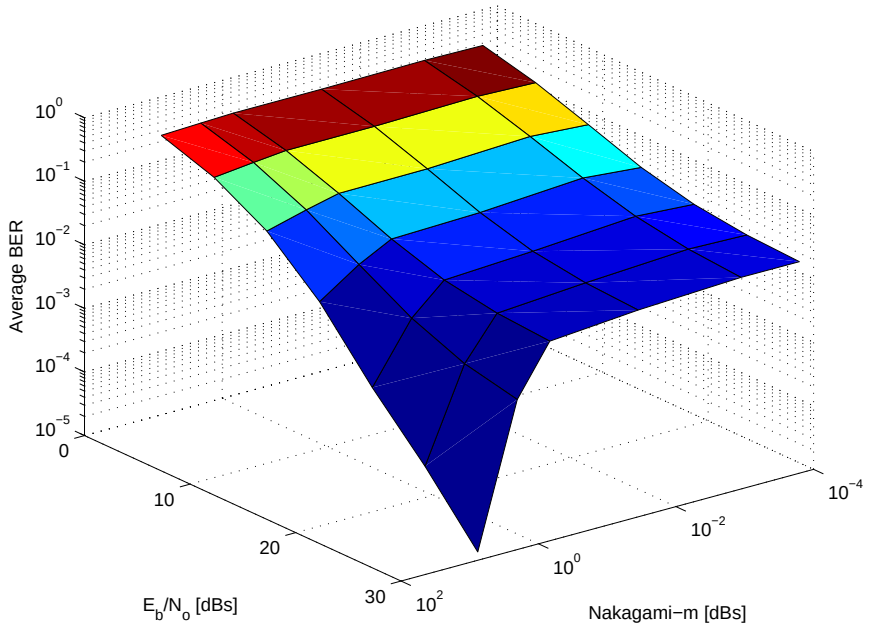

Figure 4.106: Impact of Nakagami-m variations on Average BEP of 8PSK with Rake receiver (L=3), $f = 900MHz$, Γ Exponential

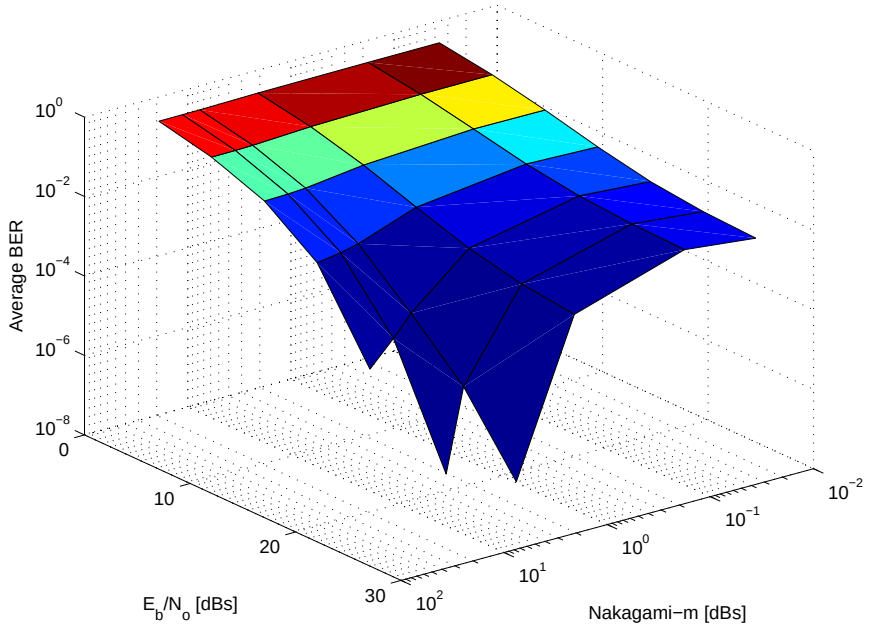

Figure 4.107: Impact of Nakagami-m variations on Average BEP of 8PSK with Rake receiver (L=3), $f = 1800MHz$, Γ Exponential

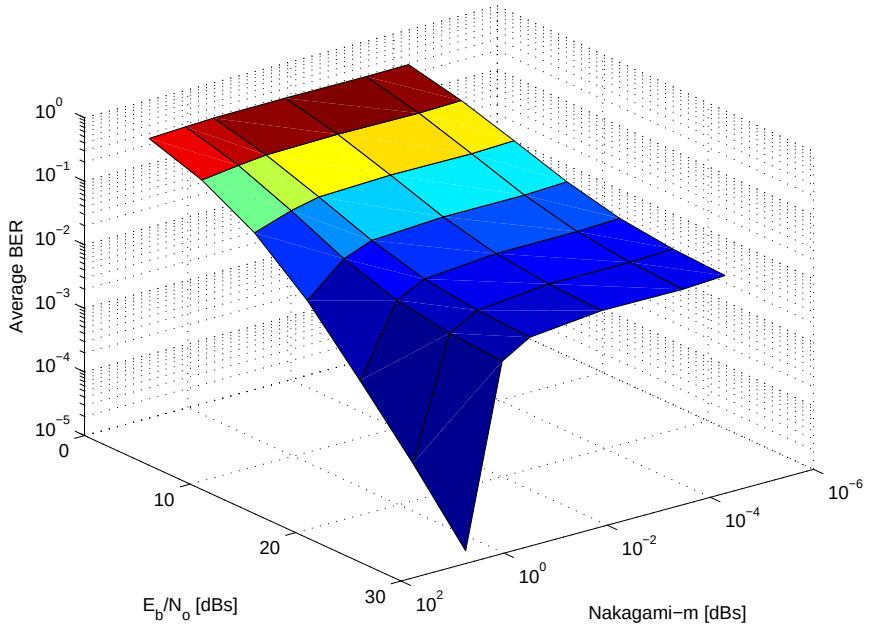

Figure 4.108: Impact of Nakagami-m variations on Average BEP of 8PSK with Rake receiver (L=3), $f = 900MHz$, Γ Half Gaussian

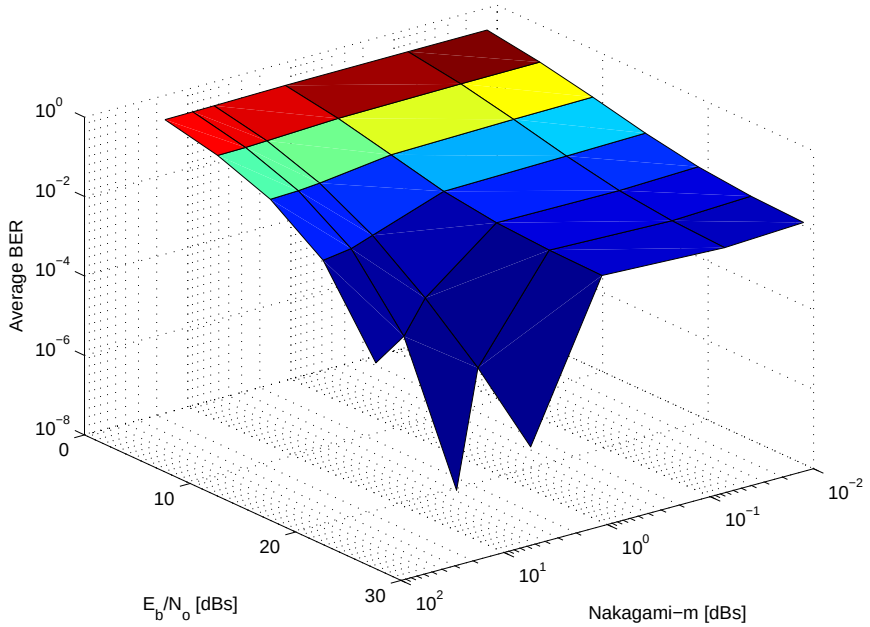

Figure 4.109: Impact of Nakagami-m variations on Average BEP of 8PSK with Rake receiver (L=3), $f = 1800MHz$, Γ Half Gaussian

Chapter 5

Conclusion and Future Work

5.1 Major Findings

The mojor findings of the study are summarized as follows:

- Development of a channel model that finds out the received direct and scattered powers at the mobile station.
- Studying the effect of varying distances between the mobile station and base station on the Nakagami-m parameter. It is found that the Nakagami-m parameter decays at a faster rate for shorter distances as compared to larger distances.
- The study reflects an impact on the performance of digital communication systems relating the distance d with m through different modulation schemes

over frequency non-selective and frequency selective multipath fading channels.

- The effect on the Nakagami-m parameter of different distributions of the reflection co-efficient Γ is studied. It is found that the exponential distribution gives larger values of m as compared to uniform and half Gaussian distribution.

- Change in the operating frequency also effects the performance of a digital communication link. It is observed that for shorter distances, operating at higher frequency gives better error rate performance but as we move away from the base station, at larger macrocellelar distances, the received power and the path loss becomes independent of the frequency thereby providing no improvement.

- A new parameter Δm is introduced in order to study the change in performance behavior of a particular modulation scheme with incresae in distance.

- The decay rate of parameter Δm is high when mobile is close to the base station and starts decreasing as it moves towards the edge of the cellular structure.

- Among the three distributions discussed (uniform, exponential, and half Gaussian), the parameter Δm reduces faster for exponential distribution of the reflection co-efficient as compared to other distributions hence providing larger values of m and better performance.

- Among the three models described (model A, model B, and model C), the

parameter m changes at a higher rate for model B in which the average distances between the receiver and the scatterers is increased, thereby reducing the received scattered power in both cellular (micro and macro) structures.

- The degraded performance of MPSK system at larger distances for smaller values of Nakagami-m parameter is studied and the error rates are improved by using Rake demodulator at the receiver.

- It is observed that the transmitter and receiver antenna heights also effects the Nakagami-m parameter and an increase in their effective value enhance the performance of the system.

- The behavior of Δm indicates that the performance of a digital communication system obeys an exponential decay.

- The tabular representation of Nakagami-m parameter indicates that its values are not integers as considered in the previous studies. However, it is stated that the Nakagami-m parameter describing the link quality is continuously changing with an increase in distance.

5.2 Future Work

It is observed that as we move away from the base station, the performance of the digital communication system degrades depending on the value of the Nakagami-m

parameter and the decay rate of parameter Δm. This behavior is observed for all the distributions of the reflection co-efficient and all the models discussed. In order to acheive uniformity throughout the cell, the concept of power control can be applied. Since, it is shown that the paramter Δm decays with the increase in distance in cellular environment, measures can be taken to control this parameter and to keep it unchanged. The performance of the link is dictated by Δm, and it is found by calculating the direct and the scattered powers between the transmitter and the receiver. To ensure a good quality of service (QoS) throughout the cell, the received signal must be strong. The power control systems have to compensate not only for signal strength variations due to the varying distance between the base station and the mobile but must also attempt to compensate for signal strength fluctuations typical of a wireless channel. These fluctuations are due to the changing propagation environment between the base station and the user as the user moves across the cell. Since the mobile terminal may move at the velocity of a moving car or even of a fast train, the rate of channel fluctuations may be quite high and the power control has to react very quickly in order to compensate for it.

Further, it can be proposed that if the scattered power from the materials that are good conducting surfaces are included or somewhat transfered into direct power at certain specified interval of distances, then the uniformity of performance and enhanced QoS may be acheived.

Bibliography

[1] Theodore S. Rappaport. Wireless communications, principles and practice. 2nd ed.

[2] Jong A. J. T. Linnartz, G. and R. Prasad. Effect of coding in digital micro-cellular personal communication systems with co-channel interference, fading, shadowing and noise. *IEEE Journal on Selected Areas in Communications*, 11:901–909, Aug 1993.

[3] M. Abdel-Hafez and M. Safak. Performance analysis of digital cellular radio systems in nakagami fading and correlated shadowing environment. *IEEE Transactions on Vehicular Technology*, 48(5):1381–1391, Sep 1999.

[4] L.G. de R. Guedes and M.D. Yacoub. Overlapping cell area in different fading conditions. *IEEE Vehicular Technology Conference*, 1:380–383, Jul 1995.

[5] William C. Y. Lee. *Mobile Communications Engineering*. McGraw-Hill Book Company.

[6] Blackard K. L. Rappaport T. S. Seidel S. Y. Feurestein, M. J. and H. H. Xia. Path loss, delay spread and outage models as functions of antenna height for microcellular system design. *IEEE Transactions on Vehicular Technology*, 43(3):487–498, Aug 1994.

[7] S.A. Abbas and A.U.H. Sheikh. Narrow-band small area microcellular mobile radio channel characterization using ray tracing technique. *IEEE Conference on Vehicular Technology*, pages 589–592, May 1993.

[8] F. Ikegami. Theoretical prediction of mean field strength for urban mobile radio. *IEEE Transactions on Antennas and Propsagation*, 39(3), Mar 1991.

[9] Rustako Jr. A. J. Radio propagation at microwave frequencies for line-of-sight microcellular mobile and personal communications. *IEEE Transactions on Vehicular Technology*, VT-40(1), Feb 1991.

[10] M. K. Simon and M. S. Alouini. *Digital Communication over Fading Channels*. Wiley series in Telecommunications and Signal Processing, second edition, 2004.

[11] J. D. Parsons. *The Mobile Radio Propagation Channel*. John Wiley Sons LTD., second edition, 2000.

[12] P. A. Bello. Characterisation of randomly time-variant linear channels. *IEEE Transaction*, 1963.

[13] D. C. Cox and R. P. Leck. Correlation bandwidth and delay spread multipath propagation statistics for 910mhz urban mobile radio channels. *IEEE Transactions*, 1975.

[14] R. H. Clarke. A statistical theory of mobile radio reception. *Bell System Technical Journal*, 47:957–1000, Jul-Aug 1968.

[15] W. C. Jakes. *Microwave Mobile Communication*. New York: Wiley, 1974.

[16] John G. Proakis. *Digital Communications*. McGraw Hill International, fourth edition, 2000.

[17] Labedz G. P. Stewart, K. A. and K. Sohrabi. Wideband channel measurements at 900mhz. *Proceesings IEEE Vehicular Technology*, pages 236–240, Jul 1995.

[18] W. R. Braun and U. Dersch. A physical mobile radio channel model. *IEEE Transactions on Vehicular Technology*, VT-40:472–482, May 1991.

[19] S. A. Abbas and A. U. Sheikh. A geometric theory of nakagami fading multipah mobile radio channel with physical interpretations. *Proc. IEEE Veh. Tech. Conf. (VTC '96)*, pages 637–641, April 1996.

[20] Hashemi H. Impulse response modeling of indoor radio propagation channels. *IEEE Transactions on Vehicular Technology*, VT-28:213–225, Aug 1979.

[21] Johnston Fine Turin, Clapp and Lavry. A statistical model for urban multipath propagation. *IEEE Transactions on Vehicular Technology*, VT-21:1–9, Feb 1972.

[22] B. Glance and L. J. Greenstein. Frequency-selective fading effects in digital mobile radio with diversity combining. *IEEE Transactions on Communication*, COM-31:1085–1094, Sept 1983.

[23] P. F. M. Smulders and A. G. Wagemans. Millimeter wave biconical horn antennas for near uniform coverage in indoor picocells. *Electronic Letters*, 28:679–681, Mar 1992.

[24] Furuno T. Ichitsubo, S. and R. Kawasaki. A statistical model for microcellular multipath propagation environment. *Proc. IEEE Veh. Tech. Conf. (VTC '97)*, pages 61–66, May 1997.

[25] Marti J. Wittmann, M. and T. Kurner. Impact of the power delay profile shape on the bit error rate in mobile radio systems. *IEEE Transactions on Vehicular Technology*, VT-46:329–339, May 1997.

[26] G. L. Stuber. Principles of mobile communication. *Boston, MA:Kluwer*, 1996.

[27] P. Hoeher. A statistical discrete-time model for the wssus multipath channel. *IEEE Transactions on Vehicular Technology*, 41:461–468, Nov 1992.

[28] M. F. Pop and N. Beaulieu. Statistical investigation of sum-of-sinusoids fading channel simulators. *Global Telecommunications Conference*, 1a:419–426, 2000.

[29] Julian Cheng and N.C. Beaulieu. Maximum-likelihood based estimation of the nakagami m parameter. *IEEE Communications Letters*, 5(3):101–103, Mar 2001.

[30] Julian Cheng and N.C. Beaulieu. Moment-based estimation of the nakagami-m fading parameter. *IEEE Pacific Rim Conference on Communications, Computers and signal Processing*, 2:361–364, Aug 2001.

[31] Julian Cheng and N.C. Beaulieu. Generalized moment estimators for the nakagami fading parameter. *IEEE Communications Letters*, 6(4):144–146, Apr 2002.

[32] C. Tepedelenlioglu and Ping Gao. Practical issues in the estimation of nakagami-m parameter. *IEEE GLOBECOM*, 2:972–976, Dec 2003.

[33] Y. Chen and N.C. Beaulieu. Estimation of ricean and nakagami distribution parameters using noisy samples. *IEEE International Conference on Communications*, 1:562–566, Jun 2004.

[34] M. Nakagami. The m-distribution - a general formula of intensity distribution of rapid fading. *Statistical Methods of Radio Wave Propagation*, pages 3–36, 1960.

[35] H. Suzuki. A statistical model for urban radio propagation. *IEEE Transactions on Communications*, COM-25:673–680, Jul 1977.

[36] A. Abdi and M. Kaveh. Performance comparison of three different estimators for the nakagami m parameter using monte carlo simulation. *IEEE Communications Letters*, 4(4):119–121, Apr 2000.

[37] Cihan Tepedelenlioglu. Analytical performance analysis of moment-based estimators of the nakagami parameter. *IEEE Vehicular Technology Conference*, 3:1471–1474, Sep 2002.

[38] Q.T. Zhang. A note on the estimation of nakagami-m fading parameter. *IEEE Communications Letters*, 6(6):237–238, Jun 2002.

[39] J. Yan and S. Kozono. Study of nakagami m parameter in mobile wide band channel, case of no line of sight. *Vehicular Technology Conference Proceedings*, 3:2162–2166, May 2000.

[40] N.C. Beaulieu and C. Cheng. An efficient procedure for nakagami-m fading simulation. *IEEE GLOBECOM*, 6:3336–3342, Nov 2001.

[41] Keli Zhang Zhefeng Song and Yong Liang Guan. Generating correlated nakagami fading signals with arbitrary correlation and fading parameters. *IEEE International Conference on Communications*, 3:1363–1367, May 2002.

[42] Keli Zhang Zhefeng Song and Yong Liang Guan. Simulation of nakagami fading channels with arbitrary cross-correlation and fading parameters. *IEEE Transactions on Wireless Communications*, 3(5):1463–1468, Sep 2004.

[43] Kuroda T. Karasawa, Y. and H. Iwai. The equivalent transmission-path model - a tool for analyzing error floor characteristics due to intersymbol interference in nakagami-rice fading environments. *IEEE Transaction on Vehicular Technology*, 46(1):194–202, 1997.

[44] T. Aulin. Characteristics of a digital mobile radio channel. *IEEE Transactions on Vehicular Technology*, VT-30:45–53, May 1981.

[45] Handforth M. Sheikh, A. U. and M. Abdi. Indoor mobile radio channel at 946mhz:measurements and modeling. *Proc. IEEE Veh. Tech. Conf. (VTC '93)*, pages 73–76, May 1993.

[46] Costa Fougere Carlson Basu, McKenzie and Whitney. 250mhz/ghz scintillation parameters in the equatorial, polar, and aural environments. *IEEE J. Select. Areas Commun.*, pages 102–115, Feb 1987.

[47] N. C. Beaulieu and A. A. Abu-Dayya. Analysis of equal gain diversity on nakagami-fading channels. *IEEE Transaction on Communications*, COM-39:225–234, Feb 1991.

[48] A. A. Abu-Dayya and N. C. Beaulieu. Microdiversity on rician fading channels. *IEEE Transaction on Communications*, COM-42:2258–2267, Jun 1994.

[49] N. C. Beaulieu. An infinite series for the computation of the complementary probability distribution function of a sum of independent random variables and its application to the sum of rayleigh random variables. *IEEE Transaction on Communications*, COM-26:1463–1474, Sept 1990.

[50] Beaulieu N. C. Dong, X. and P. H. Wittke. Signalling constellations for fading channels. *IEEE Transaction on Communications*, COM-47:703–714, May 1999.

[51] J. Gil-Pilaez. Note on the inversion theorem. *Biometrika*, 38:481–482, 1951.

[52] Q. T. Zhang. Probability of error for equal-gain combiners over rayleigh channels:some closed-form solutions. *IEEE Transaction on Communications*, COM-45:270–273, Mar 1997.

[53] Q. T. Zhanh. A simple approach to prabability of error for equal gain combiners over rayleigh channels. *IEEE Transaction on vehicular Technology*, VT-48:1151–1154, Jul 1999.

[54] Tellambura C. Annamalai, A. and V. K. Bhargava. Exact evaluation of maximal-ratio and equal gain diversity receivers for m-ary qam on nakagami fading channels. *IEEE Transaction on Communications*, COM-47:1335–1344, Sept 1999.

[55] R. Price and P. E. Green. A communication technique for multipath channels. *Proc. IRE*, 46:555–570, March 1958.

Vitae

Name: *Muhammad Imran Azam*

Birth: *February 21, 1980 - Karachi, Pakistan*

- Received Bachelor of Engineering (B.E) degree in Electrical Engineering from N.E.D University of Engineering and Technology, Karachi, Pakistan in 2002.
- Joined King Fahd University of Petroleum and Minerals, Dhahran in February 2003 as a Research Assistant to persue MS degree in Electrical Engineering.
- Conducted research both individually and as a member of team.
- Assisted the faculty members of Electrical Engineering Department in research projects through literature reviews and technical reports.
- Taught undergraduate labs (EE 201, EE 203, and EE 204).

Email: *mazam@kfupm.edu.sa*